DRDC Toronto CR 2005-121

Development of a Dynamic Biomechanical Model for Load Carriage: Phase III Part C1:

Pressure and Force Distribution Measurement for the Design of Waist Belts in Personal Load Carriage Systems

By
L.J. Hadcock

Ergonomics Research Group
Queen's University
Kingston, Ontario, Canada
K7L 3N6

Project Manager:
J. M. Stevenson (613) 533-6288

PWGSC Contract No. W7711-0-7632-06
on behalf of
DEPARTMENT OF NATIONAL DEFENCE

as represented by
Defence Research and Development Canada -Toronto
1133 Sheppard Avenue West
North York, Ontario, Canada
M3M 3B9

DRDC Scientific Authority:
Maj Linda Bossi
(416) 635-2197

August 2005

Abstract

In previous studies, two biomechanical models were developed that used pack and person geometry as well as pack mass to determine the reaction forces on the body. One perpetual problem has been determining the pack-person interface forces using Tekscan™ pressure sensors on rounded surfaces such as the shoulder and waist. The goal of this study was to determine design factors that affect force distribution of the backpack waist belt. A human-sized symmetrical lower torso (SLT) was created of wood and covered with Bocklite™. A method of calculating the directional coordinates of applied forces was developed in order to understand the reactions between pack and person. Tekscan™ Sensors were used on the surface to measure the surface pressures between the torso and the waist belt. These were converted to normal force measures based on the mathematical coordinates of each sensel. A strategy was developed for calibration of Tekscan™ on a curved surface. Calibration factors, a factor of effective sensel area and a frictional coefficient for the in situ orientation of each sensor were calculated and used for the calculation of the directional forces. Then, using selected sites on the waist belt, known forces were applied and the resulting directional forces correlated moderately well with the known applied forces (19%). The pressure distributions of three waist belts were compared and the design features were examined to account for differences in distribution. The distributions were compared to results of the previous biomechanical models and determined to be too complex to be resolved with the simplified hoop stress theory. The study determined the importance of waist belt design, frictional force from belt tightening, and influence of load in understanding the force distribution of a waist belt. A limiting factor was the lack of precision of Tekscan™ and its inability to measure shearing frictional forces, a key variable in understanding how a backpack works. It is recommended that each pack and load condition be tested using this approach if one wishes to use the waist strap force gauge to determine compressive forces on the lumbar spine and on the hips.

Résumé

Dans les études antérieures, deux modèles biomécaniques fondés sur la géométrie du sac à dos et de la personne ainsi que sur la masse du sac avaient été élaborés pour déterminer les forces de réaction corporelles. Un problème perpétuel est la détermination, à l'aide des capteurs de pression Tekscan[MC], des forces exercées à l'interface sac-personne sur des surfaces arrondies, comme les épaules et la taille. La présente étude a pour but de déterminer les facteurs de conception de la ceinture du sac à dos qui ont un effet sur la répartition des forces. À cette fin, on a fabriqué un torse inférieur symétrique (SLT) de taille humaine avec du bois et on l'a recouvert de Bocklite[MC]. Afin de comprendre les interactions entre le sac et la personne, une méthode a été élaborée pour calculer les coordonnées directionnelles des forces appliquées. Des capteurs Tekscan[MC] ont été posés à la surface pour mesurer les pressions exercées à la surface entre le torse et la ceinture. Les coordonnées mathématiques de chacun des capteurs à cellules ont servi à convertir les mesures de pression en mesures de force normale. Une stratégie a été élaborée pour l'étalonnage du Tekscan[MC] sur une surface arrondie. Les facteurs d'étalonnage, qui dépendent de la surface efficace de la cellule et du coefficient de frottement utilisés pour l'orientation de chaque capteur sur place, ont été calculés et ont servi à calculer les forces directionnelles. Ensuite, des forces connues ont été appliquées à des emplacements donnés de la ceinture; la corrélation entre les forces directionnelles obtenues et les forces connues appliquées était relativement bonne (19 %). Une comparaison de la répartition des pressions a été effectuée entre trois ceintures, et leurs caractéristiques de conception ont été examinées pour expliquer les différences de répartition. La répartition a ensuite été comparée avec les résultats obtenus au moyen des modèles biomécaniques précédents; on a déterminé qu'elle était trop complexe pour être déterminée à l'aide de la théorie simplifiée de tension de charge. L'étude a démontré l'importance de la conception de la ceinture, la force de frottement résultant du serrage et l'incidence de la charge sur la compréhension de la répartition des forces d'une ceinture. Le manque de précision du Tekscan[MC] et son incapacité à mesurer les forces de cisaillement, qui est un facteur important pour la compréhension du fonctionnement d'un sac à dos, ont limité l'étude. Nous recommandons de recourir à cette méthode pour mettre à l'essai chaque sac à dos et chaque condition de charge afin de permettre l'utilisation du dynamomètre de ceinture pour déterminer les forces de compression sur la colonne lombaire et les hanches.

Executive Summary

Introduction

This study was completed under contract PWSGC #W7711-0-7632-03 Sections 6 B and C for DRDC Toronto. Section 6B was to construct a standardized lower torso (SLT) model in order to be used in Section 6C for the validation of a waist belt model. Two previous static biomechanical models have been developed under previous DCIEM contracts (Stevenson *et al*, 1995 and Pelot *et al*, 1998). The first was a shoulder-based model that was used to help establish recommended shoulder and lumbar reaction forces and the second model added a waist belt but no load lifter or hip stabilizer straps. When Rigby (1999) attempted to add these components, results were poorer than previous models because of indeterminacy in the system. The goal of this research was to develop a valid waist belt model for future dynamic biomechanical modeling analysis.

Previous biomechanical models have made several assumptions of the waist belt, most notably a constant tension throughout the belt and frictional forces acting in a direction resisting movement of the waist belt. Section 6C used the SLT to validate these earlier models as well as determining the relationship between strap force tension and the measured pressure distribution.

Specific Objectives

The primary objectives of this research were:

1. To develop a simplified model of the human lower torso as an addition to the current suite of tools used by the Ergonomics Research Group.
2. To develop a valid waist belt model for a backpack.
3. To determine the factors affecting force distribution on a load carriage system waist belt.

To accomplish these objectives, several specific milestones were also identified:

- Determination of the frictional components of the waist belt.
- Development of a novel calibration procedure for contact pressure sensors in this application.
- Determination of the effects of the direction of strap tightening on measured pressures on the body.
- Determination of the relationship of the strap force tension in the waist belt to the measured pressures on the body.

Major Findings

A Symmetrical Lower Torso (SLT) was designed and constructed. The SLT allowed measured forces, for any point on the surface, to be resolved into directional vectors in three dimensions with the known coordinates of the point. A strategy was developed using the Tekscan™ 9600 sensors to determine waist belt compressive force distribution within an RMS error of <10N.

A calibration procedure using an effective Tekscan™ sensel area and a longitudinal frictional coefficient has been demonstrated. This is limited in application to vertical loading and was more successful in cases where the loads exceeded 50N.

Within the limitations of Tekscan™ technology, it was possible to calibrate the sensors on a curved surface. However, the need for a minimum of three repetitions to reduce random error has been demonstrated. This calibration procedure has also demonstrated the need to calibrate all

sensors, *in situ*, that are used in curved positions, or disregard the magnitudes of the measured forces.

It was possible to derive a coefficient of friction for the isolated waist belt model and to determine how factors such as the direction of belt tightening affected magnitude of the measured normal forces on the torso.

The effects of tightening direction were shown to be significant in no-load tests of waist belts. The measured forces on the hips were significantly lower on the side of the strap force transducer and these effects are reduced with an increase in load. The apparent effects due to the tightening direction of the waist belt were consistent and predictable but their relationship to the forces acting on more compliant surfaces, such as the human body cannot be extrapolated from this observation.

Previous models involving a waist belt have oversimplified the role of friction with the assumption of a constant belt tension. The complexity of the measured forces in the waist belt indicated that a direct relationship between strap force tension, measured in one location, and the forces acting on the body, was not possible. However, by testing the pack under realistic conditions (i.e. load, tension) it is possible to express hips, lumbar and abdominal tension as a multiple of waist strap tension for individual waist belts.

The application of the frictional distributions appear to depend on the materials used in the construction of the belt. In this preliminary study, the padding orientation and conical shape of the waist belt determined the severity of localized compressive forces at the base of the belt. A less conical shape created lines of pressure about the bottom of the waist belt as the effects of the belt tension were concentrated in this area due to the geometry of the SLT.

At this time, a model for an individual waist belt is limited by an inability to predict frictional force distributions. Tekscan™ instrumentation is also limited in this regard since it cannot directly evaluate the effect of shear forces on the torso.

Recommendations

The backpack must be tested under the load conditions anticipated in the field in order to determine the pressures in relation to the belt tension.

The directions of frictional forces need to be more closely examined as the impending pack motion may not be downwards as originally considered, depending on the mass of the pack and the tension in the belt. If the effective tension were higher than the effective mass on the belt, the pack would have a tendency to move upwards because of the hoop shape rather than downwards with the force of gravity. The apparent consistent effect of loading the pack and the increase in waist belt tension should be explored further. Incremental loading would better provide an understanding of this relationship.

The unbalanced forces resulting from the compressive force of belt tensioning need to be examined further. The variation in the three waist belts in this study was too great to determine with any certainty how waist belt design relates to the force and frictional distribution in the waist belt. In order to determine the actions of the waist belt padding, the properties of the material, such as compliance of the foam, and the frictional properties of the covering materials should be determined. Identical belts with different materials or different designs with the same materials would facilitate this understanding.

The effect of different lean angles of the torso on the distribution of forces should be examined. A forward lean angle of 8° would vertically orient the abdominal area of the model, more closely resembling the human body.

The padding surface of each belt may be experiencing relatively large shear forces due to circumferential pressure. These forces and their distribution are not easily modeled and would likely differ greatly when the belt interacts with the compliance of the human body. As a way of subjectively testing different materials on humans, correlations could be made through user trials and questionnaires to determine the relationship between user preferences and compliance of the padding. Belt designs could also be compared with the correlation to subjective testing.

Shear force measurement systems should be evaluated as to their applicability to quantify the frictional forces observed on the SLT.

The SLT has a number of potential uses such as: comparison of different materials used for waist belts, further improvements to the waist belt model, and comparison of novel designs in waist belt technology. A simplified shoulder can be combined with the SLT to allow for the loading of a complete pack. Tekscan™ sensors on the shoulder would allow for a more complete measurement of the forces of the upper pack and allow for complete resolution of the forces on the body. Strap force transducers on the shoulder straps would determine the relationship of the measured strap forces and the measured forces on the shoulder.

The design of different waist belt attachment points to the pack should be explored. Specifically, the ability to transmit a moment, and therefore this connection should be considered. While padding design did not show differences in the total distribution of force on the hips, the reduction of the line of pressure about the bottom was apparent in the more conical belts. The testing of a belt with an adjustable angle would help investigate this effect.

Sommaire

Introduction

La présente étude a été réalisée en vertu du contrat TPSGC n^{o} W7711-0-7632-03, sections 6 B et C, pour le compte de RDDC Toronto. La section 6B consiste en la construction d'un torse inférieur normalisé (SLT) qui sera utilisé à la section 6C pour la validation du modèle de ceinture. Deux modèles biomécaniques statiques ont été élaborés dans le cadre de contrats IMED (Stevenson *et al*, 1995 et Pelot *et al*, 1998). Le premier modélisait les épaules et a servi à établir les forces de réaction recommandées pour les épaules et la région lombaire, et une ceinture a été ajoutée au second modèle, mais sans sangle de levage de charge, ni sangle de stabilisation aux hanches. Lorsque Rigby (1999) a essayé d'ajouter ces éléments, les résultats ont été moins bons que ceux des modèles précédents en raison de l'indétermination du système. La présente étude a pour but d'élaborer un modèle valide de ceinture qui servira à une future analyse du modèle biomécanique dynamique.

Dans les modèles biomécaniques précédents, on avait fixé plusieurs hypothèses concernant la ceinture, plus particulièrement que la traction était constante dans toute la ceinture et que les forces de frottement agissaient dans la direction inverse du mouvement de la ceinture. Dans la section 6C, on a utilisé le SLT pour valider les modèles antérieurs ainsi que pour déterminer les relations entre la traction de la sangle et la répartition des pressions mesurées.

Objectifs précis

Voici les principaux objectifs de la recherche :

4. Élaborer un modèle simplifié d'un torse inférieur humain, afin de l'ajouter à l'ensemble d'outils utilisés actuellement par le groupe de recherche en ergonomie.
5. Élaborer un modèle de ceinture de sac à dos valide.
6. Déterminer les facteurs ayant un effet sur la répartition des forces dans une ceinture destinée à un système de transport de charge.

Pour atteindre ces objectifs, on a défini plusieurs étapes particulières :

- Déterminer les éléments de frottement de la ceinture.
- Mettre au point une nouvelle procédure d'étalonnage des capteurs de pression de contact pour cette application.
- Déterminer les effets de la direction de serrage de la ceinture sur les pressions corporelles mesurées.
- Déterminer la relation entre la traction de la ceinture et les pressions corporelles mesurées.

Principaux résultats

On a conçu et fabriqué un torse inférieur symétrique (SLT). Le SLT a permis de décomposer, pour tout point de la surface, les forces mesurées en vecteurs directionnels tridimensionnels à l'aide des coordonnées connues d'un point. Une stratégie a été élaborée pour déterminer, à l'aide des capteurs du Tekscan^{MC} 9600, la répartition des forces de compression de la ceinture, avec une erreur type de <10 N.

Une procédure d'étalonnage utilisant la surface utile des capteurs à cellules du Tekscan^{MC} et le coefficient de frottement longitudinal a été démontrée. Son application est limitée aux charges verticales et convient mieux aux charges supérieures à 50 N.

En dépit des limites de la technologie du Tekscan^{MC}, on a pu étalonner les capteurs sur une surface arrondie. Toutefois, pour réduire l'erreur aléatoire, il a fallu faire au moins trois tentatives. La procédure d'étalonnage indique également que tous les capteurs utilisés à des emplacements arrondis doivent être étalonnés sur place, sinon on ne doit pas tenir compte de la valeur des forces mesurées.

On a pu dériver un coefficient de friction pour le modèle de ceinture isolé et déterminer l'incidence de facteurs, comme la direction du serrage de la ceinture, sur la valeur des forces normales mesurées sur le torse.

Les effets de la direction de serrage constatés étaient considérables dans les essais des ceintures sans charge. Les forces mesurées aux hanches étaient considérablement plus faibles du côté du transducteur de restitution des efforts; les effets étaient moindres avec une charge plus lourde. Les effets apparents de la direction de serrage de la ceinture sont uniformes et prévisibles, mais les relations avec les forces agissant sur des surfaces plus flexibles, comme le corps humain, ne peuvent être extrapolées à partir de ces observations.

Dans les modèles précédents où une ceinture était utilisée, on avait trop simplifié le rôle du frottement en faisant l'hypothèse que la traction de la ceinture soit constante. La complexité des forces mesurées dans la ceinture indique qu'il n'est pas possible d'établir une relation directe entre la traction de la ceinture, mesurée à un emplacement, et les forces exercées sur le corps. Toutefois, lors d'essais menées avec le sac à dos dans des conditions réalistes (c.-à-d. de charge et de tension), il a été possible d'exprimer la traction aux hanches et dans les régions lombaire et abdominale comme un multiple de la traction de la ceinture pour des ceintures individuelles.

La répartition du frottement semble dépendre des matériaux utilisés dans la fabrication de la ceinture. Dans cette étude préliminaire, l'orientation du matelassage et la forme conique de la ceinture déterminaient l'importance des forces de compression localisées à la base de la ceinture. L'utilisation d'une forme moins conique a engendré des lignes de pression dans la partie inférieure de la ceinture, car les effets de la traction de la ceinture étaient concentrés à cet endroit en raison de la géométrie du SLT.

À l'heure actuelle, l'élaboration d'un modèle sur une ceinture individuelle est limitée par l'incapacité de prédire la répartition des forces de frottement. Les instruments Tekscan^{MC} sont

également limités à cet égard, car ils ne permettent pas d'évaluer directement l'effet des forces de cisaillement sur le torse.

Recommandations

Le sac à dos doit être mis à l'essai avec des charges en conditions réelles afin de déterminer les pressions par rapport à la traction de la ceinture.

Un examen plus approfondi des directions des forces de frottement doit être effectué, car, contrairement à l'hypothèse d'origine, le sac à dos pourrait ne pas se déplacer vers le bas, selon la masse du sac et la traction de la ceinture. Si la traction effective est supérieure à la masse effective de la ceinture, le sac devrait avoir tendance à se déplacer vers le haut en raison de sa forme arrondie, plutôt que vers le bas, attiré par la gravité. L'effet apparent du chargement du sac et l'augmentation de la traction de la ceinture devraient être étudiés plus en détail. Un chargement graduel devrait permettre de mieux comprendre cette relation.

Les forces non équilibrées résultant de la force de compression produite par le serrage de la ceinture doivent faire l'objet d'un examen plus approfondi. Les trois ceintures utilisées dans l'étude comportaient des différences trop importantes pour permettre de déterminer avec certitude la relation entre la conception des ceintures et la répartition des forces et du frottement dans la ceinture. Afin de déterminer les effets du matelassage de la ceinture, il faut identifier les propriétés des matériaux, comme l'élasticité de la mousse, et les propriétés de frottement des matériaux de recouvrement. Des essais effectués avec des ceintures identiques fabriqués avec des matériaux différents, ou avec des ceintures fabriquées différemment, mais avec les mêmes matériaux, faciliteraient la compréhension.

L'effet de différents angles d'inclinaison du torse sur la répartition des forces devrait être étudiée. L'application d'un angle d'inclinaison de 8° vers l'avant orienterait verticalement la région abdominale du mannequin, de manière à mieux simuler celle d'un humain.

La surface du matelassage de chacune des ceintures peut subir de grandes forces de cisaillement en raison de la pression circonférentielle. La modélisation de ces forces et de leur répartition n'est pas facile, car celles-ci peuvent différer grandement lors de l'interaction entre la ceinture et la surface souple du corps humain. Pour évaluer les réactions subjectives des humains à différents matériaux, on pourrait établir des corrélations en réalisant des essais avec des utilisateurs et en leur faisant remplir un questionnaire, afin de déterminer la relation entre les préférences des utilisateurs et l'élasticité du matelassage. Les différents types de ceintures seraient ensuite comparés aux résultats de la corrélation effectuée suite aux essais subjectifs.

L'applicabilité des systèmes de mesure des forces devraient être évaluée pour la quantification des forces de frottement observées sur le SLT.

Le SLT peut servir à différentes fins, notamment comparer les différents matériaux utilisés dans la fabrication des ceintures, améliorer le modèle de ceinture et comparer les nouvelles technologies de fabrication de ceinture. Une épaule simplifiée pourrait être ajoutée au SLT pour permettre le port d'un sac à dos complet. L'installation de capteurs Tekscan^{MC} sur

l’épaule permettrait de prendre des mesures complètes des forces exercées dans la partie supérieure du sac et de résoudre complètement les forces corporelles. En plaçant des transducteurs de restitution des efforts sur les sangles d’épaule, on pourrait établir une relation entre les forces mesurées sur la sangle et les forces mesurées sur l’épaule.

On devrait examiner l’effet de différents points de fixation de la ceinture au sac à dos. Plus précisément, la capacité de transmettre un moment; par conséquent, cet élément devrait être pris en compte. Même si la conception du matelassage n’a pas permis de constater des écarts dans la répartition totale des forces sur les hanches, la réduction de la ligne de pression dans la partie inférieure était apparente avec les ceintures plus coniques. La réalisation d’essais avec une ceinture dont l’angle est réglable permettrait d’examiner cet effet.

Table of Contents

List of Tables and Figures

Glossary of Terms

APLCS – Advanced personal load carriage system.

Bocklite™ – A material that acts as a skin analog. Generally for use in prosthetics, a 3mm thick, skin-coloured material that is resistant to creep as well as providing slight skin compliance.

Load Carriage System – A means of carrying loads on the human body. Designs vary greatly but for the purposes of this study the system will refer to a backpack with shoulder straps and a waist belt for connection to the trunk.

Normal Unit Vector – The surface normal converted to ratios of the vector in order to reflect only the direction and not the magnitude.

Surface Normal Vector – The direction of a vector expressed in three-dimensions that is perpendicular and tangential to a point on a body.

Suspension System – The means by which a pack is connected to the user's body. Generally consists of a waist belt and two shoulder straps held together by a cloth (internal) or metal (external) back frame. It may also have additional connection point such as load-lifter straps and hip stabilizers.

Tekscan Sensor – A flexible Mylar sheet with dimensions approximately 7.6cm x 20cm, with a thickness of 0.4mm. It is connected by a cuff to an A/D board which is read by the Tekscan software. The sensor contains resistive ink that responds to applied force with a change in resistance. This voltage is converted to pressure by knowing the applied force and the area over which it is applied.

Tekscan Sensel – An individual sensing element on a Tekscan Sensor. There are 96 sensels per sensor, each having an individual effective area of 161mm^2.

Tekscan Calibration – Procedure outlined by the manufacturer to calculate a correction factor for the individual sensors. The calibration factor is then applied to the individual sensor prior to data collection.

Tekscan Equilibration – A procedure to ensure equal loading of the Tekscan sensors. A uniform force is applied to each sensel. The software calculates an offset for each sensel and applies it to data acquired.

Waist Belt – Generally a padded strap that encircles the user's waist and connects to the pack bag to transfer some of the load onto the hips.

1.0 Introduction

Personal load carriage is performed on a daily basis throughout the world. Cultural and regional differences impact the methods, from head carriage in African and Asian countries, to pulks and sleds in Scandinavia and other northern climates. The type of loads carried and terrain covered greatly effect methods of load carriage, as does the economic status in the region.

While methods of personal load carriage vary throughout the world, first world countries tend to use the 'backpack' as the conventional method. Early aboriginal load carriage on the back started with tumplines around the forehead to support a box or basket on the back. The tumpline method allows the user to maintain a relatively upright posture although there is significant compression on the spine (Raffan, 1994). The tumpline design gradually evolved with the addition of shoulder straps. These simple packs are still in wide use for canoe travel.

Frameless backpacks developed as a simple sack with two shoulder straps. These packs evolved with the addition of a wooden frame lashed together with canvas, to which the packbag, and anything else, was attached. The true 'external frame' was an improvement as it allowed the load to be carried closer to the body with a contoured aluminum frame. The packbag was held slightly away from the body by canvas or nylon cross-straps to allow for increased ventilation. The shoulder straps were part of a crude suspension system that included the first waist belt. The load was carried higher on these frames and often interfered with head movement. They tended to be less stable over rough terrain as the centre of mass was higher due to the geometry of the pack.

Modern day heavy users of personal load carriage systems are militaries and recreational hikers. Military load carriage is more specialized than conventional recreational requirements. Compartmentalization is important for the soldier, as is complete hands-free use, ease of adjustment for different users and quick jettison of the system in emergency situations. The foot soldier's pack must be extremely versatile for different terrain, climate, and capacity. The pack must meet certain specifications for noise, visibility, and durability. Recreational hikers tend to have less specialized needs. Average hikers choose a pack by personal comfort and volume (Jenkins, 1992). Internal frame packs are most popular with hikers as they tend to reduce awkwardness, improve mobility, and allow the position of the centre of gravity of the pack to be manipulated easily. Internal dividers are common to achieve this versatility. Innovations in commercial and military designs to features such as suspension systems and load distribution are applicable across both applications.

1.1 Anatomy of a Modern Pack

The modern commercial backpack consists of a bag component with numerous pockets and attachment points and a suspension system comprised of shoulder straps, a hip belt and a frame connecting these two components. An internal frame, as seen in Figure 1.1,

is composed of aluminum or composite fiber stays that can be bent to fit the individual user's body. While external frame packs are still manufactured, they are not commonly seen displayed in equipment stores or catalogs.

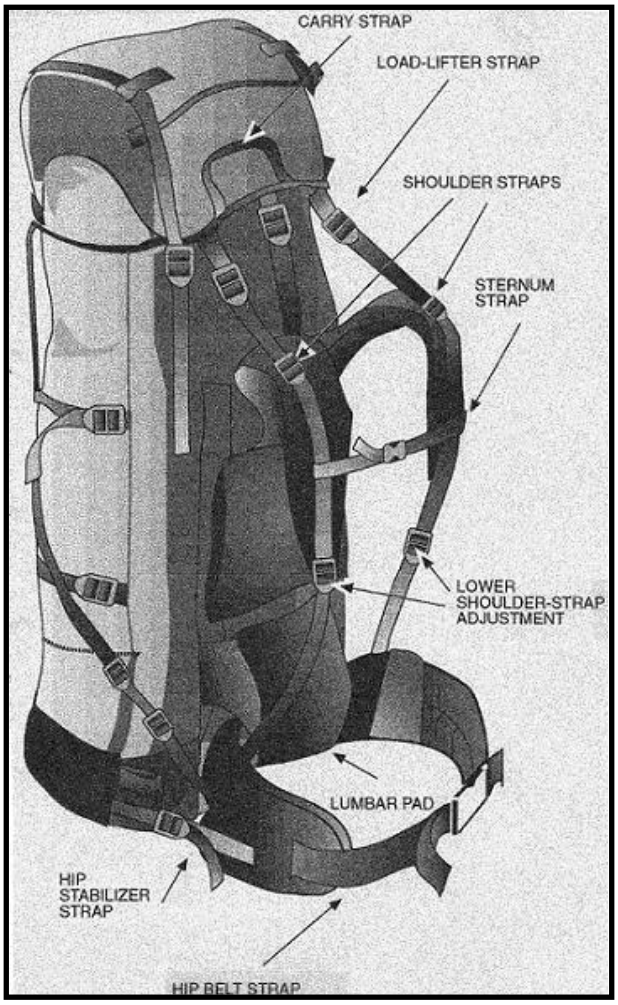

Figure 1.1 Typical Commercial Internal Frame Backpack (Stevenson, 1995)

The main bag or pack section is sewn into one side of the internal frame and additional padding sewn on the other side. The combination of bag, straps, padding and the attachment components of the hip and shoulder straps gives the internal frame both stiffness and the ability to form to the user's shape. The shoulder straps may have additional straps called load lifter straps and generally a small sternum strap between the shoulder straps. Most commonly today, the shoulder straps consist of 50-90mm wide, 10mm thick foam covered with a cordura or similar fabric, and are attached to the pack with nylon webbing. The upper orientation of the straps vary, either single point attachment or separate attachment points. The straps may be contoured or straight, and are often available in men's and women's sizes. The load lifter straps' attachment points are from the shoulder strap at approximately the user's shoulder to the top of the frame stays. Their purpose is to adjust the load's resultant force to different sites on the shoulder and provide greater stability. The sternum strap helps to maintain some lateral stability

and take some load but is needed primarily to prevent the shoulder straps from drifting into the axilla.

1.2 Role and Design of Waist belts

There is great variation in waist belt design between manufacturers. In general, the waist belt is attached to the pack at the lumbar pad area and fastens in the front over the user's abdomen. The material used for padding varies, as does the thickness and shape. Many belts are reinforced with a plastic frame sheet on the outside of the belt. Hip stabilizer straps connect the side of the waist belt with the lower edges of the pack.

The waist belt should carry the majority of the load to prevent fatigue of the upper body (Jenkins, 1992). The load can be transferred between the shoulders and hips to minimize discomfort over long periods. The waist belt is used as a support to inhibit the front-to-back and side-to-side movement of the pack, independent of the user's body. It should rest over the iliac crests of the user to transmit the load onto the hips. With the load on the hips, the weight of the pack is being carried by the relatively large musculature of the legs instead of the smaller muscles of the upper body. The waist belt should be tight enough to minimize slipping and rubbing, while loose enough to not inhibit respiration or cause discomfort or compression of the abdomen. The waist belt can be attached to the pack in many different configurations, from static single-point or multiple-point sewn attachments, to plastic pivots or dynamic attachments. The use of a packframe with a well-padded waist belt reduces loads on the shoulders, reduces incidences of some injuries and results in less perceived pain (Knapik, et al., 1996).

The commercial backpack market is constantly changing waist belt designs and materials and marketing it as the latest 'technology'. These biomechanical effects are not generally quantified with measurable results. Dana Design™ attaches the waist belt behind the frame for 'positive load transfer, not sag' and their belts have 'contour molded' foam (Dana Design, www.danadesign.com). The North Face™ offers 'dual-density' foam padding of their waist belts as well as separate men's and women's designs (www.thenorthface.com). Serratus™ offers 'thermo-molded' foam, men's and women's styles and special sewing techniques that eliminate wrinkling of the belt covering material (Serratus, www.serratus.com). Mountainsmith™ has designed an auto-centering waist belt buckle (www.mountainsmith.com). Lowe Alpine™ uses two-position belt tensioners and has a bi-laminate construction (www.lowealpine.com). Arc'Teryx™ uses four layer, thermo-molded foam construction, an articulating or floating attachment point, an adjustable waist belt angle, and lateral load transfer rods (Arc'Teryx, www.arcteryx.com). Although each of these companies markets their products based on design features, there are no scientific data available to support the design shape or materials used.

Only two studies were found that examined the lumbar reaction forces at the level of the L3-l4 vertebrae. Reid (1999) examined the effects of lateral rods in a commercial design by measuring the forces and moments at the level of L3-L4 vertebra. The addition of the

lateral rods reduced the vertical load applied to the shoulders by 10% without increasing the shear load on the lumbar spine. This experiment was performed under static conditions. In another study, Reid et al (1998) examined the effects of various locations of attachment points for the lower shoulder strap. Based on comparing the shoulder and lumbar reaction forces across 12 different attachment points, a location was identified that optimized the shoulder and lumbar reaction forces.

As can be seen from the lack of scientific evidence, design in the area of backpacks lacks vigor. Most of the design features have evolved historically or have been developed through experience. Only recently has instrumentation been developed to undertake a more scientific approach to pack design, specifically the waist belt.

1.3 Introduction to Backpack Modeling

Two ways to determine the reaction forces on the shoulders and lumbar pad during load carriage are by direct measurement of forces or pressures on these areas and by modeling these forces through a biomechanical model of the backpack. If a biomechanical model is being developed, it must be evaluated though comparison to an independent measure, such as a direct measure. This concept is easy to understand but often difficult to perform. It is problematic to validate a biomechanical model of a backpack, as there are concerns with finding a reliable direct measurement device and concerns with the complexity of the biomechanical model.

If an accurate biomechanical model of a backpack can be developed and validated, then there are several important uses for such a model. Firstly, the model can be very helpful for the design and comparison of novel concepts and materials. Secondly, the model can be used to understand the importance of change in load location and load mass. Each of these factors may have implications on the amount of shoulder and lumbar reaction force needed to carry a backpack. Finally, a biomechanical model can be used to recommend tissue tolerance limits based on subjective discomfort scores. Although direct measures can also be used to interpret subjective discomfort, it is often more convenient and cost effective to make these interpretations with a biomechanical model.

To develop a valid biomechanical model for a backpack, it is reasonable to separate the components and develop a model for shoulder straps separately from the waist belt. MacNeil (1996) developed and validated a shoulder strap biomechanical model where no waist belt was considered. Pelot (1998) developed and improved a model that included a waist belt with moderate success. However, when Rigby (1999) attempted to add additional features such as load lifter straps and hip stabilizer straps, the model failed to predict shoulder and waist belt forces. Some of the concerns that Rigby (1999) identified were that the strap force sensors did not truly reflect the waist belt's responses, that friction might play a larger role than he anticipated and that the waist belt connection point to the suspension system should not be modeled as a pin joint nor should the anterior-posterior force by the waist belt be considered zero.

Based on Rigby's recommendations, the primary objectives of this thesis were to develop a valid waist belt model for a backpack and to determine the factors affecting force distribution on a load carriage system waist belt. To accomplish these objectives, several specific objectives were also identified:

1. Determination of the frictional components of the waist belt.
2. Development of a novel calibration procedure for contact pressure sensors in this application.
3. Determination of the effects of the direction of strap tightening on measured pressures on the body.
4. Determination of the relationship of the strap force tension in the waist belt to the measured pressures on the body.

2.0 Applications of Modeling and Pressure Measurements to Load Carriage Research

While many different load carriage systems have been designed and used for both military and civilian purposes, objective measurements for evaluation of designs is a relatively new area of research. Weight limits for load carriage have been recommended based on various measures: heart rate scores, blood pressure (Sagiv, 1994), perceived exertion (Goslin, 1986), and VO_2 maximal tests (Epstein et al., 1988). While the largest area of research is simply the amount of load carried, load placement has been examined by comparing physiological measures (Legg et al., 1992) and loss of performance with load position (Holewijn and Lotens, 1992). Inverse dynamic biomechanical modeling to determine joint forces with varying loads has been used (Goh, 1998).

Subjective measures have been observed with the use of questionnaires (Jenkins, 1992). The primary measures have been subjective and relating to performance, such as obtaining feedback from user groups (e.g. expert trekkers and military personnel). As individual opinion varies greatly, subjective measures do not provide clearly defined advantages and disadvantages between designs. No studies have examined psycho-social factors that may contribute to an individual's perception of pack comfort and design properties, such as: physical anthropometry of the individual, pack colour and appearance, preconceived opinions of a pack design based upon the manufacturer's reputation, peer pressure, or mood during testing.

It is especially difficult to determine optimal design features through subjective opinions alone. One solution to design problems is to construct a means of objectively testing packs that minimize human variability when analyzing design features for load carriage. In this way, the comparison of features can be quantified objectively under controlled conditions.

The approach has been to compare a number of packs and subjects' opinions of load control and load transfer features with specific measured outputs from standardized measurement tools (Stevenson, 1996). By correlating subjects' opinions with objective measurements, it was possible to validate the objective measures.

One main tool has been a Load Carriage (LC) Simulator that is pneumatically operated by computer controls and programmed to simulate gait cadence at various speeds (Stevenson, 1995). The mannequin of the LC Simulator is used to determine the forces, moments, pressures and relative motion of the body because of the pack design, load and method of wearing the pack. Secondly, a pack compliance testing mannequin is capable of bending at the level of the third and fourth lumbar vertebrae (L3/L4) about the principal axis of rotation for torsion, lateral bending or forward bending. For this device force-displacement profiles show the resistance to motion of the pack suspension system. Finally, a load distribution mannequin has force and moment measurement capabilities both at L3 and at the base of the mannequin. This device allows researchers to partition the upper and lower body reaction forces that support a backpack.

The models used for basic measurement and evaluation for load carriage tools are anthropometrically sized and weighted commercial mannequins that are covered with Bocklite™, a skin-analog. The sizes of mannequins available for research are 5th and 50th percentile women and 50th and 95th percentile men (Reid, et al., 1997). While these systems evaluate overall response of the load carriage system to torso motion, they do not specifically measure characteristics of waist belt design.

If a valid and reliable approach could be developed, then a means of comparing different waist belt designs and materials, independent of the rest of the pack features, could be developed. However, the difficulty comes in validating a waist belt model with a surface contact pressure measurement system. These systems generally consist of thin, mylar, resistive ink technology sensors attached to the surface. The Tekscan™ system has proven to be non-linear on curved surfaces (Bryant, et al 1999). Hence, a revised lower torso that is mathematically simpler than a human torso must be developed first, in order to validate a waist belt model with Tekscan™ F-Scan sensors. The most appropriate device to use is the load distribution mannequin as it has been used for biomechanical modeling (MacNeil (1996), Pelot (1998), Rigby (1999)). Its current design is configured with a 50th percentile male torso where it is expected that entire packs would be assessed as a unit. Using the lower torso only, the relationship between the forces acting on the body and the measured tension in the waist belt can be examined.

2.1 Models of Load Carriage Systems

A number of load carriage system models have been developed through the efforts of DRDC Toronto (formerly DCIEM) in the design of the 2004 issue Clothe the Soldier Load Carriage System (Stevenson, 1995). In addition to hardware tools, the Ergonomics Research Group at Queen's University has created three biomechanical load carriage models. The first model consisted simply of a shoulder model with two shoulder straps and no waist belt. As shown in Figure 2.1, MacNeil (1996) determined the forces in the T_1 and T_2 straps by knowing the mass in the pack, the lean angle of the pack based on the wearer's standing posture and specific pack geometry such as shoulder strap angles, distances to straps and location of the centre of gravity. The T_1 and T_2 strap tensions and strap angles in relation to the pack (θ_1 and θ_2) were determined based on the three equations for the sum of X forces, Y forces, and moments in the system. From these equations, T_1, T_2, and the lumbar reaction force (F_x) could be determined. The T_1 and T_2 tensions along with their strap angles from the horizontal (ω_1 and ω_2) were examined in relation to the shoulder so that the shoulder reaction force (S^N) could be determined.

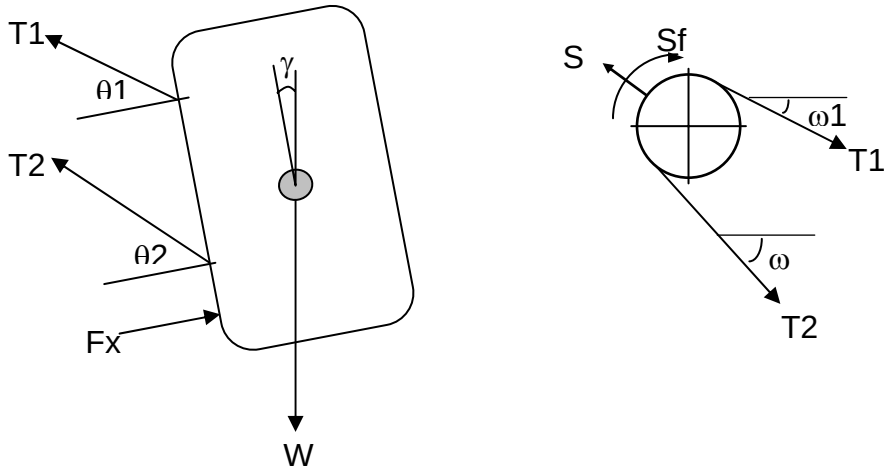

Figure 2.1 Shoulder Model for a Backpack.

T_1=Upper shoulder strap, T_2=Lower shoulder strap, υ_1=Upper strap angle in relation to the pack, υ_2=Lower strap angle in relation to the pack, F_x=Lumbar reaction force, W=Weight of the pack, γ=Lean angle of the pack, S^N=Shoulder reaction force, S_f=Frictional force on the shoulder, ϖ_1=Upper shoulder strap angle from the horizontal, ϖ_2=Lower shoulder strap angle from the horizontal.

MacNeil (1996) determined a frictional force, S_f, using a coefficient of static friction measured with an inclined plane. The differences between T_1 and T_2 were considered to be due to the effects of this frictional force.

This model was successful (r^2=0.95) in estimating the reaction force on the shoulder but was rather simple with the exclusion of the waist belt. Despite this limitation it was quite successful at predicting subjects' opinions based on backpack design data. However, for most modern commercial and military load carriage systems that employ a waist belt, this model was limited primarily to daypacks or children's backpacks.

The second model that was created by Rigby (1997) and Pelot (1998) expanded the MacNeil model to include a waist belt. This model kept the same features for modeling the shoulder reaction force but incorporated a waist belt that was treated as a pin joint with no horizontal transmission of force to the waist belt. The waist belt itself was treated as a hoop and modeled as a thin-walled cylinder with hoop stress. No contact or friction was assumed to be present on the back.

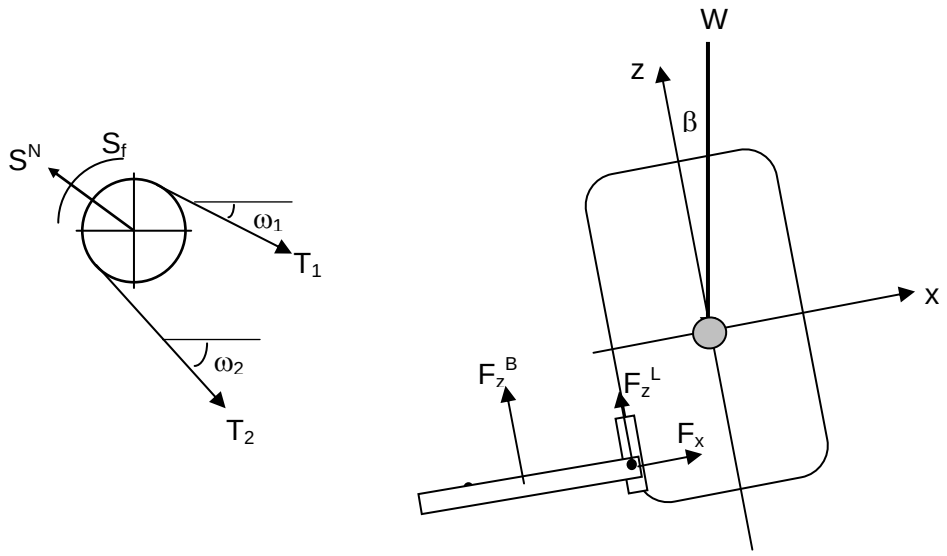

Figure 2.2 Waist belt Model with Lumbar Forces

Where:
X = coordinate along pack depth
Z = coordinate along pack height
W = the force of the mass of the pack
β = body lean angle
T_1 = tension in upper shoulder strap
T_2 = tension in lower shoulder strap
F_X = reaction force of lower back on pack in the X-direction
F_z^B = lift provided by the waist belt resting on the hips
F_z^L = lift on the pack from friction and angle at lower back

This second model was tested by Pelot and Rigby (1998) using seven different backpacks on the load distribution mannequin. Both the shoulder and lumbar reaction forces averaged within 5% error, however features such as load lifter straps were not included.

The third model developed by Rigby (1999) involved the addition of load lifter straps that increased its complexity but reduced its effectiveness. Load lifter straps were modeled in such a way that the shoulder strap force was split into sub-components. The waist belt attachment to the framesheet was modeled as a pin joint. As well, there was assumed to be no net horizontal force transmitted from the waist belt to the body. There was a horizontal force component acting on the lumbar area from the mass of the pack.

Rigby (1997) identified other features that could also have affected the accuracy of the model. The division of the load between the shoulders and waist and the effect of friction was assumed and simplified. For example, the force of friction was considered to be dependent on the percentage of load carried on shoulders and the waist. When the entire load was carried on the shoulders there was no force of friction about the waist to prevent the pack from sliding down. When there was any weight transferred to the waist through the belt, its value depended on both the weight downward and the tension of the waist

belt itself. Another feature of the Rigby model was that the forces acting at the waist belt and lumbar area were not isolated, but were measured as a single value, neither the directional vectors of this force, or the actual values of these forces were determined.

2.2 Waist belt Models

The isolated waist belt was modeled previously using the theory of hoop stress in a thin-walled pressure vessel (Hibbeler, 1993). As shown in Figure 2.3, the internal pressure, P is related to the stress in the wall by:

$$\sigma_H = \frac{P \times r_H}{t}$$

Where σ, P, r_H, and t represented the tension in the waist belt, internal pressure, average radius of the waist belt at the hips, and thickness of the belt, respectively. The tension in the belt was assumed to be constant, such that $T = \sigma_H tw$, where w is the belt width.

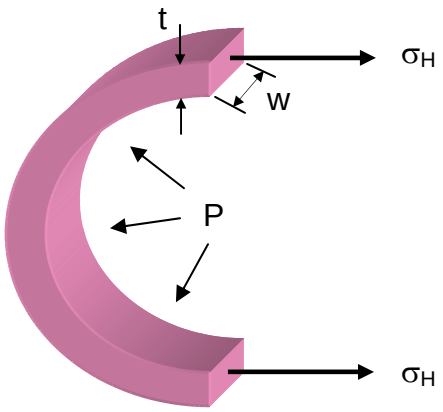

Figure 2.3 Hoop stress in the waist belt

Since hoop stresses equilibrate internally, $\sum F_x = \sum F_y = 0$ as shown in Figure 2.4. Forces in the vertical direction on the body by the unloaded waist belt were equal and opposite to the force of gravity acting on the waist belt.

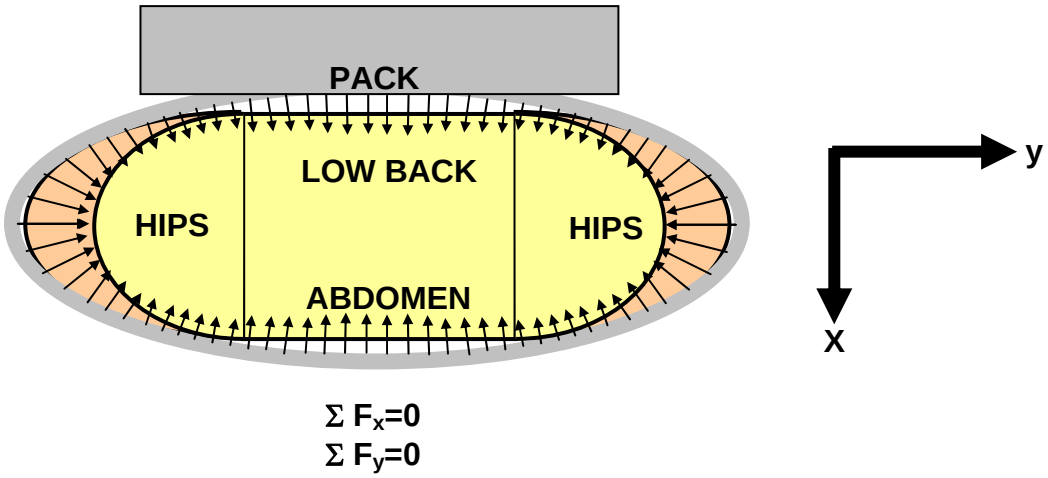

Figure 2.4 Assumed pressure distribution on the torso from the belt in the x-y plane.

Several simplified assumptions of the waist belt were common to the Pelot (1998) and Rigby (1999) models. The waist belt tension was considered constant and the belt attachment to the pack was modeled as a pin joint, and therefore did not exert a moment on the back. Also, there was no compressive force on the back or abdomen by the belt, merely tension (T_3) in the waist belt (Figure 2.5).

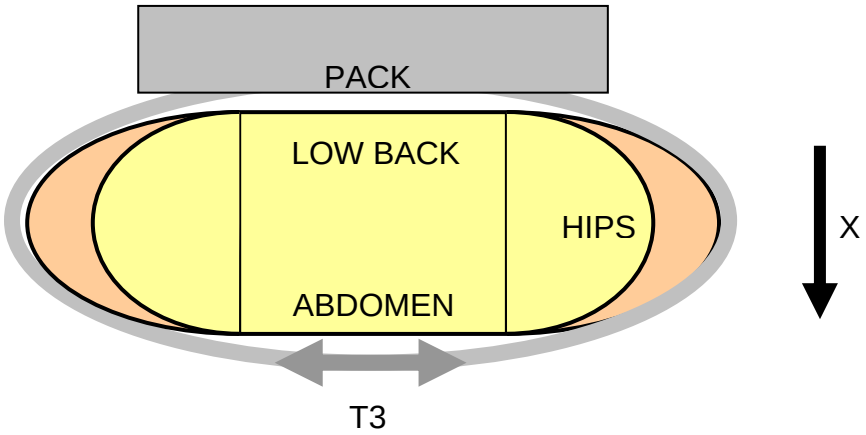

Figure 2.5 Tension in the Waist belt

One major limitation of the models was the determination and assumption of independent forces in the Z-direction by the lumbar pad (F_z^L) and the waist belt (F_z^B) as in Figure 2.2.

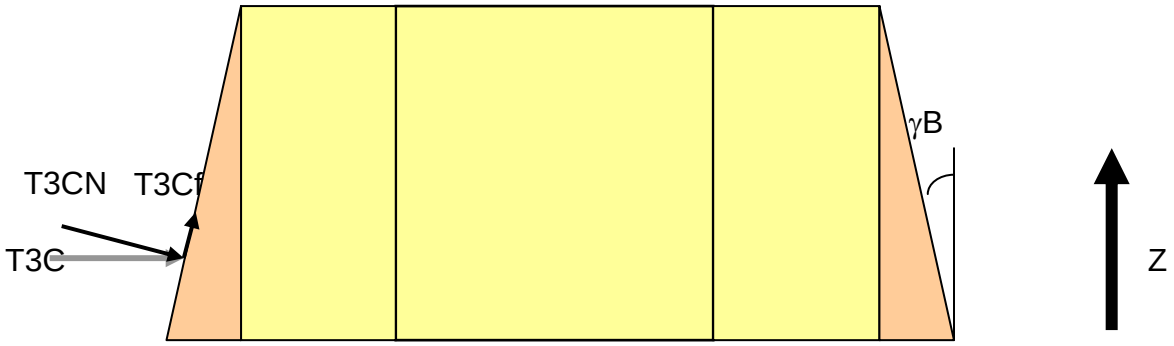

Figure 2.6 Compressive Forces on the Hips

Where:
T_{3C} = compressive force that T_3 apples around the hips
T_{3C}^{N} = normal force component of T_{3C}
T_{3Cf} = force of friction
γ_B = anatomical hip angle from vertical

The waist belt applied a compressive force about the hips. This compressive force acted in the horizontal direction and was resolved into a normal force to the surface, T_{3C}^{N}, and a frictional force acting along the surface, T_{3C}^{f} as shown in Figure 2.6. As well, it was assumed that the low back angle created a vertical lift force as well as a force due to friction. The elements of the compressive force could not be individually determined from the model as the normal unit vector direction of the point of force application was unknown.

2.3 Experimental Methods for Waist belt Contact Mechanics

The complexity of the irregular curvatures of the mannequins used in the previous studies made the directions of the measured forces difficult to calculate. Without the directional information, the forces could not be resolved. In addition, the contact pressures on the body by the waist belt have not been measured in conjunction with the strap force tension and a comparison of these measurements has not been possible. These problems could be addressed by constructing a quantitative measurement tool, a symmetrical lower torso, where there is a simple model to determine individual resultant forces. Contact pressures could be measured in conjunction with strap force tensions to determine their relationship. A symmetrical lower torso would allow for the applied forces to be easily resolved using the known geometry at the point of application of pressures. The current torso models have geometrically complex surface contours that make the resolution of vectors difficult. In order to do this, it was necessary to measure surface contact pressure.

2.4 Contact Pressure Measurement

Various methods of surface pressure measurement are available commercially. The two most common systems are the Tekscan™ F-scan system and Novel™ Electronics PEDAR system. Rash, et al (1997) compared the two systems and found no significant difference in the systems' abilities to measure uniform average pressure, although more sensor-to-sensor variation was found in the Tekscan™ system. The size and relatively low cost of the Tekscan™ sensors, as well as their reported favorable comparison to the PEDAR system facilitated their use. Therefore, the surface pressure measurement tools used for research on load carriage in the Biomechanics laboratory at Queen's University were the Tekscan™ F-Scan sensors, Figure 2.7.

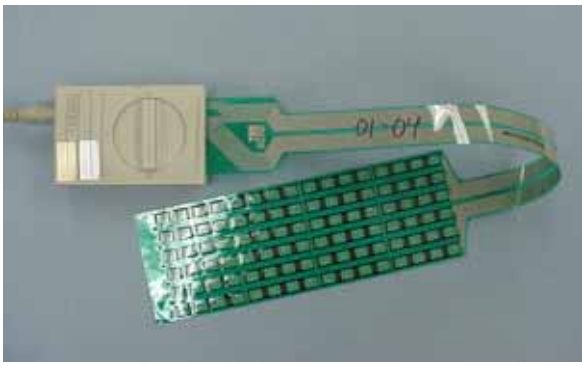

Figure 2.7 Tekscan Sensor and Cuff

Each sensor consists of a flexible Mylar sheet with dimensions approximately 7.6cm x 20cm, with a thickness of 0.4mm. The sensor contains resistive ink that responds to applied force with a change in resistance. They are connected by a cuff and cable to an A/D board in the computer that is read by the Tekscan™ software. This voltage is converted to pressure by an algorithm, stated by the manufacturer, using the effective area of the individual sensel and the voltage converted to a force with a regression line calculated during calibration. These sensors are affixed to the surface of the mannequins, a difficult task since they have a tendency to wrinkle over various protruding landmarks. Symmetrical placement of these sensors over a region of the mannequin's anatomy is also difficult due to the slight dissimilarities and curvatures of the body surfaces. The normal directions of points on the surface are generally unknown and therefore the measured forces are difficult to resolve.

This resistive ink technology has achieved varying success. These sensors have been shown to have an average calibration error of 4%, creep of 19%, and hysteresis of 12% (Woodburn and Helliwell, 1997). As well, the measurements between sensors have significant variability and the calibration protocol determined by the manufacturer is inaccurate (Woodburn and Helliwell, 1997). Average pressure results on flat surfaces have an accuracy of 4% and precision of 9.6%, while peak pressure measurements have both an accuracy and precision of 14% (Bryant, et al., 1999).

In addition to the surface compliance effects and time dependency, various additional factors affecting sensor accuracy have been determined. For example, a temperature range from 24° to 37°C resulted in a 50% increase in sensor output (Luo, 1998). For the current study however, the temperature for calibration and experimentation was held a constant at 21ºC.

When the sensors were used on a curved surface, there was inherent change of the surface geometry with the nature of the contact surfaces. This resulted in an increased gain for radii of curvature greater than 50mm (MacNeil, 1996). This response had also been shown by Buis and Convery (1997) to attenuate with a radius of curvature of less than 50mm. The sensitivity has been shown to decrease with the addition of pliable material (Sumiya, 1998) yet is not suitable for use on hard surfaces such as plexiglas (Luo, 1998). An additional limitation with the Tekscan™ system is that the F-Scan™ sensors are not calibrated for use on curved surfaces. Equilibration is possible, but difficult and inconsistent on the surface of the mannequins. The manufacturer makes no claims to their accuracy or precision when used on curved surfaces. Bryant, *et al* (1999) attempted to overcome some of these concerns by constructing a hand-held pressure calibrator that would apply a constant force regardless of the surface shape.

As a result of calibration difficulties, Tekscan™ sensors have been used in a limited manner only. They have proven to be a useful comparison tool for peak pressure areas and the relative magnitude, but not the actual values of the forces (Stevenson, et al., 1996). Developing a calibration method to cope with rounded surfaces on human mannequins to enhance the Tekscan™ F-Scan accuracy form one of the objectives of this study. Pelot and Rigby (1998) endeavored to use pressure sensors in his biomechanical model to measure body forces, however, he confined his analysis to peak pressure points and a comparison of peak pressures between packs. Although he also measured strap tensions in the waist belt and lower shoulder strap, he did not correlate these two measures.

To develop a scientific approach to waist belt design, it is important to understand how they work. Stevenson *et al*. (1995) have used a waist belt strap sensor in all of their research on the LC Simulator and LC Compliance tester to standardize the tension for all pack testing. However, the impact of this standard tension due to different waist belt designs is unknown. Neither Pelot (1998) nor Rigby (1999) used the waist belt strap tension gauge in their hoop stress modeling of waist belt design. Rigby (1999) was particularly sensitive to the need to examine the waist belt by itself as his model could not resolve the lumbar forces.

A lower torso model with a method of measuring applied forces and resolving those forces into their respective resultants in the X, Y, Z directions is necessary to further the biomechanical model as shown in Figure 2.8, the current models use the sum of the measurements from the sensor to determine the average force acting on the area as well as peak pressure locations on the body. The lack of directional information for the measured forces limits the ability to resolve the measured force vectors. This is necessary

to gain an understanding of the applied pressures at the waist and to determine the effects at the lumbar area independent of the rest of the system.

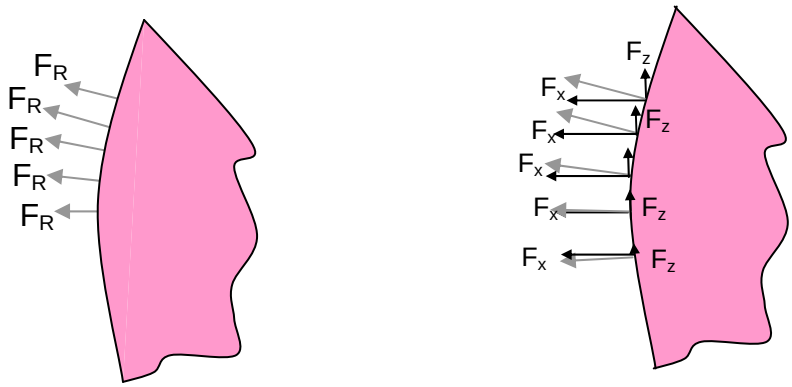

a) Current System

Known: ΣF_R

b) Proposed System

Known: ΣF_R, ΣF_x, ΣF_y, ΣF_z

Figure 2.8 Reaction Forces on the Body Under the a) Current System and b) Proposed System.

F_x and F_z cannot be determined from the current system as the coordinate of the point of pressure measurement and the normal direction of the applied force is not known. With the proposed system, the measured force can be resolved into directional components as the direction of the normal force is known.

A direct comparison of pressure and force distribution of different belt designs and materials has not been performed, nor has the relationship between belt tension and the force distribution been examined. The ability to quantify the differences between designs and measure the effects of proposed changes would be of great importance to backpack manufacturers.

3.0 Methodology

3.1 Design of the Symmetrical Lower Torso

The Symmetrical Lower Torso Model (SLT) was designed to provide a simple method of determining the surface normals of applied forces. The previous torsos were commercial mannequins with non-symmetrical curves and irregular bony landmarks. As well, it was difficult to place the Tekscan^{TM} sensors on the surface of the previous models without creating bubbles and wrinkles (Bryant, et al., 1999).

A simple cylinder was considered for the torso model similar to the simplified shoulder representation of MacNeil (1996). However, due to the vertical orientation of the torso compared to the horizontal orientation of the shoulder, a conical model was considered more representative of the human body. It was hypothesized that there would be lower tensions in the waist belt than on the shoulder and that friction would play a greater part to prevent slippage of the belt.

The waist size of the SLT corresponded with the waist dimensions of the 50th percentile male upper torso. The waist-to-hip ratio was determined as the average of the 5th and 50th percentile female and 50th and 95th percentile male mannequins currently in use. A waist-to-hip ratio of 0.85 was chosen, as it was also consistent with ratios for healthy males or females as reported by McArdle (1996). The SLT was designed to fit on the base platform of the load distribution mannequin and had a similar appearance to the previous model. The distance from waist-to-hip was measured from the existing load carriage mannequins as well as from 10 human subjects (5M, 5F) of average fitness level, with mean age 29 years +/-11yrs. The distance from the narrowest part of the waist to the height of the largest circumference about the buttocks was measured. As a result the SLT was designed to be unisex.

The height of the SLT was 318mm and corresponded to the previous model (Appendix A). The centre rectangular section was added to signify the relative flatness of the lower back and abdomen. The SLT had symmetrical quadrants, consisting of a hip-shaped cone with an 8° angle that was vertically split into two halves and glued to the sides of the three-dimensional trapezoid of the back and abdomen (Figure 3.1).

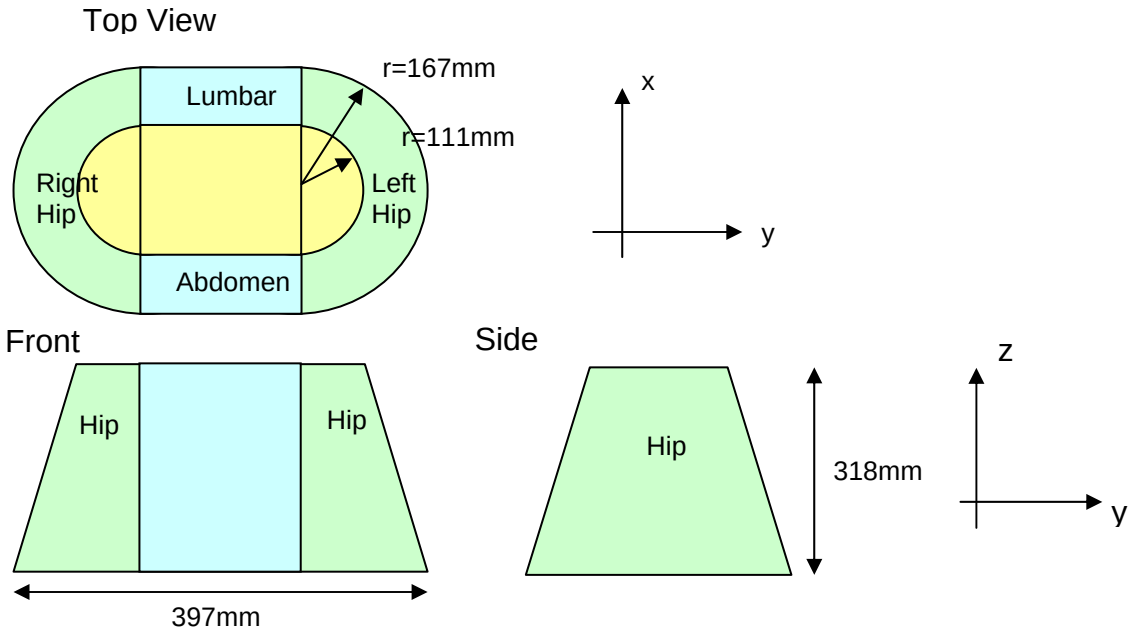

Figure 3.1 Symmetrical Lower Torso - Physical Model in three views

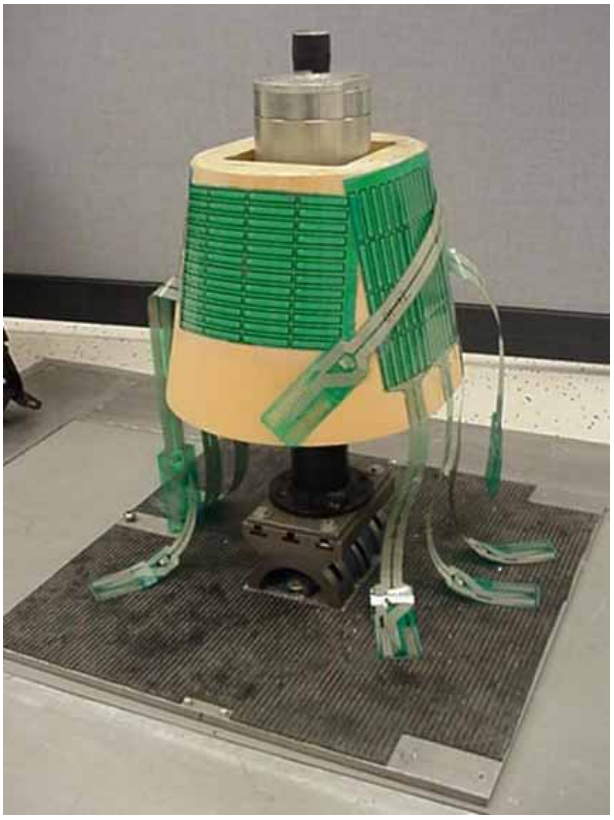

Figure 3.2 Symmetrical Lower Torso – View of SLT on in-floor force plate with Tekscan™ Sensors.

The SLT was constructed with laminated basswood that was machined on a CNC lathe with further sanding and finishing performed by hand to remove any irregularities. The finished wood was covered with 3mm Bocklite™, a skin analog that provided slight surface compliance (Rigby and MacNeil, 1996).

A steel pipe, outer diameter 47.8mm, was inserted into the bottom of the SLT and fit into an attachment on the base plate. The attachment mechanism allowed for alteration of the lean angle of the torso. The base plate was designed to fit on top of the AMTI Force Plate, Model LG6-4-2000, with the centre axis of the SLT passing through the centre of the plate.

Tekscan™ 9811 F-Scan sensors were affixed to the torso in a pattern that provided the easiest repeatability and most accurate symmetry of coverage of the waist region. To accomplish this goal, some of the sensors were placed longitudinally and some transversely as shown in Figure 3.3.

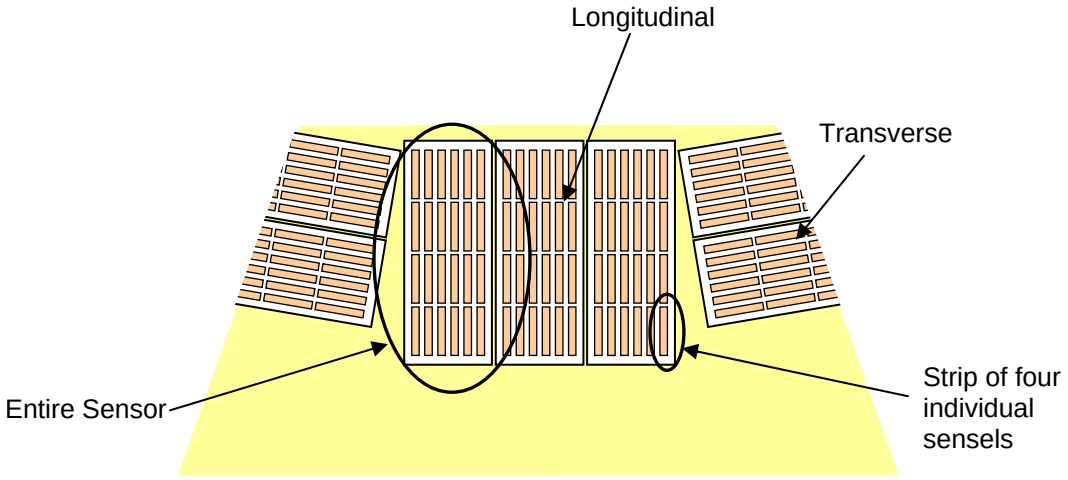

Figure 3.3 Sensor Placement on the SLT

Three waist belts were placed on the SLT with the mid-line of each belt in the same place. The edges of each belt were marked and the sensors were laid out in a pattern that was a minimum of approximately 1.5 times the width of the widest belt. Complete coverage was not possible due to the rectangular shape of the sensors. Although the sensor design allowed them to be cut lengthwise to separate the columns of sensels, this approach limited the ease and accuracy of replacing sensors into the same positions. As well, interpolation when determining the sensel locations would not have been possible and the assumed mirror images would have been less exact. The hip, lumbar, and abdominal areas had complete coverage while small sections of the transitional areas between the flat and curved were left uncovered. To compensate for minor lack of coverage, sensors were positioned in the same locations in each quadrant. These transitional areas were regions of the least precision for calculations as slight imperfections in machining and finishing were most apparent in these sections. The area of these regions was 2% of the total coverage of sensors. Therefore the error in

measurement of these sections can be approximated as 2% lower than the actual measurement. Once the precise locations were determined, the Tekscan™ sensors were fixed into position with 3M™ 810D tape.

3.2 The Development of the Mathematical Model

A point of interest on the SLT was defined as the centre of a sensel. Since there were ten sensors with 96 sensels each, there was a total of 960 points. Prior to experimentation, the coordinates of each point of interest on the surface were determined and the unit vector normal to the surface was calculated. During experimentation, the pressures measured by the Tekscan™ Sensors were converted to forces at each sensel and these forces were resolved into x, y, and z components using the normal unit vectors.

3.2.1 Determination of SLT Coordinates

The main origin (0,0,0) for the coordinate system was the geometric centre of the base of the SLT as seen in Figure 3.4. Two additional coordinate systems were used for the hip sections, one for each side. This allowed calculations to be performed on the hip sections purely as a function of the radius and angle in the x-y plane.

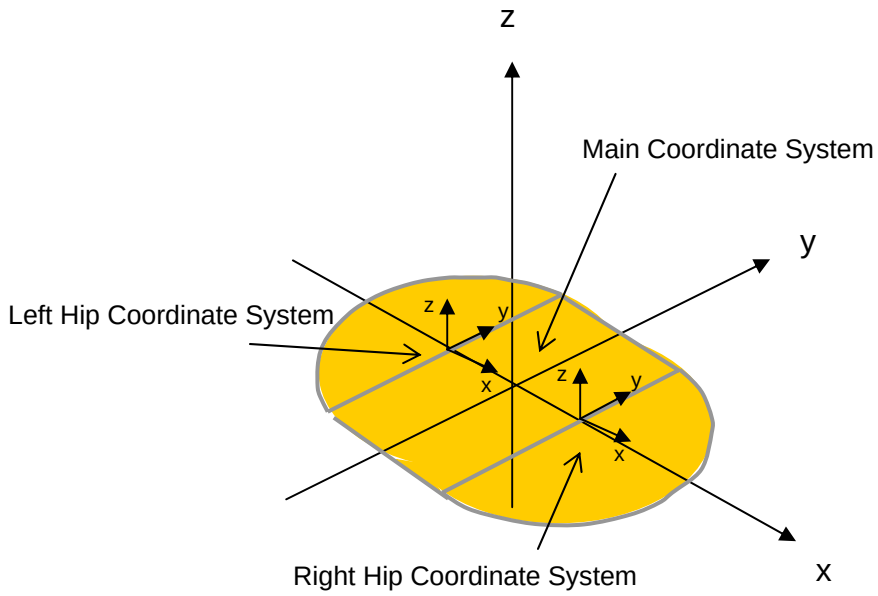

Figure 3.4 Coordinate Systems on Base of SLT

Each point on the surface of the curved hip sections of the SLT had a single set of three-dimensional coordinates and a normal vector common to all points on a tangential plane from the base of the model to the mathematical apex of the conical section. This plane contained the triangle ABC as shown in Figure 3.8.

A point was defined on the circumference of the hip according to the polar coordinates z, θ, where z is the height above the base plane and θ is the angle from the y-axis. θ was measured on the top of the SLT with a protractor for each point. The distance from the base of the SLT on the surface of the cone was measured. Using the right-angle triangle rule, the distance in the vertical z-direction was calculated. This z-value allowed for the calculation of the radius of the cone at the point of interest. This radius was resolved using the right-angle triangle rule, resulting in the coordinates of the point of interest (x_0, y_0).

For the right hip, the base plane is shown in Figure 3.5. The equation of the tangent to the circle at the given point is given in point-slope form:

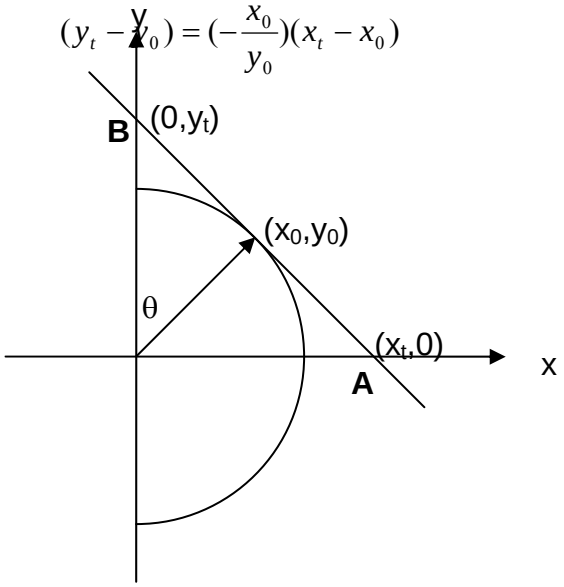

Figure 3.5 Tangent to the Circle

For the x intercept of the tangent:

$$y_t = 0$$

$$(0 - y_0) = (-\frac{x_0}{y_0})(x_t - x_0)$$

$$x_t = (-y_0)(-\frac{y_0}{x_0}) + x_0$$

For the y intercept of the tangent:

$$x_t = 0$$

$$(y_t - y_0) = (-\frac{x_0}{y_0})(0 - x_0)$$

$$y_t = y_0 + (-\frac{x_0}{y_0})(-x_0)$$

The z-intercept of the plane, C, was calculated through extrapolation of the height of the cone, as shown in Figure 3.6:

$$z_0 = r \tan \alpha$$

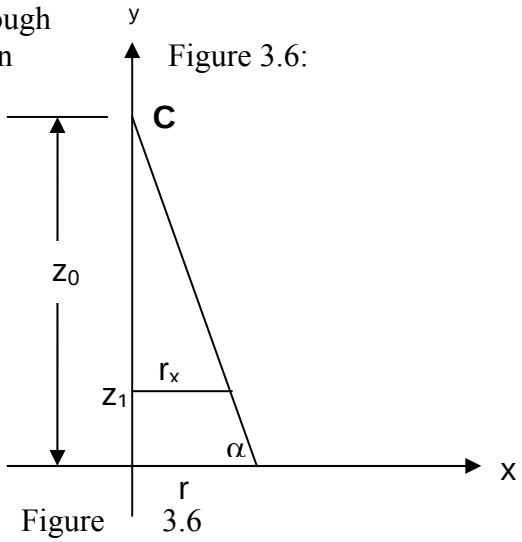

Figure 3.6

Using the three intercepts, (A, B, C), the normal to the plane that they created was calculated as shown in Figure 3.7. This plane provided the normal vector (ñ) for every point on the plane containing A, B, C.

$$A = (x_t, 0, 0)$$
$$B = (0, y_t, 0)$$
$$C = (0, 0, z)$$

$$\vec{u} = B - A$$
$$\vec{v} = C - A$$

$$\vec{n} = \vec{u} \times \vec{v}$$

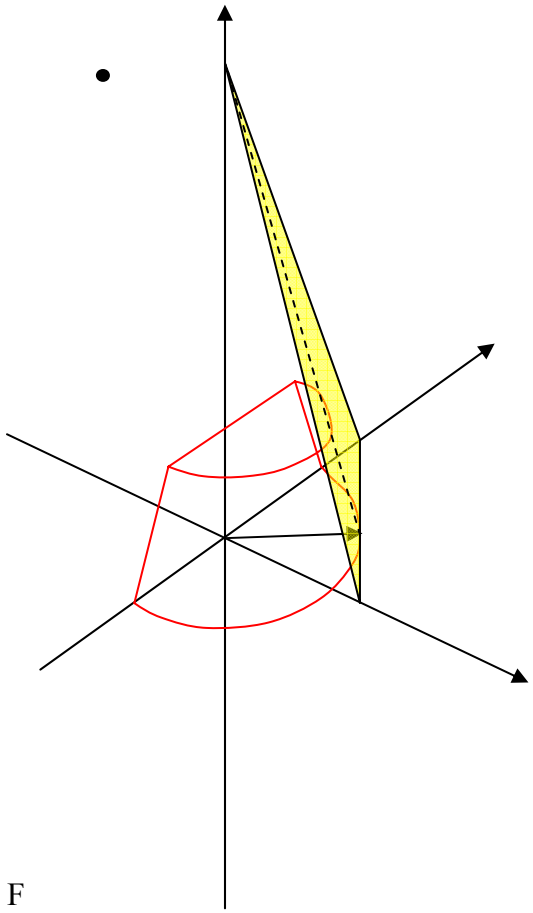

Figure 3.7 Normal Plane to a line of points on the surface of the SLT.

These normal unit vectors were calculated for each angle from the y-axis in 0.5° increments. These vectors were imported into the EXCEL™ spreadsheets for each sensor calculation template. Simple calculations for this method are shown in Appendix B.

The directions of the forces on the centre abdominal and lumbar sections were more simply calculated, as the normal vectors were the same for all of the points on the plane, as shown in Figure 3.8. The equations of the planes were calculated, as in the above section, using three known points: the z intercept, and the two bottom corners of the non-curved section.

For the radius at $z=z_1$

$$\alpha = 82^o$$
$$z_0 = 1143.4mm$$
$$z_1 = measured$$
$$r = \frac{z_0 - z_1}{\tan \alpha}$$

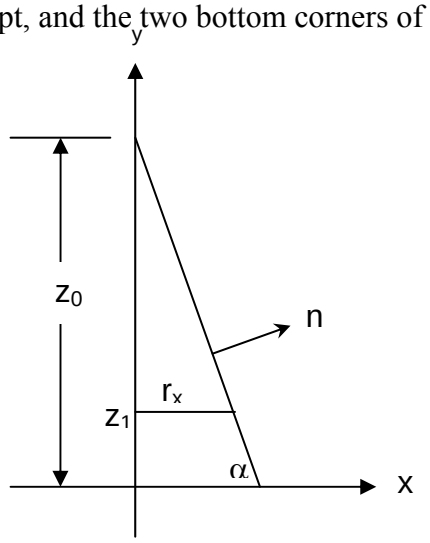

Figure 3.8 Normal Plane - Lumbar and Abdomen

3.2.2 Estimation of the Coefficient of Friction

MacNeil (1996) and Rigby (1999) believed that the static coefficient of friction was major source of error when resolving measured pressures since Tekscan™ sensors did not measure shear forces directly. One method to account for this is to use an estimated coefficient of friction. MacNeil (1996) estimated the frictional coefficient to be 0.116 by differences in strap tension tests whereas Rigby (1999) used 0.35 measured on an inclined plane for his waist belt model. Because friction was such an important force, especially in the waist belt, a strategy was needed to determine the frictional coefficient.

An inclined plane experiment was performed using the materials and conditions of the actual model. A static coefficient of friction (μ) was calculated using an inclined plane, protractor and 605 g block of wood. The inclined plane was covered with Bocklite™ and the Tekscan™ sensor. The plane was tilted and the angle at which the block started to slide was recorded. The average of 10 trials was taken, with μ ranging from 0.35 to 0.41, and an average value of μ=0.38. A frictional force (f_f) was then estimated as $f_f = \mu \times F_N$.

The directional unit vectors of the frictional force on the curved surfaces were calculated using the equation of the line connecting the point of application of the normal force with

the z-coordinate of the theoretical top of the cone. This assumed that any impending motion is in the longitudinal direction. As such,

$$f_{N\,dir} = (x, y, z) - (0,0, z_o)$$
$$f_{N\,dir} = (x, y, (z - z_0))$$

In dimensionless form:
Where:

$$f_N = (i, j, k)$$

$$j = \frac{y}{\sqrt{x^2 + y^2 + (z - z_0)^2}}$$

$$k = \frac{(z - z_0)}{\sqrt{x^2 + y^2 + (z - z_0)^2}}$$

Each of these unit vectors was multiplied to the frictional force to generate the friction component in the x, y, and z directions respectively.

The normal vectors on the non-curved surfaces of the abdomen and back were the same for the entire plane. The vectors were calculated using the z coordinate of the theoretical top of the cone and the centre of the base of the plane, the y coordinate of the plane (Figure 3.7). The frictional force was given by:

$$f_{N\,dir} = (0, y, 0) - (0,0, z_o)$$
$$f_{N\,dir} = (0, y, (-z_0))$$
$$f_N = (i, j, k)$$
$$j = \frac{y}{\sqrt{y^2 + (-z_0)^2}}$$

In dimensionless form:

$$k = \frac{-z_0}{\sqrt{y^2 + (-z_0)^2}}$$

Where:

$$i = \frac{x}{\sqrt{x^2 + y^2 + (z - z_0)^2}}$$

F_x, F_y, F_z, f_x, f_y, and f_z were each summed for the entire sensel. These values were automatically copied to the EXCEL™ summary sheet to be combined with the rest of the sensors to provide an entire data set.

3.3 Tools Used for Calibration and Validation Experiments

3.3.1 Tekscan™ Calibration

To measure pressures on the body created by the waist belt, Tekscan™ F-Scan 9811 Pressure Sensors were used. These sensors consisted of an array of 96 individual sensels, 16 rows by six columns. The array was on a thin, flexible Mylar sheet, each sensel measuring 6mm by 7mm. Each sensel contained a homogenous layer of resistive ink, sandwiched between two conductive sheets. When a force was applied, the resulting resistance between the two sheets was measured as a voltage. The software took this voltage value, determined it to be acting across the entire sensel area of 161.29 mm^2, and subsequently calculated the pressure acting on the sensel.

A calibration jig (Bryant, *et al*., 1999) was developed to calibrate each Tekscan™ F-Scan sensor. The jig consisted of a rectangular bladder sandwiched between two metal plates with the corners of the plates kept in place with four bolts. Each sensor was placed on top of the lower plate, with the bladder and upper plate placed on top. The sensor was taped in place to inhibit movement. The bladder was then inflated to 10psi and the data input to a calibration algorithm (Bryant, *et al*., 1999). The data sets were converted to a calibration line with linear regression. Each calibration line consisted of a constant and a slope, representing the offset and gain respectively for each sensel.

3.3.2 Force Plate

The model LG6-4-2000 (AMTI Incorporated, Boston, USA) force platform was built into the floor of the testing facility. The force platform measured forces and moments simultaneously in the X, Y and Z directions using four measurement gauges, one at each corner. The output voltages were proportional to the force applied to the system. The voltage signal was amplified with a Model SGA6-4 (AMTI Incorporated) and input to a National Instruments BNC-2090 connection box and sent througha 25-pin connector to an A/D board in the CPU of the computer. This signal was then captured using Labview Software (National Instruments Inc.). Potter (1998) showed that the force plate had an average percent error in the vertical direction of 0.078% and a standard deviation of 0.34%. He also showed a resolution of 0.002kg and r^2=0.999. Finally, the precision of standard deviation in the z-direction was shown to be equal to 0.374 mV. The output voltages were converted to Newtons using a linear procedure defined by the manufacturer. The force plate instrumentation was zeroed across all six channels. One data set was recorded for 5 seconds at 50Hz with the plate unloaded. The force plate was then loaded with weight in the following increments: 2.27kg, 4.55kg, 9.09kg, 22.73kg, 45.45kg, 90.91kg. The voltages were recorded for each trial.

The raw voltages were plotted against the applied forces in the Z-direction. As the masses were not of uniform size or material, the comparison of any of the other forces could not easily be calculated as the exact centre of pressure for each mass is unknown. Regression

analysis was performed on the plotted points. Significant values were r^2=0.99. P values for the X and Y-axes were 0.002 and 0.001, respectively (Appendix C).

To determine the centre of pressure of the force platform, a small, cylindrical, uniform mass of 2.27kg was placed on the force plate in different positions. The forces were recorded and the position was calculated and compared with the known position. Three data sets were recorded for each position, with the mass being repositioned for each set. The results showed a good correlation between the measured positions and the known positions although the positions were consistently underestimated in the x-direction while overestimated in the y-direction. The standard deviations ranged from 2.8mm to 21.9mm, with standard errors ranging from 0.2mm to 12.7mm. (Appendix C)

3.3.3 Strap Force Transducer

The strap force transducers (Stevenson, 1995) consisted of four strain gauges arranged in a full wheatstone bridge on a small aluminum 'dog-bone' shaped base as shown in Figure 3.9. The transducers were sewn into the webbing section of belt to the right of the front buckle. These transducers have been shown to have a maximum standard error of between 1.5N and 2.6N for loads ranging from 44.5N to 177.5N. The data were highly linear with correlation coefficients of r^2 >0.99 (Stevenson, 1996). A calibration curve was calculated for the sensor by hanging a known mass from the gauge and plotting the output voltage versus the applied mass (Appendix C).

Figure 3.9 Strap Force Transducer

3.3.4 Force Gauge

The Shimpo™ MF-100 push-pull gauge was a handheld force-measuring instrument. A bracket was designed to allow it to be linked in series with a 50.8 mm (2") webbing strap to measure the tension in a strap. The gauge has a capacity of 445.9N (100lb) and had an analog dial measured in increments of 2.2N (0.5lb). The accuracy, specified by the manufacturer, was 0.2% full scale, or 0.9N (0.2lb) (www.shimpoinst.com). A simple calibration performed by suspending known masses from the gauge produced standard errors between 0.04N and 0.2N (0.01 and 0.05 lbs.). The errors for this gage were higher than the manufacturer specifications, perhaps due to reading of the gauge or setting the baseline load (Appendix C).

3.4 Analysis Methods

Using Microsoft Excel as the analysis program, each sensor resulted in two worksheets in the calculation template (Appendix B). The first sheet was an input page for the measured Tekscan™ force data. The input data consisted of the averaged sensel measurements for 40 data sets measured at 50 Hz. The frequency and number of data sets were chosen as representative of the measurements after being compared with higher and lower frequencies and numbers of data sets. The averaged data were converted to Newtons prior to being pasted onto the input worksheet.

The second sheet consisted of the coordinates and calculations of each sensel on the sensor. Each sensor consisted of six columns and sixteen rows of individual sensels.

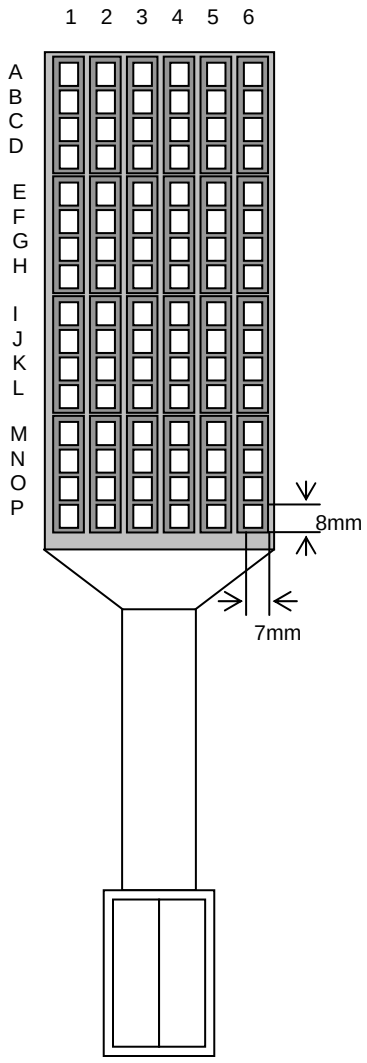

Figure 3.10
Tekscan™ Sensor

The columns were numbered one through six while the rows were lettered A through P. Sensel designations were consistent regardless of the placement orientation of the sensor. Each sensor was on a separate worksheet with the name of the worksheet indicating the sensor number. The sensors were numbered with the year purchased and the order of calibration (e.g. 01-12). This numbering system corresponded to the file names of the calibration matrix.

The layout of columns for all sensors followed the same format whereby the first column of data was the label for the rows. The second column was the x-coordinates for the first column of sensels on the

sensor; the second was the y-coordinate and the third, the z-coordinate. Two columns for the radius and angle from the y-axis followed this, respectively.

The angle from the y-axis was input as a constant for each sensel, as measured from the torso. The z-coordinate was also input as a constant for the sensel as it was measured from the torso. These two values were used to compute the radius of the cone at the point and subsequently the x and y coordinates.

Once the x,y,z locations were entered, the normal unit vector with the corresponding angle from y was input from the normal calculation spreadsheet. The vector was broken down into *l, m,* and *n* directions corresponding to the X, Y and Z directions respectively. To match the x,y,z location with the Tekscan™ force, each sensor's input was pasted into a separate worksheet that was linked to the main calculation page for each sensor. The force measured by Tekscan™ was input into the corresponding sensel location on the calculation page. This scalar value was multiplied by each directional vector of the normal unit vector. The resulting normal Tekscan™ force vectors in each of the x, y, and z directions were placed in the next three columns respectively. The directional vectors for friction, f_x, f_y and f_z, were calculated in the next three columns by multiplication with the coefficient of friction.

3.4.1 Robustness of the Mathematical Model: Internal Verification of the Calculations

Several tests were conducted to ensure that the spreadsheet manipulations were correct. The precision of the mathematical model was tested with the input of uniform forces for each sensel. A force value of 1N was input for each sensel in the system. The forces in the X and Y directions summed to zero. As the z values were not expected to equilibrate to zero, a comparison calculation was made by summing the resultant vertical component of each 1N force. These results showed the model was correct in the calculation of the coordinates and normal vectors for each point. As a secondary test, values of zero for each of the measured forces were input to the model. This acted as a troubleshooting measure to verify that cell references were correct.

4.0 Validation and Calibration of Testing Apparatus

4.1 Loading Validation

Tekscan™ sensor output was directly compared to that of the force plate and force gauge measurements in a simulation of waist belt loading. The loading system is shown in Figure 4.1. A zero lean angle was used to maximize symmetry for initial testing. A length of 50.8mm (2") wide webbing was wrapped around the left side of the SLT and connected to the force gauge. The angle of the webbing corresponded to the slope of the SLT in order to maximize contact with the sensor and provide a normal force to the surface. A spreader bar was inserted between the SLT and the gauge to hold the strap out from the sides of the SLT as contact on only one sensor on a hip was being tested. Mathematical proof that the spreader bar did not change the external forces acting on the system is shown in Appendix D. The belt was constrained vertically to support the weight of the spreader bar.

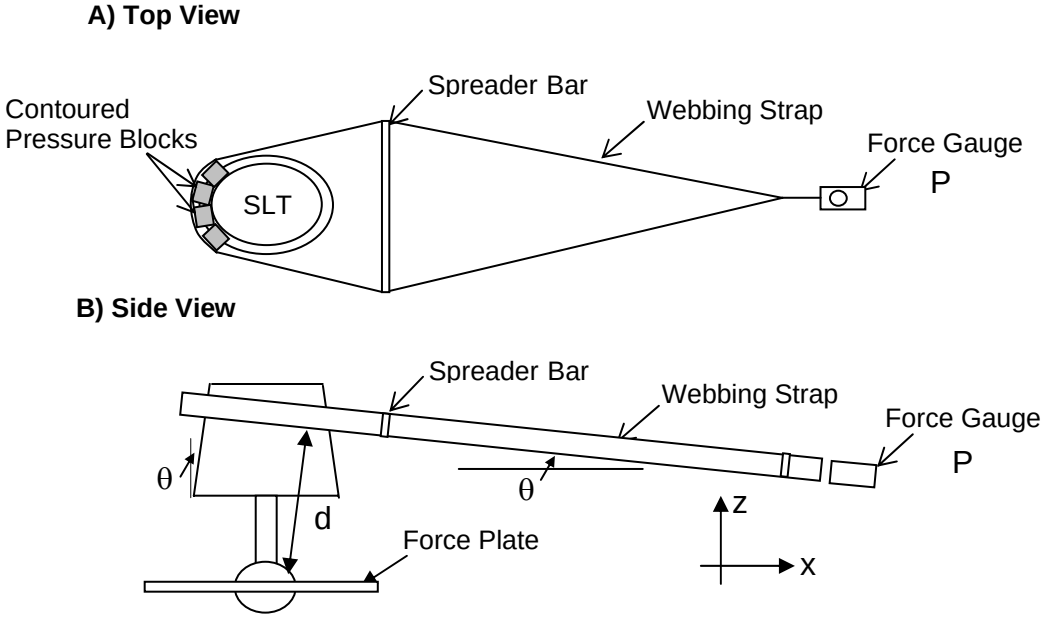

Figure 4.1 Calibration Set-up. Where F_x=Pcosθ, F_z=-Psinθ, and M_y=Pd.

Small blocks covering 16 Sensels were designed to concentrate the forces, as shown in Figure 4.2. These blocks were constructed of a square of high density styrofoam contoured with the shape of the curve of the hip region. One side was covered with closed-cell foam to maximize the surface area contact of the block. One to four of these blocks were used with the resulting measured forces resolved into a single point application of force in the centre of the block.

Figure 4.2 Calibration Block

Loads ranging from 25 to 110N were randomly applied to the waist belt and maintained. Readings were taken simultaneously with the Force Plate and the Tekscan™ sensors. The force gauge was read at the start and finish of data collection to ensure the consistency of the applied force.

Expected moments and forces on the load cell were calculated from the equilibrium expressions shown in Figure 4.1. The values measured by the Tekscan™ sensors were also input to the mathematical model to determine the resultant forces.

The loading validation results are shown in Table 4.1. The force plate and force gauge measurements had good correlation with an average percentage difference of 2.5%, averaged over forces and moments The results showed that the applied force using the strap was consistent with the Force Plate. In contrast, these results indicated discrepancies between the measurements of the three systems. The percentage difference between the Tekscan™ sensors and the applied force were largely unacceptable, ranging from 43.4% to 73.8% below the expected values.

Table 4.1a Tekscan Expected and Measured Forces

	Force Gauge				Tekscan				
Trial	Force	Expected (N)			Measured (N)			Percent Difference	
	(N)	X	Y	Z	X	Y	Z	X	Z
1	91.4	90.5	0	12.7	40.4	-3.5	6.9	44.6	54.3
2	87.4	86.5	0	12.2	35.2	-4.7	6.2	40.7	50.8
3	119.5	118.3	0	16.6	61.7	-7.1	10.5	52.2	63.3
4	68.7	68	0	9.6	28.2	1.1	5	41.5	52.1
5	72.2	71.5	0	10.1	29	-3.8	5.2	40.6	51.5
6	85.6	84.8	0	11.9	35.7	-3.2	6.2	42.1	52.1
7	104.3	103.3	0	14.5	48.6	-4.7	8.3	47	57.2
8	103.7	102.7	0	14.4	44.6	-5.3	7.8	43.4	54.2
9	67.8	67.1	0	9.4	37	-1.5	6.2	55.1	66
10	93.2	92.3	0	13	58.1	-2.6	9.6	62.9	73.8
11	90.1	89.2	0	12.5	47.7	-2.8	8.1	53.5	64.8

Table 4.1b Force Plate Expected and Measured Forces

	Force Gauge				Force Plate				
Trial	Force	Expected (N)			Measured (N)			Percent Difference	
	(N)	X	Y	Z	X	Y	Z	X	Z
1.0	91.4	90.5	0.0	12.7	92.4	-0.3	16.0	2.1	26.0
2.0	87.4	86.5	0.0	12.2	91.0	-0.6	13.1	5.2	7.4
3.0	119.5	118.3	0.0	16.6	124.6	-0.5	13.9	5.3	-16.3
4.0	68.7	68.0	0.0	9.6	71.3	-0.8	10.8	4.9	12.5
5.0	72.2	71.5	0.0	10.1	72.9	-0.9	11.7	2.0	15.8
6.0	85.6	84.8	0.0	11.9	85.7	-1.1	10.5	1.1	-11.8
7.0	104.3	103.3	0.0	14.5	104.9	-0.9	13.6	1.5	-6.2
8.0	103.7	102.7	0.0	14.4	104.2	-0.9	13.8	1.5	-4.2
9.0	67.8	67.1	0.0	9.4	69.3	-0.6	10.3	3.3	9.6
10.0	93.2	92.3	0.0	13.0	91.2	-0.8	11.9	-1.2	-8.5
11.0	90.1	89.2	0.0	12.5	86.6	-0.9	12.9	-2.9	3.2

Table 4.1c Force Place Expected and Measured Moments

		Force Plate						Percent
Trial	Force	Expected (N)			Measured (N)			Difference
	(N)	Mx	My	Mz	Mx	My	Mz	My
1.0	91.4	0.0	66.8	0.0	4.8	72.1	1.3	7.9
2.0	87.4	0.0	63.9	0.0	2.1	61.0	2.5	-4.5
3.0	119.5	0.0	87.4	0.0	2.5	89.9	3.3	2.9
4.0	68.7	0.0	50.2	0.0	6.2	54.1	8.2	7.7
5.0	72.2	0.0	52.8	0.0	5.6	58.2	1.6	10.3
6.0	85.6	0.0	62.6	0.0	6.1	66.3	1.8	6.0
7.0	104.3	0.0	76.2	0.0	4.7	71.2	2.9	-6.6
8.0	103.7	0.0	75.8	0.0	3.5	77.9	3.1	2.8
9.0	67.8	0.0	49.6	0.0	3.6	52.0	1.2	4.9
10.0	93.2	0.0	68.1	0.0	4.7	70.6	1.8	3.6
11.0	90.1	0.0	65.9	0.0	4.9	68.1	1.8	3.4

4.2 In-Situ Calibration

Initial data collection of Tekscan™ pressure sensors mounted on the SLT produced results that varied greatly from the applied force values. To improve the calibration, a modified procedure was developed that incorporated compensation for sensor curvature. The manufacturer stated that the effective sensel area was 161mm^2 when the sensor was used on a flat surface (Tekscan™, 2000). However, it was hypothesized that curvature effects would introduce a scale factor to the relationship between sensor output and applied force. As such, this factor could be treated as a change in effective area of the sensor. By treating the sensor area as a variable, the effective sensel area for each sensor in its curved position could be determined through optimization. As the exact coefficient of friction was also unknown, these two inputs were optimized to minimize the difference between the predicted loads from the Tekscan™ system and the expected loading from the external force gauge.

4.2.1 Calibration Procedure

The initial calibration procedure was the same for that of the initial calibration of the SLT (Appendix D). The sensors on the hip areas were loaded independently and the applied force was distributed through the 50.8mm (2”) wide webbing belt over four blocks of rigid Styrofoam with 10mm thick closed cell foam padding on each. The belt position in the vertical direction was varied to minimize the effects, if any, of different belt shapes in the z-direction.

The sensors on the outer edges of both the abdomen and lumbar area were loaded in pairs to ensure symmetrical load application. The sensors were each loaded with one of the blocks of foam with padding underneath the 50.8mm (2”) wide webbing belt.

The centre sensors on the abdomen and lumbar sections were loaded using a different procedure as their geometry made it impossible to use the same calibration procedure (Appendix D). The SLT was tilted to an angle from the horizontal between 10° and 13° and a mass, acting as an applied force, was placed on the SLT solely on the sensor being calibrated. This experimental design allowed for the sensors on the lumbar and abdominal areas to be isolated for calibration. The sensor measurements were taken and the results compared with the resultant forces of the applied mass.

To test repeatability of sensel measures, nine trials of data were collected for each sensor. These data sets of applied force ranging from 36N to 154N were collected in random order and over three days. Initial testing indicated that the sensor values measured for applied forces of less than 48N were below the capability of the sensors. Therefore, the applied forces used for calibration were always above this value. These trials were input into the spreadsheets for each sensor where the values for the effective sensel area and the friction coefficient were input as variables. Any trials that had greater than 10% of the

total applied force in the y-direction, before optimization, were discarded as this indicated that the testing apparatus was not symmetrical in the loading of the applied force.

4.2.2 Optimization Method

The sum of the squared errors between the Tekscan™ forces and applied forces were calculated and minimized using the effective sensel area and coefficient of friction variables. This is illustrated in Figure 4.3. The initial calibration procedure was applied to the raw Tekscan™ data and the calibrated sensel data were input to the waist belt model. The sensel forces were calculated, summed, and compared to the applied forces. The root mean square error (RMS) for each sensor was calculated as a measure of precision. For this calculation, the sum of squared errors for each sensor was divided by the number of trials.

$$RMS = \sqrt{\frac{SSE}{n}}$$

If this value was not a minimum, the coefficient of friction and the effective area values were adjusted and the waist belt model calculations were performed again.

Figure 4.3. Flow chart of optimization procedure.

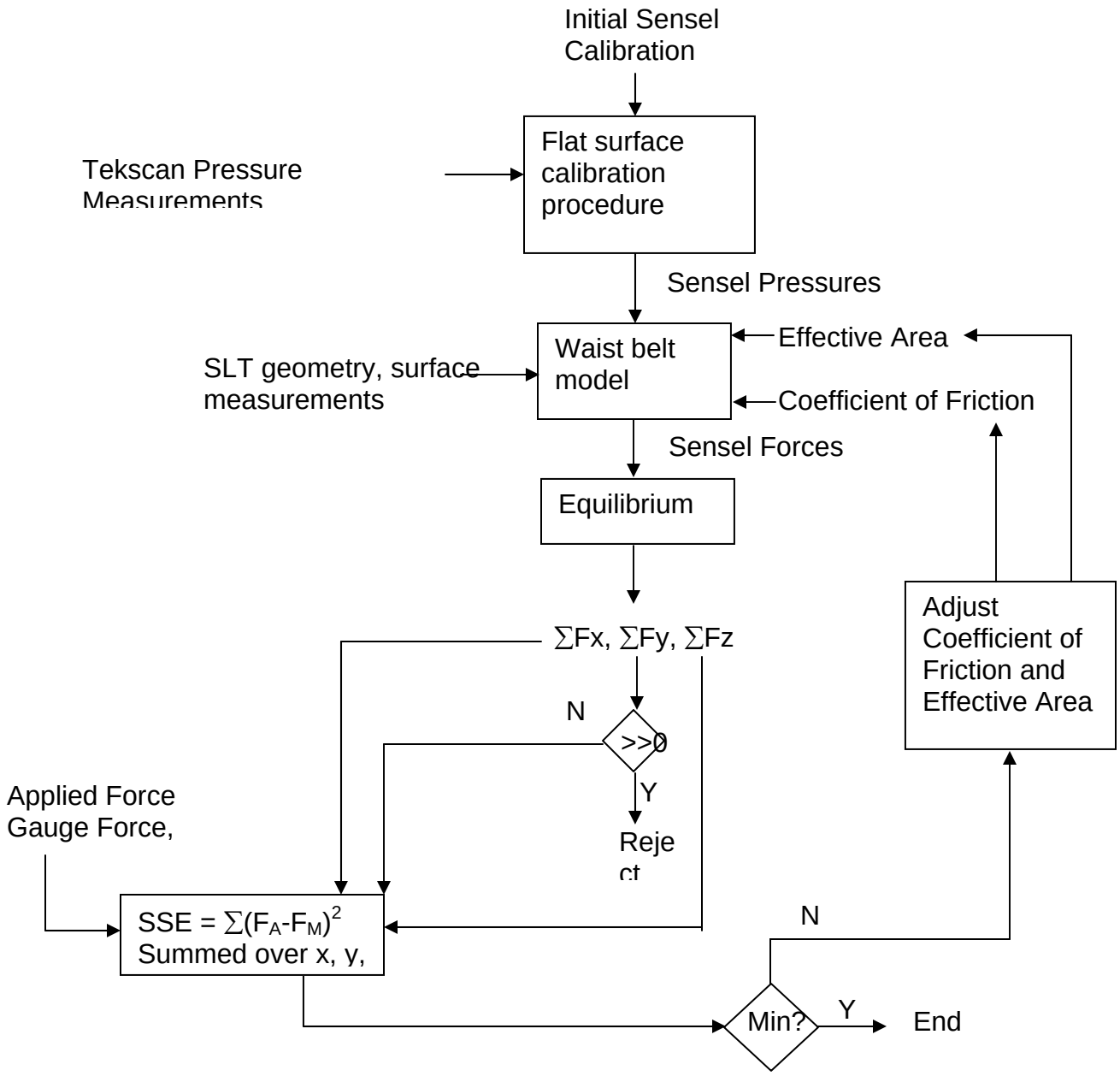

The pressure measurements were input to the waist belt model and the output was compared to the applied force using the sum of squared errors. If this value was not a minimum, the coefficient of friction and the effective area were adjusted and the process was repeated until the minimum was calculated.

4.2.3 Calibration Results

The root mean square error values in Newtons are seen in Table 4.2. Every sensor had an RMS error of less than 8 Newtons, indicating good precision. Sensors 01 and 05 were located on flat surfaces and were not considered to have an effect of curvature.

Table 4.2 RMS Values (N)

Sensor	SSE	RMS
01	-----	-----
03	289.39	7.61
05	-----	-----
06	122.33	6.39
07	227.29	7.54
09	66.47	4.71
10	122.33	6.39
12	103.49	5.87
13	289.39	7.61
15	245.71	6.40

Table 4.3 shows the effective sensel area for each sensor after optimization. Excellent correlation occurred between sensors located in opposite positions, sensors 01-12 and 01-09 had a difference of 5.4%, sensors 01-07 and 01-15 had a difference of 2%. While sensors 01-12 and 01-15, located on the same side, had a difference of 27%, and sensors 01-09 and 01-07, also located on the same side, had a difference 24%.

Table 4.3 Effective Sensel Area

Sensor	**Effective Area (mm^2)**
01	-----
03	205.3
05	-----
06	207.5
07	167.8
09	221.7
10	207.5
12	234.7
13	205.3
15	171.2

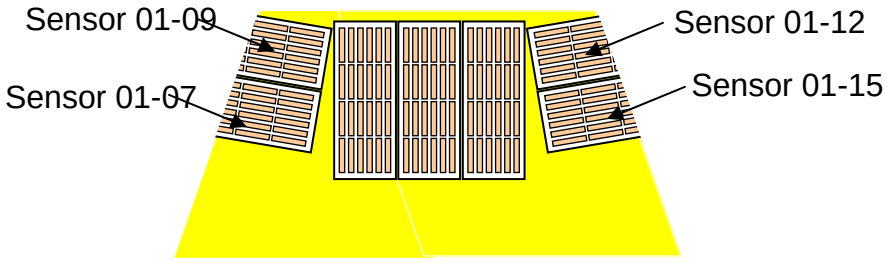

Figure 4.4 Location of Sensors on the Hip Sections

The results indicated a difference in curvature affected the effective sensel area as the radius of curvature changed with position in the z-direction. The optimized values for the effective sensel area of each sensor were considered to be constant for each sensor, providing the locations of the sensors were not changed.

As expected, the optimized coefficients of friction were below the previously determined experimental coefficient of static friction (μ=0.38), shown in Table 4.4. Generally, the sliding coefficient of friction is 25% lower than the static coefficient (Hibbeler, 1995). The standard error between all of the measured values was small enough to consider the average of the values to be a constant to two decimal places, μ=0.26. This assumption resulted in a change in RMS errors of less than 0.05N.

Table 4.4 Optimized Coefficient of Friction

Sensor	Coefficient of Friction
01	-----
03	0.26
05	-----
06	0.26
07	0.26
09	0.25
10	0.26
12	0.24
13	0.26
15	0.25

Each of the values for the effective sensel area was considered to be a calibration factor for the particular sensor in its current location. This calibration procedure would need to be repeated if the position of the sensor was changed or the actual sensor was moved to a different location. As well, due to variation between sensors (Bryant, et al., 1999), the procedure should be repeated if a different sensor was used in the location. The coefficient of sliding friction was considered to be a constant for all further testing on the SLT.

These calibration results showed that the Tekscan™ Sensors could be calibrated *in situ* for use on curved surfaces. The addition of a scale factor to the measured pressures permitted calculation of forces that were within 19% of a known applied load, within the error of the measurement system. The symmetry between scale factors and the radius of curvature of opposite sensors indicated that these scale factors were not random but dependent on the radius of curvature. Therefore, based on sensor location, separate scaling factors were used for each sensor.

4.3 Reproducibility in Waist belt Testing

In order to determine the applicability of the system to waist belt assessment and design, an experiment was required to study the effects of random error and determine the number of trials required to produce acceptable results.

4.3.1 Method

A simple waist belt with built-in lumbar pad was loaded onto the SLT as seen in Figure 4.5. It was tightened to a random belt tension, within the pre-determined limits of the system. Data were first collected in this configuration. Without adjustment or movement of the belt, uniform masses were added about its circumference by means of commercial ankle weights attached end-to-end in a circle a second data set was collected. Three trials were completed with complete set-up of the apparatus between trials.

Figure 4.5 Simple Waist belt

The pressure data were input into the mathematical model for each set of trials. In order to minimize the effect of non-uniform belt tension caused by the direction of tightening, the forces from each trial with the unweighted belt were subtracted from those of the corresponding weighted belt trial to isolate the effect of the applied mass.

4.3.2 Results

For a single measurement, the model predictions were inconsistent with the applied load and between trials, ranging from 69.7% below to 37.2% above the expected values in the z-direction, as shown in Table 4.5.

Table 4.5 Measured and Expected Values for Isolated Mass

	Expected	Measured	
Trial	Fz (N)	Fz (N)	Percent Difference
1	44.6	32.5	-27.0
2	44.6	60.9	36.5
3	44.6	22.5	-49.6
4	44.6	59.2	32.8
5	44.6	13.5	-69.7
6	44.6	61.2	37.2
7	44.6	14.0	-68.6
8	44.6	32.9	-26.3
9	44.6	30.7	-31.2
	Average	34.4	-18.4

This indicated the possibility of excessive random error in the system. Further trials were performed to determine the number of trials needed to reduce these random errors to obtain acceptable results. A plot of the standard errors of the means for the x, y, and z values of nine trials are seen in Figure 4.6.

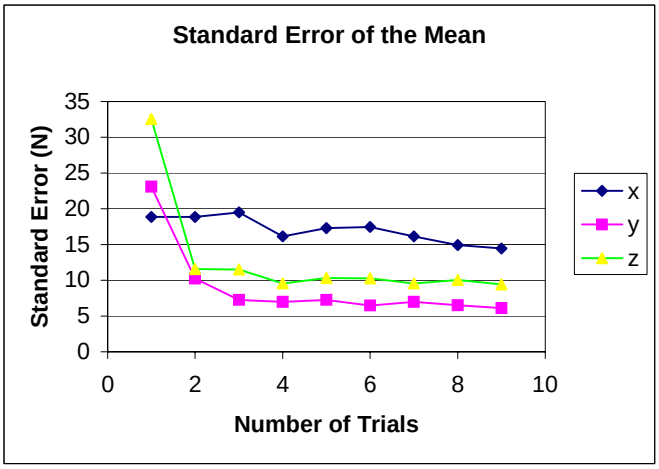

Figure 4.6 Standard Error of the Mean of summed forces in the x, y, and z directions over nine trials

A distinct break point was seen at three trials although the errors decreased minimally until the ninth trial. These results indicated that three trials were sufficient to reduce random error. In subsequent testing as many as ten trials and as few as three trials were used in each set-up, depending on the level of concern over precision.

5.0 Effect of Strap Tension Contact Force Distribution in Waist belts

In previous studies of load carriage performance, Tekscan™ sensors have been used in conjunction with strap force transducers (Stevenson, 1995). The values measured by the transducers were input into earlier biomechanical models as variables in the calculation of the forces in the system, however this has proven inconclusive. Since the system is statically indeterminate, the purpose of this experiment was to determine the correlation between the measured strap tension and resultant pressure measurements.

5.1 General Analysis Method

In order to examine the relationship between tension and pressure, a simple equilibrium expression was first developed. The pressure data were divided into halves, medially and laterally, and the forces in the X and Y-directions were calculated for each half as shown in Figure 5.1.

The tension was considered to be constant throughout the belt and was expected to correspond to the measured forces as in the theorized relationship of the strap force tension to the measured forces in Figures 5.2 and 5.3. This assumed that any frictional forces, if present, are in equilibrium along the length of the belt. As the measured tension differed slightly between trials, the resulting forces were normalized by expressing them as a factor of the applied tension, as read by the strap force sensor.

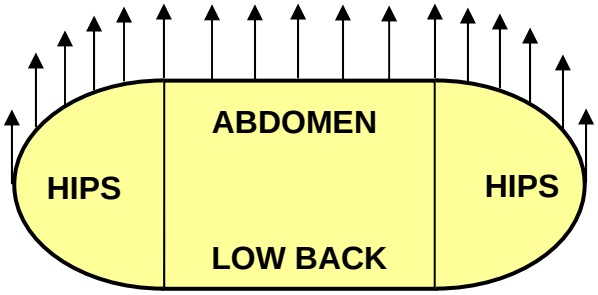

a) Summation of forces on the Abdominal area

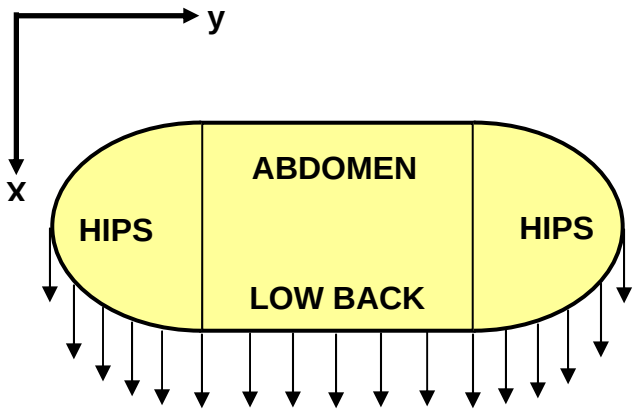

b) Summation of forces on the Lumbar area

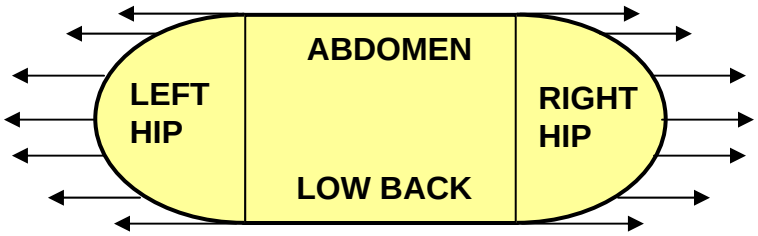

c) Summation of forces on the right and left hips

Figure 5.1 Summation of Forces measured on the SLT by the waist belt on the a) abdominal area b) lumbar area and c) right and left hips

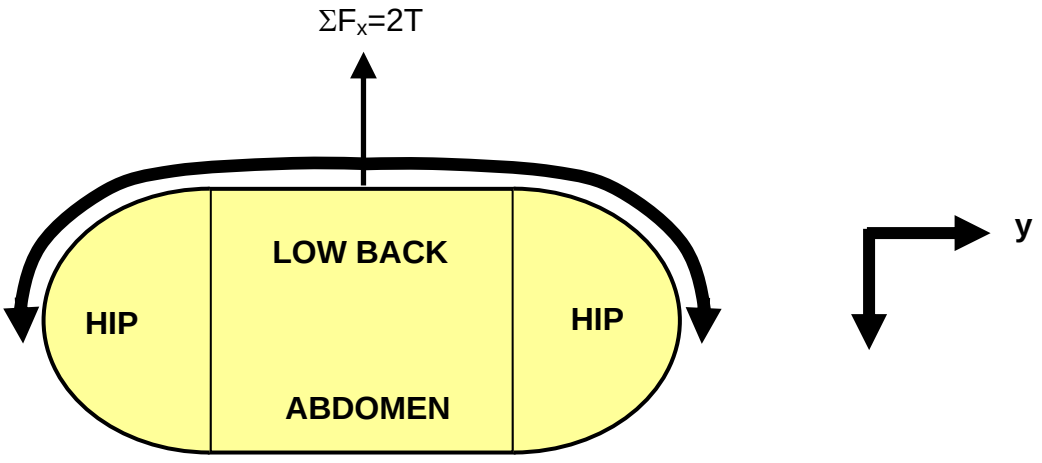

Figure 5.2 Estimated forces on the lumbar area due to belt tension

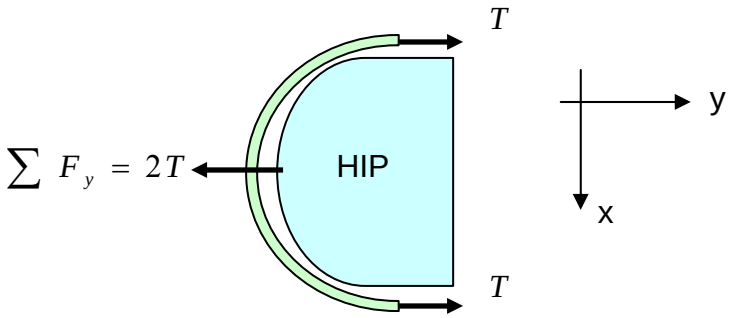

Figure 5.3 Estimated forces on the hip due to belt tension

5.1.1 Method and Results

A strap force transducer was mounted on the simple waist belt. The waist belt was then placed on the SLT and tightened to approximately 50N. The strap tension and pressure measurements were recorded. Ten trials were completed with resetting of the apparatus between each trial.

The results are shown in Table 5.1. The column labeled “front’ refers to the ratio of measured force to belt tension in the x-direction across the entire anterior half of the SLT. ‘Rear’ refers to the ratio of measured force to the belt tension in the x-direction across the entire posterior half of the SLT. The left and right hips referred to the ratio in the y-direction across the entire left and right sides of the SLT, respectively.

In order to insure that the SLT was symmetrical in the anterior and posterior directions, three trials were completed with the waist belt on in the opposite orientation. The results were not significantly different than those in the first orientation and are shown in Table 5.1b.

Table 5.1 Ratio of Measured Force to Belt Tension, Belt #1

		Ratio of Measured force to Belt Tension			
Trial	**Belt Tension (N)**	**Front**	**Rear**	**Left Hip**	**Right Hip**
1.0	44.5	-1.3	3.1	-1.0	2.1
2.0	50.4	-1.3	3.0	-1.6	2.3
3.0	54.4	-1.2	3.1	-1.9	2.3
4.0	40.5	-1.4	3.5	-1.6	2.2
5.0	43.0	-1.5	3.7	-2.5	2.3
6.0	47.4	-1.5	3.8	-2.1	2.3
Average:	46.7	-1.4	3.4	-1.8	2.2
	Average:	2.4		2.0	

Table 5.1b Ratio of Measured Force to Belt Tension, Belt #1, Opposite Orientation

		Ratio of Measured force to Belt Tension			
Trial	**Belt Tension (N)**	**Front**	**Rear**	**Left Hip**	**Right Hip**
1.0	46.9	-1.1	3.1	-2.0	2.3
2.0	52.1	-1.3	3.4	-1.9	2.1
3.0	50.4	-1.2	3.3	-1.7	2.3
Average:	49.8	-1.2	3.3	-1.9	2.2
	Average:	2.3		2.1	

With six repetitions averaged, the force on the right hip was equal to 2.2 times the strap tension. Of note is that this side had the strap force transducer. Force on the left hip was a factor 1.8 times the strap tension. The average force on the front was 1.4 times the strap tension. The average force on the rear was 3.4 times the strap tension.

The sum of the forces on the hips in the y-direction had unexpected inequalities as the hips were symmetrical. It was hypothesized that the tensions on the hips were not equal due to the direction of tightening of the belt. The strap force transducer placement interfered with the tightening of the belt and dictated that it could be tightened on one side only, the right side.

The average ratio of summed force to strap force tension on the right and left hips were examined to determine a possible correlation of the effects of directional belt tensioning. The average of these two values was the expected 2.0 times the strap tension acting on each hip. However, the lumbar area force averaged 3.4 times the belt tension and the abdomen 1.4 times. The resultant effects on the lumbar and abdomen areas averaged 2.4 times the belt tension and suggested that secondary force distributions may be present.

5.1.2 Secondary Force Distributions

To study a possible secondary pressure distribution, the forces acting in the x-direction on the flat surface of the lumbar and abdomen were isolated as shown in Figure 5.4.

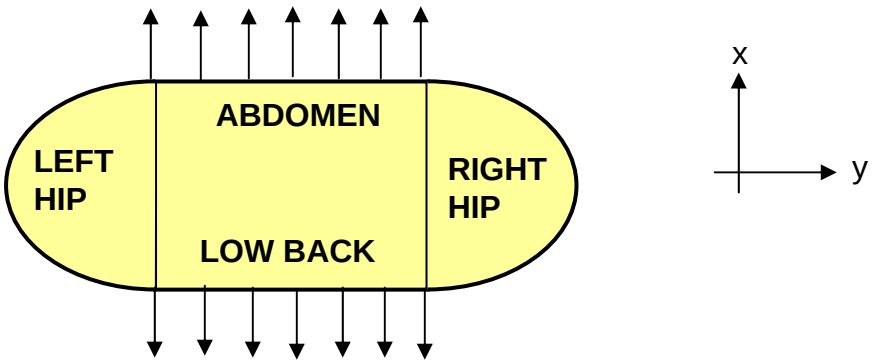

Figure 5.4 Summation of Forces on the Isolated Lumbar and Abdominal Areas

The forces were summed from forces measured by the sensels located only on the flat surfaces. The results are shown in Table 5.2. The abdomen experienced an average force of 0.5 times the strap tension while the lumbar region experienced an average factor of 0.7 times the strap tension. These values were both expected to be zero as there is no net force in the x-direction assumed to be acting on the flat surfaces by the waist belt.

Table 5.2 Ratio of Measured force to Belt Tension Secondary Calculation – Belt #1

		Ratio of Measured force to Belt Tension	
Trial	**Belt Tension (N)**	**Abdomen**	**Lumbar**
1.0	44.5	-0.4	0.7
2.0	50.4	-0.4	0.7
3.0	54.4	-0.4	0.7
4.0	40.5	-0.5	1.0
5.0	43.0	-0.5	1.4
6.0	47.4	-0.5	1.1
Average:	46.7	-0.5	0.9

Several theories exist to explain the results shown in Table 5.2 that appear to violate Newtons Law. A ‘pressure fit’ effect might be occurring due to the materials and orientation of the system. This involves the effect of compression of the padding in the waist belt as the geometry of the system indicated that there should be no force in the Y-direction on the flat surfaces of the lumbar and abdomen areas. Deformation of the belt over these areas could be contributing forces in this direction.

The abdomen area might be experiencing subsequent buckle pressure caused by the deformation of the ends of the belt padding as it wraps around the front shown in Figure 5.5. The horizontal tension of the webbing section would be compressing the ends of the padding non-uniformly. The transitions from curved to flat surfaces might also be presenting an artifact in these regions.

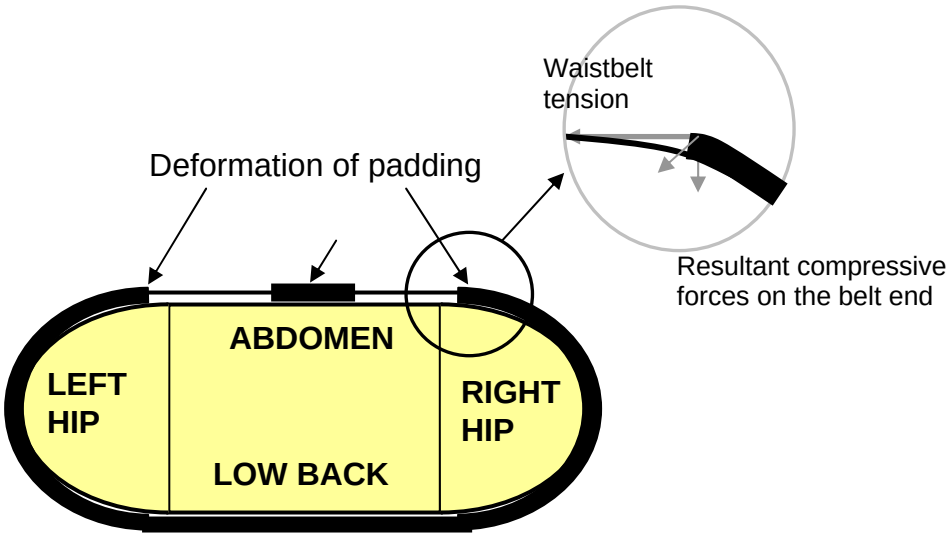

Figure 5.5 Deformation of the padding on the ends of the waist belt

An additional effect might be occurring in the form of uneven pressure distribution as the belt did not necessarily have a shape that perfectly corresponded to the shape of the SLT. Therefore, different pressures might be occurring at the top and bottom of the belt. Pressure profiles clearly showed increased force around the bottom of the belt, indicating that the belt was tighter around the bottom than the top of its circumference and, therefore, of less conical and more cylindrical shape than the SLT, as shown in Figures 5.6a and 5.6b. The pressure distribution shown on the hip in Figure 5.6a resulted from full coverage of the sensor by the belt, although the pressure map did not show this as the pressures were not evenly distributed.

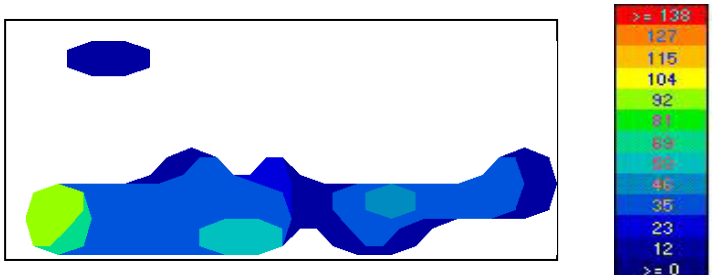

Figure 5.6a. Tekscan pressure profile on hip

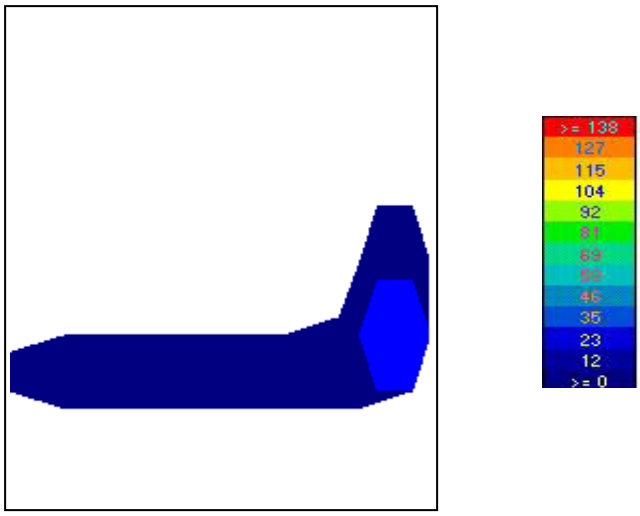

Figure 5.6b Tekscan pressure profile on lumbar area

The profile shown on the lumbar area, shown in Figure 5.6b, exhibited a similar pattern to that of the hip area. A distinct line of pressure was seen around the bottom of the waist belt even though there appeared to be full contact of the waist belt over the sensor.

In summary, results of these experiments did show the expected relationship of the tension to contact pressure for the hips but did not for the abdomen and lumbar areas. To determine if these results were related to the design of the belt, additional waist belts of different styles were tested.

5.2 Effect of Design on Contact Force Distribution

As the previous trials were completed with the use of only one waist belt, the distribution and loading may be specific to a particular belt. In order to determine this, the effect of a number of waist belt design parameters on pressure and force patterns were examined.

5.2.1 Methods

A second belt of a different design was evaluated under similar conditions to the initial study. Belt #2 was of a different covering material, a rougher, looser weave nylon cordura. The larger lumbar pad was a separate piece from the belt that attached with Velcro^{TM}, it was approximately 1.7 times the width of the belt. The padding was more compliant and sectioned in vertical compartments, as seen in Figure 5.7. As well, the belt had a partial plastic framesheet on the outer side of the belt.

Figure 5.7 Testing Belt #2

A strap force transducer was mounted on the waist belt and the waist belt was then placed on the SLT and tightened to approximately 50N. The strap tension and pressure measurements were recorded. Four trials were completed with resetting of the apparatus between each trial.

A third belt was also tested as in Figure 5.8. It was a commercial design that was not detachable from the backpack. The effect of the pack was minimized by suspending the packbag from above so its mass was not affecting the belt attachment. This third belt had a very distinct and separate lumbar pad as well as stiff foam padding that had less compliance than the other two belts. The padding pattern was similar to that of Belt #2.

Figure 5.8 Testing Belt #3

5.2.2 Results

The results of the second belt testing are shown in Table 5.3, with the secondary calculations shown in Table 5.4. With four repetitions averaged, the force on the right hip was equal to 2.0 times the strap tension. Of note is that this side had the strap force transducer. Force on the left hip was a factor of 0.9 times the strap tension. The average force on the front was 1.7 times the strap tension. The average force on the rear was 2.8 times the strap tension.

For the secondary calculations, the abdomen experienced an average force of 0.4 times the strap tension while the lumbar region experienced an average factor of 0.6 times the strap tension. These values were both expected to be zero as there is no net force in the y-direction force assumed to be acting on the flat surfaces by the waist belt.

The force distribution for the second waist belt was similar to the first waist belt in the general distribution of forces, though not in the magnitudes. The left and right hips had the same inequalities likely due to tightening and the lumbar forces exceeded the abdominal forces. The second belt indicated a better distribution of the forces, especially at the lumbar and abdominal regions. The effect of tightening direction was seen as in the previous waist belt. Inequalities were again seen as a non-balanced system.

Table 5.3 Ratio of Measured Force to Belt Tension: Belt #2

		Ratio of Measured force to Belt Tension			
Trial	**Belt Tension (N)**	**Front**	**Rear**	**Left Hip**	**Right Hip**
1.0	47.9	-1.6	2.5	-0.9	2.0
2.0	46.4	-1.8	2.5	-0.7	1.9
3.0	50.9	-1.5	2.6	-1.1	2.0
4.0	46.4	-1.8	3.4	-1.0	2.0
Average:	47.9	-1.7	2.8	-0.9	2.0
	Average:	2.3		1.5	

Table 5.4 Ratio of Measured Force to Belt Tension Secondary Calculation: Belt #2

		Ratio of Measured force to Belt Tension	
Trial	**Belt Tension (N)**	**Abdomen**	**Lumbar**
1.0	47.9	-0.3	0.6
2.0	46.4	-0.4	0.6
3.0	50.9	-0.3	0.5
4.0	46.4	-0.7	0.6
Average:	47.9	-0.4	0.6

The results of the third belt testing are shown in Table 5.5, with the secondary calculations shown in Table 5.6. With four repetitions averaged, the force on the right hip was equal to 2.2 times the strap tension. Of note is that this side had the strap force transducer. Force on the left hip was a factor 1.5 times the strap tension. The average force on the front was 2.3 times the strap tension. The average force on the rear was 2.1 times the strap tension.

For the secondary calculations, the abdomen experienced an average force of 0.1 times the strap tension while the lumbar region experienced an average factor of 0.9 times the strap tension. These values were both expected to be zero as there is no net force in the y-direction assumed to be acting on the flat surfaces by the waist belt. The left and right hips exhibited the effects due to direction of tightening seen in all of the other belts.

Table 5.5 Ratio of Measured Force to Belt Tension: Belt #3

		Ratio of Measured force to Belt Tension			
Trial	**Belt Tension (N)**	**Front**	**Rear**	**Left Hip**	**Right Hip**
1	44.0	-2.3	2.4	-1.3	2.2
2	51.4	-2.3	1.9	-1.4	2.0
3	50.4	-2.3	2.0	-1.6	2.3
Average:	48.6	-2.3	2.1	-1.5	2.2
	Average:	2.2		1.9	

Table 5.6 Ratio of Measured Force to Belt Tension: Secondary Calculation: Belt #3

		Ratio of Measured force to Belt Tension	
Trial	**Belt Tension (N)**	**Abdomen**	**Lumbar**
1	44.0	0.3	-0.7
2	51.4	0.0	-1.1
3	50.4	0.1	-0.8
Average:	48.6	0.1	-0.9

As the SLT is symmetrical in quadrants, the forces in each quadrant were summed as shown in Figure 5.9 and Table 5.7. This summation was expected to balance as inequalities would cancel out in the opposite quadrants. The forces in the X and Y directions for each quadrant were expected to be equal to T, based upon a constant tension throughout the waist belt.

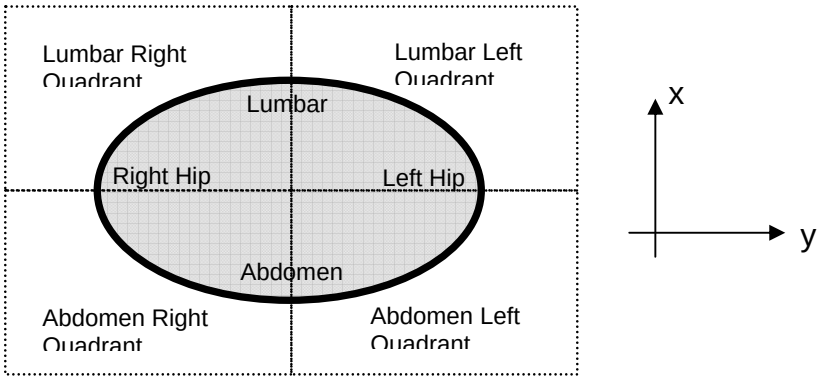

Figure 5.9 Division of quadrants for summation

The results of the summation in quadrants is shown in Table 5.7 for all three belts. There is some correlation between all three waist belts. The Y-direction force is consistently higher than the X-direction force in the Lumbar Left quadrant for all three waist belts. The Lumbar Right Y-direction force is consistently 0.2T higher than the Lumbar Left force for all three waist belts. Averaging across all measurements, Belt 1 had the highest values in both the x and y-directions, while Belt 2 and 3 were lower and more similar.

Table 5.7 Comparison of Belt Styles in X and Y Directions

	Ratio of Measured Force to Belt Tension					
	Belt 1		Belt 2		Belt 3	
	X	Y	X	Y	X	Y
Abdomen Left	0.6	0.9	0.4	0.8	0.5	0.4
Abdomen Right	1.2	0.5	0.7	0.9	0.6	0.5
Lumbar Right	1.1	1.6	1.3	0.9	1.6	1.3
Lumbar Left	1.1	1.4	0.6	0.7	1	1.1

The forces in the Z-direction are displayed visually in Figure 5.10 as measured forces in Newtons in each of the four quadrants.

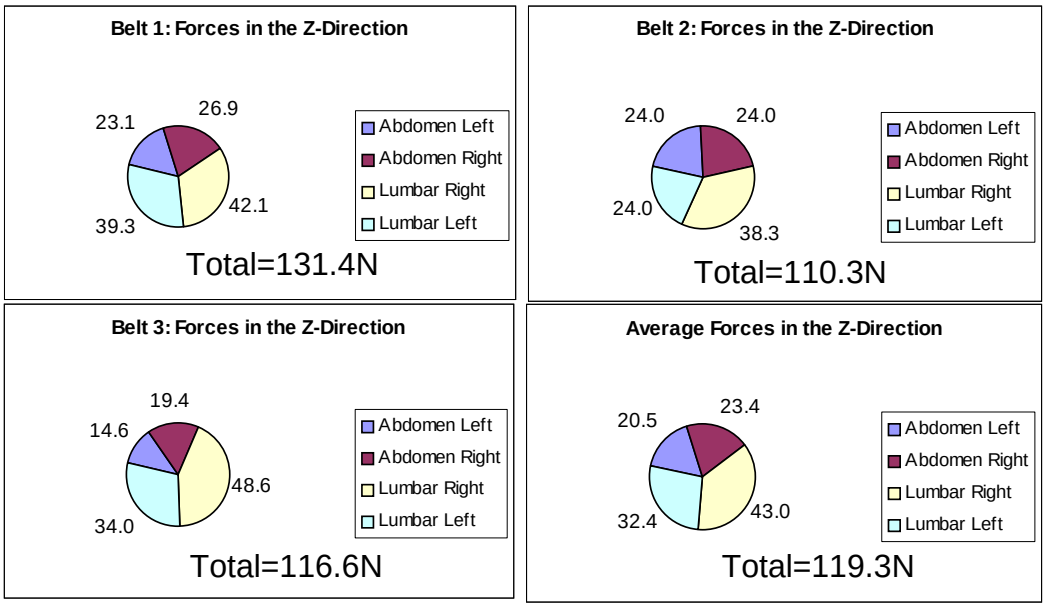

Figure 5.10 Forces in the Z-direction (Newtons)

In this study, the measurements in the z-direction were overestimated in comparison to the mass of the waist belt as the expected total Z-direction force is 33.4N while the average Z-direction force of the three belts was 119.3N. These results showed a consistent trend of higher Z-direction force in the lumbar right quadrant compared to the lumbar left. As well, the abdomen right forces were higher than the abdomen left across all three belts. These findings correlated with the force inequalities due to the direction of waist belt tensioning. The larger forces in the lumbar quadrants matched those of the initial testing results although they were not expected according to the constant tension modeling assumptions.

Internal forces in the belt, particularly in the lumbar and abdominal areas might indicate that the belt was not acting in the assumed orientation. There might be shear effects seen in the transition areas from flat to curved.

5.3 Force Distribution of the Waist belt: Unloaded vs. Loaded Pack

In order to examine the pressure effects of the waist belt of a loaded pack, the third belt was tested again in both unloaded and loaded configurations. The backpack was set up on the SLT as in Figure 5.11. The waist belt was fastened with an approximate 50N tension and the pressure values and horizontal force on the force gauge were recorded. Without adjusting the waist belt, the pack was loaded with 178.4N (40lb). The pressure values and waist belt tension of this new configuration were recorded. Three trials were completed for each configuration.

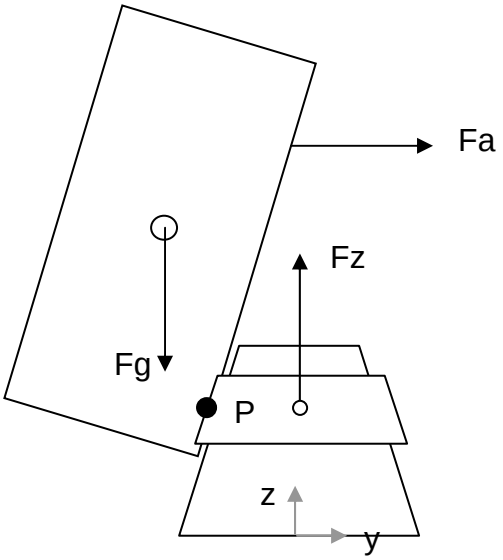

Figure 5.11 Placement of the backpack with waist belt on the SLT with an external force, F_A, balancing the pack in the Y-direction.

The magnitude of the moment transmitted through he waist belt connection (P) was not determined, however. Although F_A was applied to prevent tipping of the pack, some of the moment to resist tipping is also provided by the connection at P.

5.3.1 Expected Loading

The free body diagram of the forces expected during pack-on conditions are shown in Figure 5.12.

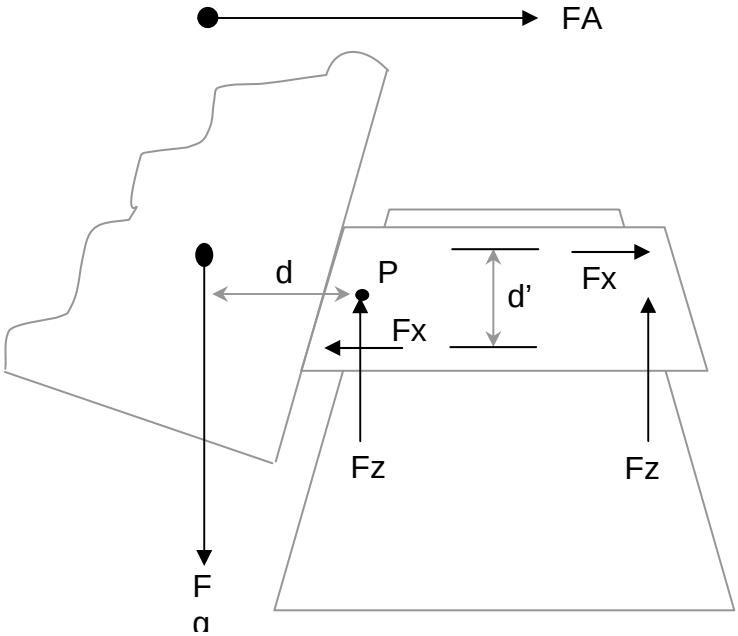

Figure 5.12 Forces on the waist belt with loaded pack

Where:

F_g = Force of gravity acting on the pack mass
d = Distance from centre of gravity of the pack to the waist belt connection
F_z = Force in the z-direction counteracting F_g
F_x = Force in the X-direction
P = Location of the single point connection between the pack and the waist belt
F_A = Force applied to prevent pack from tipping

The force of gravity creates a moment about P with the moment arm, d. Part of this is resisted by the external force F_A, and the balance is counteracted by F_x at the top of the belt in the abdominal area and the base of the belt in the lumbar area, separated by the distance d'.

5.3.2 Results

The measured pressures were summed as in the previous section. The forces in the x and y-directions are shown in the diagrams in Figure 5.12. It was shown that the system was not in equilibrium in the x and y-directions. With the addition of the mass in the pack, the inequalities shown in the right and left hips due to the direction of waist belt tightening

were reduced and nearly equilibrated. The forces on the lumbar and abdominal areas remained non-balanced. The tension in the waist belt consistently increased with the addition of mass, to a factor of 2 times the unloaded tension.

The external forces were minimized and used only to prevent the pack from tipping backwards. These forces ranged from 13N to 34N. The higher forces were observed in the loaded condition. The direction of application was along the x-axis.

Expected measurement errors were the same as those measured in the calibration procedure. The RMS errors ranged from 4.7N to 7.6N for the optimization.

Figure 5.13 X and Y Forces on the SLT with Unloaded and Loaded Backpack

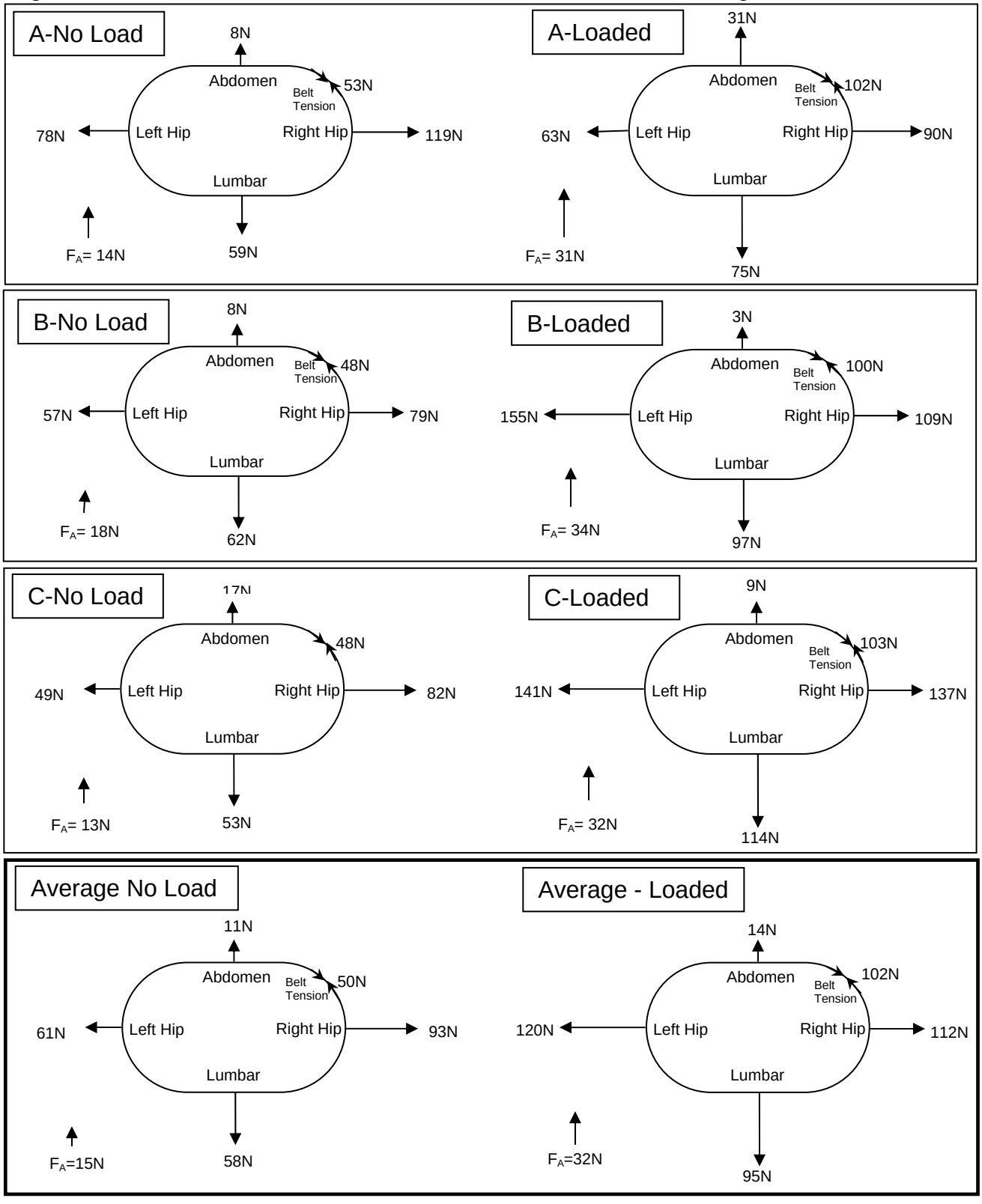

The z-values were also summed in Figure 5.14. The z-direction forces in the unloaded condition were not as expected as the mass of the empty pack was a constant known value of 33N (7.5lb). The averaged measured force was 105.4N. The measured z-values under loaded pack conditions showed that there was equilibrium as the z-force exerted directly by the pack was known. The expected z-direction force was 212N (47.5lb). The average measured force in the z-direction for the loaded pack was 205N. The average measured force in the z-direction when the pack was loaded was within 4% of the expected value (r^2=0.964).

Figure 5.14 Vertical Z forces on the SLT with Unloaded and Loaded Backpack: Measured in Newtons

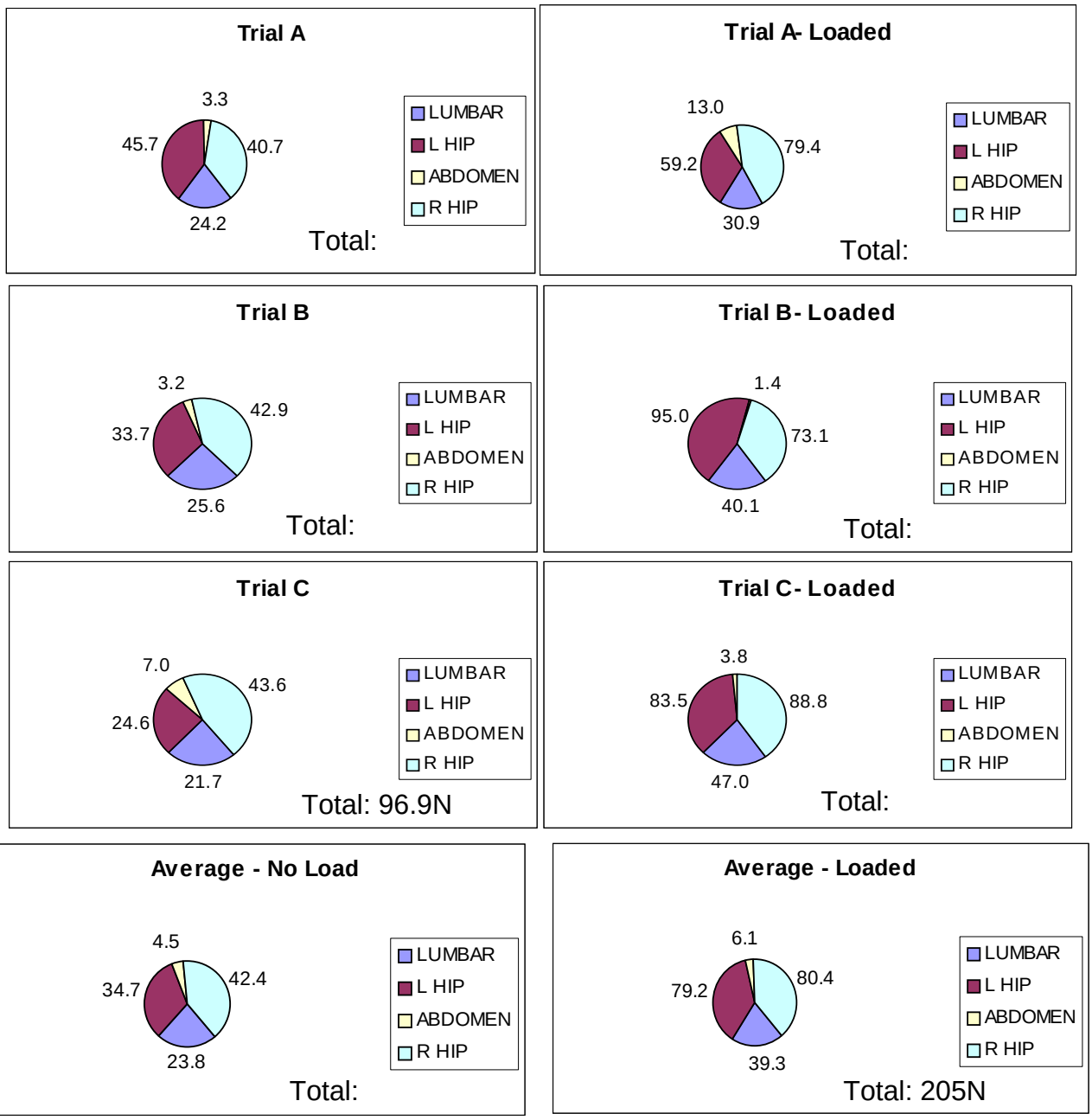

With load in the pack, the measured force in the z-direction was within 4% of the expected value. When the belt was isolated with no load in the pack, the forces in the z-direction had major discrepancies, with an average measurement error of 315%. This result indicated that the forces of friction and belt geometry were misrepresented by the mathematical model at low loads. As balance was not shown in the x and y directions during unloaded and loaded conditions, there appeared to be more complex frictional and tension factors than originally modeled. The tension in the belt may not be a constant as was assumed for calculations and previous biomechanical models. This created an indeterminate problem as these forces cannot be measured with one strap force

transducer. The typical geometry of a waist belt with padding and lumbar pad does not allow for placement of multiple transducers to measure the tension in more than two places.

Friction may not be acting as originally predicted. Although the simple friction model was effective in initial calibration on the curve for isolated sensors, the effects with load in the z-direction may indicate that the frictional forces may not be acting solely in the directions assumed. There may be a geometry change with loading that is indeterminate. This problem of the indeterminacy of friction is seen in the derivation of the equation for wrap angle as the model for friction in a pulley:

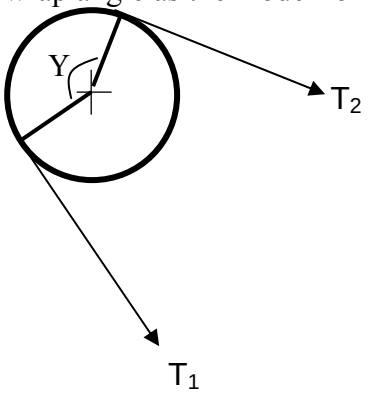

Figure 5.15 Friction on a pulley. T_1 and T_2 are the lower and upper straps respectively and Y is the wrap angle.

Where T_1 and T_2 are the upper and lower strap tensions, respectively, μ is the coefficient of friction and θ is the angle of the wrap. The tensions cannot be individually calculated from the strap force angle and the coefficient of friction, only the ratio.

$$\frac{T_1}{T_2} = e^{\mu\theta}$$

6.0 Discussion

A model torso was developed that allowed the normal directions of each point of interest on the surface to be calculated. The measured force vectors were resolved into directional components to further understand the forces acting on the body by a backpack waist belt. A calibration procedure was developed for use of the Tekscan™ sensors on a curved surface. The procedure also determined a coefficient of sliding friction for Tekscan™ over Bocklite™.

The discussion has been broken down into two sections. The first section deals with the potential of measurement errors which could have affected the results. The second section deals with interpretation of results from the biomechanical testing of waist belt designs.

6.1 Measurement Error

Push-pull gauge. The display of the push-pull gauge was in increments of 0.23kg (0.5 lb) on an analog dial. Measurement reading error was present, accounting to an accuracy of +/- 0.23kg (0.5lb). This error would have contributed to discrepancies during calibration of the SLT set-up. Depending on the force applied, this attributed to range 2.2N of error. The z-axis angle of the applied force was measured with inclinometers. Error in the reading of the inclinometer could account for error in the resolution and comparison of the applied force vector. Sensitivity analysis was performed by changing the measured angle in the calculations by +/- three degrees. The result had an average standard error of 0.36. The applied force was assumed to be in the x-direction but discrepancies may have occurred.

Force Plate. The centre of the force plate was not marked by the manufacturer but was measured from the edges after installation. Placement of the SLT apparatus was assumed to be at the origin of the force plate although experimental centre of pressure measurements taken showed the force plate to be off-centre by an average of 4.5mm (Appendix C). Noise and cross-talk present in the system was assumed to be negligible after subtraction of an averaged baseline value. Vibration of the floor in which the force plate was installed was considered a source of error but assumed to be negligible.

Strap force transducer. The strap force transducers are not calibrated *in situ* and therefore may introduce some error when used in different applications. The transducer was sewn into the webbing of the belt by hand, while great care was taken to ensure the sensor was in line with the hoop force of the belt, some error can be expected. In some cases there was contact on the underside of the transducer by the excess webbing. This may have induced some bending of the transducer.

Tekscan™. The Tekscan™ sensors were initially calibrated on a flat surface but used on a curved surface. The sensors were not equilibrated as each sensel was being summed individually so the inequalities should cancel out. No forces were shown to be present

when the sensors were affixed to the curved surface and unloaded. When calibrated in situ, the sensors exhibited favorable results although the large experimental error of 28% (Helliwell, 1992) could be accounting for a great deal of the unbalanced measured forces. Wear of the sensors in this study was a concern as they were used over 12 months although no apparent degradation was seen in the data. As well, the pressures applied in this study were in the lower range of the sensor capabilities and therefore may have been less accurate than higher forces. The inability of the sensors to measure shear forces limited their usefulness.

Limitations of the mathematical model. The locations of the sensels were measured on the SLT. There was error involved with the exact location as several assumptions were made. The active sensel areas were assumed to be of the identical size as well as the sensor being placed on the SLT in a symmetrical arrangement. The sensels in each quadrant corresponded to those in opposite locations. Each normal vector calculation was dependent upon the measured sensel location. Surface irregularities on the model may have caused slight variations on the actual location and angle of the sensel. The sensors did not provide complete coverage due to the shape of the sensor. The uncovered area was the same in each quadrant so it was assumed to provide consistent error. These gaps would result in a slight under-measurement (2%) of the Tekscan ^{TM} forces compared to the applied force. The RMS errors calculated in the calibration optimization procedure showed the accuracy expected from the model. The RMS values were below 8N.

In summary, the most significant source of error in the equipment is the random measurement error of the Tekscan^{TM} system. With repeated testing, the effects of random error are reduced with a minimum of three trials. In relation to the errors observed with the unbalanced measured forces during waist belt testing, the equipment errors were less significant, as the sensors were calibrated *in situ* with an accuracy of >8N RMS. The unbalanced effects, due to unknown frictional forces were more significant than those inherent in the equipment.

6.2 Waist belt Design Effects

The three waist belts tested varied significantly in design, as did the force distributions on the lower torso. The padding pattern of the first belt was the simplest with the division of padding into two sections along the transverse plane. The covering material was stiff and wrinkles were present in it. The second and third belts were more similar in their padding pattern of multiple longitudinal sections of padding. The covering materials were less stiff and there were fewer wrinkles than in the first belt. The second belt appeared to have slightly more compliant padding than the third. The lumbar area of the first belt was the same as the rest of the padding with no distinct area. The second belt had a large lumbar pad, approximately 1.3 times the width of the waist belt. The lumbar pad had square corners and was not contoured. The third lumbar pad was highly rounded and approximately 1.7 times the width of the waist belt.

The results of the force distribution measurement for the first belt indicated a correlation to the hoop stress as modeled on the hips, but the forces on the lumbar and abdominal areas were not explained by this theory. The large load on the lumbar area indicated that there were forces acting on the torso that were not accounted for by the hoop stresses. Distinct differences between the top and bottom of the waist belt were shown on the pressure maps. The belt did not perfectly match the shape of the SLT and was tighter around the bottom than the top as it was less conical. The lack of contours and sections in the padding of the first belt was expected to result in symmetrical coverage of the torso and a subsequent even pressure distribution; this was not the case.
The second and third belts were expected to have more similar distributions compared to that of the first belt due to the similarity in padding style. There was no consistency between the belts although there was less of a distinct line of pressure around the bottom of the belt. The vertical sections of foam may have allowed for more compression of the padding and distribution of the pressure internally in the foam. The space in between the vertical padding sections would have allowed for spreading of the foam more than in the first belt that would not have allowed spreading in the lateral direction.

The three belt designs were of different lengths which meant that the padding did not always end at the same location on the abdomen. The ends of the waist belt appeared be compressed by the angle of the webbing strap dependent on their location. The shorter the waist belt, the further the ends of the padding would be from the flat abdominal section and therefore the webbing attachment would be at an angle, instead of straight across the abdomen. This created subsequent compression of the ends of the belt. The length of the belt also determined the amount of contact of the buckle on the abdomen. The higher pressure points on the abdomen were due to the buckle when the waist belt length was shorter.

One visible pattern in the force distribution data for each waist belt was the consistency of higher forces on the right hand side of the torso. The left abdominal side was consistently lower than the right while the left lumbar was lower or equal to the right side. The consistency of these results suggested that the direction of belt tightening had a distinct effect on the force distribution. The strap force transducer was located on the left hand side in a constrained position that did not facilitate the tightening of the belt in both directions. This inequality in the system rendered the theory of constant belt tension oversimplified.

Large discrepancies of measured forces in the Z-direction in the unloaded condition, regardless of belt design, indicated large measurement errors. The Tekscan^{TM} sensors for this condition were measuring in the lower range of their capabilities. Alternatively, these discrepancies may represent frictional forces that were not accounted for. The calibration of the sensors in the curved position accounted for friction with the calculation of a constant coefficient of sliding friction when a force was applied. The measurement accuracy determined during calibration of the sensors was >8N RMS for the system. The unbalanced forces observed in subsequent waist belt testing indicated frictional forces caused by the waist belt that were not accounted for in the analysis of friction during calibration. The addition of forces in the circumferential direction by the waist belt

changed the frictional distributions. This distribution was not consistent between the belts, suggesting a design dependency for the friction distribution. This distribution and the relationship to strap force tension was not determined. The discrepancies of measured to applied forces and the degree to which they were unbalanced during waist belt testing indicated that unknown frictional components were a significant source of error.

The addition of mass in the pack increased the belt tension by a factor of two consistently over the three trials. The force in the z-direction was not consistent with the unloaded belt but became consistent with the addition of mass. This indicated that the significance of the frictional forces acting on the body in the z-direction as a result of the circumferential pressures was reduced relative to the force in the z-direction. Therefore, it appears that the higher the mass and tension in the belt, the lower the effect of internal shear forces of the padding.

7.0 Conclusions and Future Work

1. A strategy was developed to determine waist belt compressive force distribution within an RMS error of <10N. A calibration procedure using an effective sensel area and a longitudinal frictional coefficient has been demonstrated. This is limited in application to vertical loading and was more successful in cases where the loads exceeded 50N.
2. Within the limitations of Tekscan™ technology, it was possible to calibrate the sensors on a curved surface. However, the need for a minimum of three repetitions to reduce random error has been demonstrated. This calibration procedure has also demonstrated the need to calibrate all sensors, *in situ*, that are used in curved positions, or disregard the magnitudes of the measured forces.
3. It was possible to derive a coefficient of friction for the isolated waist belt model and to determine how factors such as the direction of belt tightening affected magnitude of the measured normal forces on the torso. The effects of tightening direction were shown to be significant in no-load tests of waist belts. The measured forces on the hips were significantly lower on the side that the strap force transducer was on and these effects are reduced with an increase in load. The apparent effects due to the tightening direction of the waist belt were consistent and predictable but their relationship to the forces acting on a more compliant surfaces, such as the human body cannot be extrapolated from this observation.
4. Previous models involving a waist belt have oversimplified the role of friction with the assumption of a constant belt tension. The complexity of the measured forces in the waist belt indicated that a direct relationship between strap force tension, measured in one location, and the forces acting on the body, was not possible.
5. The application of the frictional distributions appear to depend on the materials used in the construction of the belt. In this preliminary study, the padding orientation and conical shape of the waist belt appeared to determine the severity of localized compressive forces at the base of the belt. A less conical shape created lines of pressure about the bottom of the waist belt as the effects of the belt tension were concentrated in this area due to the geometry of the SLT.
6. At this time, a model for an individual waist belt is limited by an inability to predict frictional force distributions. Tekscan™ instrumentation is also limited in this regard since it cannot directly evaluate the effect of shear forces on the torso.

7.1 Future Work

1. The directions of frictional forces need to be more closely examined as the impending pack motion may not be downwards as originally considered, depending on the mass of the pack and the tension in the belt. If the effective tension were higher than the effective mass on the belt, the pack would have a tendency to move upwards rather than downwards with the force of gravity. The apparent consistent effect of loading the pack and the increase in waist belt

tension should be explored further. Incremental loading would better provide an understanding of this relationship.

2. The unbalanced forces resulting from the compressive force of belt tensioning need to be examined further. The variation in the three waist belts in this study was too great to determine with any certainty how waist belt design relates to the force and frictional distribution in the waist belt. In order to determine the actions of the waist belt padding, the properties of the material, such as compliance of the foam, and the frictional properties of the covering materials should be determined. Identical belts with different materials or different designs with the same materials would facilitate this.
3. The effect of different lean angles of the torso on the distribution of forces should be examined. A forward lean angle of 8° would vertically orient the abdominal area of the model, more closely resembling the human body.
4. The padding surface of each belt may be experiencing relatively large shear forces due to circumferential pressure. These forces and their distribution are not easily modelled and would likely differ greatly when the belt interacts with the compliance of the human body. As a way of subjectively testing different materials on humans, correlations could be made through user trials and questionnaires to determine the relationship between user preferences and compliance of the padding. Belt designs could also be compared with the correlation to subjective testing.
5. The Tekscan™ pressure measurement system was limited in its ability to measure shear. Future testing should be performed when shear measurement technology becomes more widely available.
6. The SLT has a number of potential uses such as: comparison of different materials used for waist belts, furthering of the waist belt models, and comparison of novel designs in waist belt technology. A simplified shoulder can be combined with the SLT to allow for the loading of a complete pack. Tekscan™ sensors on the shoulder would allow for a more complete measurement of the forces of the upper pack and allow for complete resolution of the forces on the body. Strap force transducers on the shoulder straps would determine the relationship of the measured strap forces and the measured forces on the shoulder. The inconsistencies measured during tightening needs to be examined.
7. The design of different waist belt attachment points to the pack should be explored. Specifically, the ability to transmit a moment, and therefore this connection should be considered. While padding design did not show differences in the total distribution of force on the hips, the reduction of the line of pressure about the bottom was apparent in the more conical belts. The testing of a belt with an adjustable angle would help investigate this effect.

8.0 References

AMTI (1989). Biomechanics Platform Set Instructions Manual. Boston, Mass.

Bryant, J.T., Reid, S.A., Morin, E., Stevenson, J.M., Pelot, R.P. (1999). Development of a Calibration Jig for the F-Scan Pressure measurement system. PWGSC Contract # W7711-7-7405/SRV, (58 pages).

Buis, A.W.P. and P. Convery (1997). Calibration problems encountered while monitoring stump/socket interface pressures with force sensing resistors: Techniques adopted to minimize inaccuracies, *Prosthetics and Orthotics International* 21:179-182.

Epstein, Y., Rosenblum, J., Burstein, R., Sawka, M. (1988). External load can alter the energy cost of prolonged exercise, *European Journal of Applied Physiology*, 57:243-7.

Goh, J-H, Thambyah A, Bose K**.** (1998). Effects of varying backpack loads on peak forces in the lumbosacral spine during walking, *Clinical Biomechanics*, 13(1):26-31.

Goslin, B.R., Rorke, S. (1986). The perception of exertion during load carriage, *Ergonomics*, 29(5):677-86.

Hibbeler, R.C. (1993). Statics and Mechanics of Materials, Macmillan Publishing Company, NY.

Holewijn, M. (1990). Physiological strain due to load carrying. *European Journal of Applied Physiology*, 59:237-45.

Holewijn, M., Lotens, W.A. (1992). The influence of backpack design on physical performance, *Ergonomics*, 35(1):149-157.

Jenkins, M. (1992). The Weekend Pack Test, *Backpacker*, October, pg 53-57.

Knapik, J., Harman, E., Reynolds, K. (1996). Load carriage using packs: A review of physiological, biomechanical and medical aspects, *Applied Ergonomics*, 27:207-16.

Legg, S.J., Ramsey, T, Knowles, D.J. (1992). The metabolic cost of backpack and shoulder load carriage, *Ergonomics*, 35(9):1063-8.

Legg, S.J., Mahanty, A. (1985). Comparison of five modes of carrying load close to the trunk, *Ergonomics*, 28(12):1653-60.

Luo, Z.P., L.J. Berglund and K.N An (1998). Validation of F-Scan Pressure Sensor System: A Technical Note, *Journal of Rehabilitation Research and Development*, 35:186-191.

MacNeil, S.K. (1996). Validation and Development of a Mathematical Model of the Shoulder for load Carriage, Master's Thesis, Queen's University, Kingston, ON.

MacNeil, S.K. Rigby, W.A. (1996). Determination of an appropriate substitute skin. Queen's University, Kingston, On. (unpublished).

McArdle, W.D., F. Katch, V. Katch (1996). Exercise Physiology: Energy, nutrition, and human performance, 4th, Ed., Williams & Wilkins, Maryland, USA.

McPoil, T.G.P.P.A., et al (1995). A Comparison of Two in-shoe plantar pressure measurement systems, *The Lower Extremity*, 2:95-103.

Morin, E, Reid, S.A, Bryant (1998). Research and Development of an Advanced Personal Load Carriage Measurement System, Phase IV: Section E Applicability of the F-Scan System for Humane Pressure Assessment, PWGSC Contract No. W7711-7-7420/A Report to the Defense and Civil Institute of Environmental Medicine.

Pelot, R.P., Pinter, J., Rigby, A., Bryant, J.T., Stevenson, J.M. (1998) Section F: Phase II of Parametric Analysis of Advanced Personal Load Carriage Systems. PWGSC Contract # W7711-7-7420/A (45 pgs).

Pelot, R.P., Rigby, A., Bryant, J.T., Stevenson, J.M. (1998) Section C: Phase II of a Biomechanical Model for Load Carriage Assessment. PWGSC Contract # W7711-7-7420/A (45 pgs).

Potter, D.W. (1998) AMTI (Boston, Mass.) Force Platform: a technical note. School of Physical and Health Education. Queen's University, Kingston, Ontario. (unpublished).

Raffan, J. (1995). Load Carriage Backgrounder. *Report for Ergonomics Research Group*, Queen's University. (unpublished).

Reid, S.A., Bryant, J.T., Morin E., Stevenson, J.M., Doan, J.E. (1999). Clothe the Soldier: Phase IIID: Effect of Back Pack Shoulder Strap Lower Attachment Point on the Load Distribution to the Torso, PWGSC Contract # W7711-7-7412/001/SRV, (29 pages).

Reid, S.A., Bryant, J.T., Morin E., Stevenson, J.M., Doan, J.E. (1999). Clothe the Soldier: Phase IIID: Effect of Lateral Rods and No Rods in the Suspension System of the Pack, PWGSC Contract # W7711-7-7412/001/SRV, (39 pages).

Reid, S.A., Doan, J, Bryant, J.T., Morin, E., Sui, D. (1997) Research and Development of an Advanced Personal Load Carriage System (Phases II and III) Section A: Futher Developemtn of Comprehensive Measurement Systems, PWGSC Contract #WW7711-5-7273/001/TOS, (42 pages).

Rigby, W.A. (1999). Development of a Biomechanical Model and Validation of Assessment Tools for Personal Load Carriage Systems, Master's Thesis, Queen's University, Kingston, ON.

Rigby, W.A., McNeil, S.K. (1996) Determination of an Appropriate Substitute Skin, Queen's University, Kingston, ON. (unpublished).

Sagiv, M, et al. (1994). Left Ventricular responses during prolonged treadmill walking with heavy load carriage, *Medicine and Science in Sports and Exercise*, 26:285-8.

Shimpo Instruments Inc. Website, www.shimpoinst.com

Stevenson, J.M., Bryant, J.T., Reid, S.A. and Pelot, R.P. (1996). Research and Development of an Advanced Personal Load Carriage System: Section D, Validation of the Load Carriage Simulator, PWGSC Contract No. W7711-7-7225/01-XSE Report to the Defence and Civil Institute of Environmental Medicine.

Stevenson, J.M., Bryant, J.T., Morin, E.L., Pelot, R.P., Reid, S.A., Doan, J.B. (1998). Research and Development of an Advanced Personal Load Carriage Measurement System, Phase IV, PWGSC Contract No. W7711-7-7420/A Report to the Defense and Civil Institute of Environmental Medicine.

Stevenson, J.M., Bryant, J.T., dePencier, R.D., Pelot, R.P., and Reid, J.G. (1995). Research and Development of an Advanced Personal Load Carriage System (Phase I-D). DSS Contract # W7711-4-7225/01-XSE (350 pgs).

Stewart, J, Ed.(1991). Calculus, Second Edition, Brooks/Cole Publishing Company, California.

Sumiya, T, Suzuki, Y., Kashahara, T., Ogata, H. (1998). Sensing Stability and Dynamic Response of the F-Scan in-shoe sensing system: a technical note, *J Rehabil Res Dev*, 35(2):186-91.

Tekscan F-Scan Pressure Assessment System, User's Manual. Tekscan, Inc, Boston, MA, 2000.

Wilke, H-J, Neef, P., Hinz, B., Seidel, H., Claes, L (1992). Intradiscal Pressure together with anthropometric data – a data set for the validation of models. *Clinical Biomechanics*, 16(1): S111-S126.

Woodburn, J. and P.S. Helliwell (1996). Observations on the F-Scan in-shoe pressure measuring system, *Clinical Biomechanics* 11:301-304.

Appendix A - Symmetrical Lower Torso Design

Anthropometric Data

Listed below are the anthropometric data necessary to construct the SLT physical model.

Dimensions from the 50th percentile male mannequin at the waist:
Circumference, C_m = 0.84 m
Width (Transverse plane) = 0.292m
Depth (Midsagittal plane) = 0.229m

Using the depth as the diameter for the ends:
$C_{ends} = \pi d$
C_{ends} = 0.719 m

For the lumbar and abdomen:
$C_m - C_{ends} = C_{LA}$
$C_{LA}/2$ = Width of lumbar section
C_{LA} = 0.121 m
$C_L = C_A$ = 0.0605 m

The width with these dimensions does not quite correspond with the current torso model, so 0.00125m was added to the sides for a better match.

Therefore, $C_L = C_A$ = 0.06175 m

The total circumference with these values is 0.8429 m.

The desired waist to hip ratio is 0.85.

$$\frac{W}{H} = 0.85$$
$$H = \frac{W}{0.85}$$
$$H = \frac{0.8429}{0.85}$$
$$H = 0.992\ m$$

Determination of the radius and angulation at the hips:

$$Circumference = 2\pi r + 2(side)$$
$$0.992 = 2\pi r + (0.1235)$$
$$r = 0.1382m$$

Waist to Hip Ratio Calculations

Mannequin	Waist (m)	Hip (m)	W-H distance	Ratio
50% F	0.792	0.967	0.18	0.8190279
5% F	0.636	0.806	0.19	0.7890819
50% M	0.862	0.984	0.21	0.8760163
95% M	0.966	1.072	0.22	0.9011194
			Average:	0.8463114

Waist to Hip Distance

Subject	distance (m)
1	0.235
2	0.182
3	0.196
4	0.214
5	0.22
6	0.184
7	0.198
8	0.204
9	0.195
10	0.194
Average:	0.2022

Calculation of SLT Measurements

50th % M

Circumference	0.84	m
Width	0.292	m
Depth	0.228	m
Height	0.3175	m

Depth as diameter of ends

d=	0.228	m
circ ends	0.716	m
Circ sides	0.124	m

Bocklite consideration: 3mm on all sides

d=	0.222	m
circ ends	0.6974336	m
circ sides	0.124	

Bottom no Bocklite

d=	0.333	m
circ ends	1.0461504	m
circ sides	0.124	

Total top	0.8214336	m
Hip (/0.85)	0.9663924	

RH Triangle for angle

h=	0.2	m
b=(diff/2)	0.0724794	m

Flare angle

arctan(h/b)	70.079627	

Appendix B - Mathematical Model Spreadsheets

Summary Sheet for Single Trial

Date: 10-May
Load: cdn belt N
Tension: N/A

			Force			Friction		
Sensor	Friction	Eff Area	X	Y	Z	fx	fy	fz
3	0.257	4.87056	-0.0338	28.9847	4.0760	0.0012	-1.0475	7.4536
5	0.257	4.5413	0.0000	-16.1095	2.2640	0.0000	0.5819	4.1401
6	0.257	4.821583	10.7179	-62.8996	9.0741	-0.3871	2.2734	16.5934
7	0.257	5.959539	-50.7786	-10.4442	8.1912	1.8341	-0.3772	14.9788
9	0.257	4.5066	-72.7495	-13.8913	12.6065	2.6276	-0.7351	23.0529
10	0.257	4.821583	-7.0958	-63.0574	9.0253	0.2560	2.2785	16.5041
12	0.257	4.262788	78.1762	-49.3790	14.0966	-2.8236	1.7835	25.7777
13	0.257	4.87056	3.3321	8.3025	1.2590	-0.1203	-0.2999	2.3023
14 (01)	0.257	4.4604	0.0000	39.6413	5.5712	0.0000	-1.4318	10.1878
15	0.257	5.843816	62.7379	-4.7702	9.7143	-2.2660	0.1723	17.7640

Sum			24.3063	-143.6227	75.8783	-0.8782	3.1980	138.7548

Total			23.4281	-140.4246	214.6331

Main Spreadsheet

Spreadsheet Input/Calculations

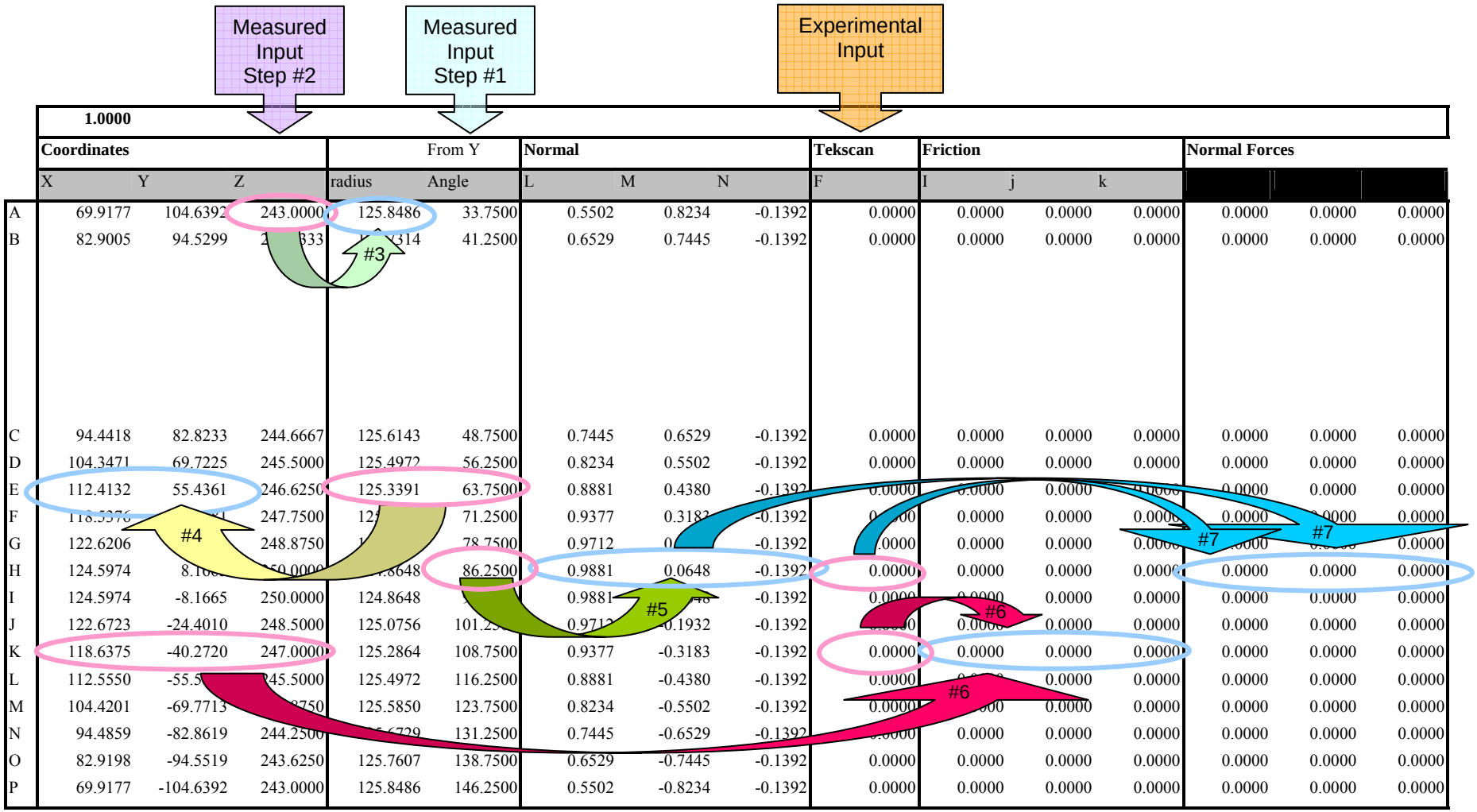

	Coordinates			From Y		Normal			Tekscan	Friction			Normal Forces		
	X	Y	Z	radius	Angle	L	M	N	F	I	j	k			
A	69.9177	104.6392	243.0000	125.8486	33.7500	0.5502	0.8234	-0.1392	0.0000	0.0000	0.0000	0.0000	0.0000	0.0000	0.0000
B	82.9005	94.5299	[illegible]	[illegible]	41.2500	0.6529	0.7445	-0.1392	0.0000	0.0000	0.0000	0.0000	0.0000	0.0000	0.0000
C	94.4418	82.8233	244.6667	125.6143	48.7500	0.7445	0.6529	-0.1392	0.0000	0.0000	0.0000	0.0000	0.0000	0.0000	0.0000
D	104.3471	69.7225	245.5000	125.4972	56.2500	0.8234	0.5502	-0.1392	0.0000	0.0000	0.0000	0.0000	0.0000	0.0000	0.0000
E	112.4132	55.4361	246.6250	125.3391	63.7500	0.8881	0.4380	-0.1392	0.0000	0.0000	0.0000	0.0000	0.0000	0.0000	0.0000
F	[illegible]	[illegible]	247.7500	125	71.2500	0.9377	0.3183	-0.1392	0.0000	0.0000	0.0000	0.0000	0.0000	0.0000	0.0000
G	122.6206	[illegible]	248.8750	[illegible]	78.7500	0.9712	0.1932	-0.1392	0.0000	0.0000	0.0000	0.0000	0.0000	0.0000	0.0000
H	124.5974	8.1665	250.0000	124.8648	86.2500	0.9881	0.0648	-0.1392	0.0000	0.0000	0.0000	0.0000	0.0000	0.0000	0.0000
I	124.5974	-8.1665	250.0000	124.8648	[illegible]	0.9881	[illegible]	-0.1392	0.0000	0.0000	0.0000	0.0000	0.0000	0.0000	0.0000
J	122.6723	-24.4010	248.5000	125.0756	101.25	0.9712	-0.1932	-0.1392	0.0000	0.0000	0.0000	0.0000	0.0000	0.0000	0.0000
K	118.6375	-40.2720	247.0000	125.2864	108.7500	0.9377	-0.3183	-0.1392	0.0000	0.0000	0.0000	0.0000	0.0000	0.0000	0.0000
L	112.5550	-55.5	245.5000	125.4972	116.2500	0.8881	-0.4380	-0.1392	0.0000	[illegible]	0.0000	0.0000	0.0000	0.0000	0.0000
M	104.4201	-69.7713	[illegible]	125.5850	123.7500	0.8234	-0.5502	-0.1392	0.0000	[illegible]	0.0000	0.0000	0.0000	0.0000	0.0000
N	94.4859	-82.8619	244.2500	[illegible]	131.2500	0.7445	-0.6529	-0.1392	[illegible]	0.0000	0.0000	0.0000	0.0000	0.0000	0.0000
O	82.9198	-94.5519	243.6250	125.7607	138.7500	0.6529	-0.7445	-0.1392	0.0000	0.0000	0.0000	0.0000	0.0000	0.0000	0.0000
P	69.9177	-104.6392	243.0000	125.8486	146.2500	0.5502	-0.8234	-0.1392	0.0000	0.0000	0.0000	0.0000	0.0000	0.0000	0.0000

0.0000	0.0000	0.0000	0.0000	0.0000	0.0000

Sum of Forces

N

Fx	Fy	Fz	fx	fy	fz
15.9993	-14.4713	-3.0585	-0.6071	0.5491	5.8759

Step 1: Angle from Y measured and input directly.
Step 2: Z-value measured from base of SLT and calculated with the angle on the top of SLT.
Step 3: Z-value used to calculate the radius.
Step 4: Radius and angle from Y used to calculate coordinates.
Step 5: Angle used to input normal unit vector (calculated previously).
Step 6: Coordinates and measured force used to calculate directional frictional components.
Step 7: Normal unit vectors and measured force used to calculate directional force components.

Main Spreadsheet – Single Sensor

	1.0000															
	Coordinates			From Y		**Normal**			**Tekscan**	**Friction**			**Normal Forces**			
	X	Y	Z	radius	Angle	L	M	N	F	I	j	k	I	j	k	
A	69.9177	104.6392	243.0000	125.8486	33.7500	0.5502	0.8234	0.1392	2.8566	-0.0568	-0.0850	0.7270	1.5716	2.3520	0.3976	
B	82.9005	94.5299	243.8333	125.7314	41.2500	0.6529	0.7445	0.1392	2.6000	-0.0613	-0.0699	0.6617	1.6976	1.9357	0.3618	
C	94.4418	82.8233	244.6667	125.6143	48.7500	0.7445	0.6529	0.1392	2.1925	-0.0590	-0.0517	0.5580	1.6324	1.4315	0.3051	
D	104.3471	69.7225	245.5000	125.4972	56.2500	0.8234	0.5502	0.1392	5.7943	-0.1723	-0.1151	1.4747	4.7709	3.1878	0.8064	
E	112.4132	55.4361	246.6250	125.3391	63.7500	0.8881	0.4380	0.1392	1.6223	-0.0520	-0.0257	0.4129	1.4408	0.7105	0.2258	
F	118.5376	40.2381	247.7500	125.1810	71.2500	0.9377	0.3183	0.1392	0.4923	-0.0167	-0.0057	0.1253	0.4616	0.1567	0.0685	
G	122.6206	24.3908	248.8750	125.0229	78.7500	0.9712	0.1932	0.1392	0.7464	-0.0262	-0.0052	0.1899	0.7249	0.1442	0.1039	
H	124.5974	8.1665	250.0000	124.8648	86.2500	0.9881	0.0648	0.1392	0.0000	0.0000	0.0000	0.0000	0.0000	0.0000	0.0000	
I	124.5974	-8.1665	250.0000	124.8648	93.7500	0.9881	-0.0648	0.1392	0.0000	0.0000	0.0000	0.0000	0.0000	0.0000	0.0000	
J	122.6723	-24.4010	248.5000	125.0756	101.2500	0.9712	-0.1932	0.1392	0.0000	0.0000	0.0000	0.0000	0.0000	0.0000	0.0000	
K	118.6375	-40.2720	247.0000	125.2864	108.7500	0.9377	-0.3183	0.1392	0.0000	0.0000	0.0000	0.0000	0.0000	0.0000	0.0000	
L	112.5550	-55.5060	245.5000	125.4972	116.2500	0.8881	-0.4380	0.1392	0.0000	0.0000	0.0000	0.0000	0.0000	0.0000	0.0000	
M	104.4201	-69.7713	244.8750	125.5850	123.7500	0.8234	-0.5502	0.1392	0.0000	0.0000	0.0000	0.0000	0.0000	0.0000	0.0000	
N	94.4859	-82.8619	244.2500	125.6729	131.2500	0.7445	-0.6529	0.1392	0.0000	0.0000	0.0000	0.0000	0.0000	0.0000	0.0000	
O	82.9198	-94.5519	243.6250	125.7607	138.7500	0.6529	-0.7445	0.1392	0.0000	0.0000	0.0000	0.0000	0.0000	0.0000	0.0000	
P	69.9177	-104.6392	243.0000	125.8486	146.2500	0.5502	-0.8234	0.1392	0.0000	0.0000	0.0000	0.0000	0.0000	0.0000	0.0000	
										-0.4443	-0.3582	4.1494	12.2998	9.9185	2.2691	

Sum of Forces

N

Fx	Fy	Fz	fx	fy	fz
27.3370	11.1622	5.1349	-0.9874	-0.4032	9.3900

2.0000															
Coordinates					**Normal**			**Tekscan**	**Friction**			**Normal Forces**			
X	Y	Z	radius	Angle	L	M	N	F	I	j	k	I	j	k	
72.2330	105.0996	231.0460	127.5286	34.5000	0.5609	0.8161	0.1392	3.0731	-0.0623	-0.0906	0.7821	1.7237	2.5080	0.4277	
85.0870	94.8310	231.9061	127.4077	41.9000	0.6613	0.7371	0.1392	3.0731	-0.0734	-0.0818	0.7821	2.0323	2.2651	0.4277	
96.5005	83.0035	232.7662	127.2868	49.3000	0.7508	0.6458	0.1392	1.8085	-0.0490	-0.0422	0.4603	1.3577	1.1678	0.2517	
106.2862	69.8170	233.6263	127.1659	56.7000	0.8277	0.5437	0.1392	2.0409	-0.0610	-0.0401	0.5194	1.6892	1.1096	0.2840	
114.2549	55.4792	234.7197	127.0123	64.1000	0.8908	0.4326	0.1392	0.0000	0.0000	0.0000	0.0000	0.0000	0.0000	0.0000	
120.3030	40.2528	235.8131	126.8586	71.5000	0.9391	0.3142	0.1392	0.0000	0.0000	0.0000	0.0000	0.0000	0.0000	0.0000	
124.3346	24.3935	236.9066	126.7049	78.9000	0.9717	0.1906	0.1392	0.0000	0.0000	0.0000	0.0000	0.0000	0.0000	0.0000	
126.2875	8.1666	238.0000	126.5513	86.3000	0.9882	0.0639	0.1392	0.0000	0.0000	0.0000	0.0000	0.0000	0.0000	0.0000	
126.2875	-8.1666	238.0000	126.5513	93.7000	0.9882	-0.0639	0.1392	0.0000	0.0000	0.0000	0.0000	0.0000	0.0000	0.0000	
124.3760	-24.4016	236.6066	126.7471	101.1000	0.9717	-0.1906	0.1392	0.0000	0.0000	0.0000	0.0000	0.0000	0.0000	0.0000	
120.3830	-40.2796	235.2131	126.9429	108.5000	0.9391	-0.3142	0.1392	0.0000	0.0000	0.0000	0.0000	0.0000	0.0000	0.0000	
114.3687	-55.5344	233.8197	127.1388	115.9000	0.8908	-0.4326	0.1392	1.0322	-0.0332	0.0161	0.2627	0.9195	-0.4465	0.1437	
106.3450	-69.8556	233.1263	127.2362	123.3000	0.8277	-0.5437	0.1392	0.0000	0.0000	0.0000	0.0000	0.0000	0.0000	0.0000	
96.5360	-83.0341	232.4329	127.3337	130.7000	0.7508	-0.6458	0.1392	0.0000	0.0000	0.0000	0.0000	0.0000	0.0000	0.0000	
85.1027	-94.8485	231.7394	127.4311	138.1000	0.6613	-0.7371	0.1392	0.0000	0.0000	0.0000	0.0000	0.0000	0.0000	0.0000	
72.2330	-105.0996	231.0460	127.5286	145.5000	0.5609	-0.8161	0.1392	0.0000	0.0000	0.0000	0.0000	0.0000	0.0000	0.0000	
									-0.2789	-0.2385	2.8066	7.7225	6.6040	1.5348	

3.0000															
Coordinates					**Normal**			**Tekscan**	**Friction**			**Normal Forces**			
X	Y	Z	radius	Angle	L	M	N	F	I	j	k	I	j	k	
74.5721	105.5171	219.0920	129.2086	35.2500	0.5715	0.8087	0.1392	0.0000	0.0000	0.0000	0.0000	0.0000	0.0000	0.0000	
87.2909	95.0945	219.9789	129.0840	42.5500	0.6697	0.7295	0.1392	0.0000	0.0000	0.0000	0.0000	0.0000	0.0000	0.0000	
98.5712	83.1518	220.8657	128.9593	49.8500	0.7569	0.6385	0.1392	0.0000	0.0000	0.0000	0.0000	0.0000	0.0000	0.0000	
108.2332	69.8853	221.7526	128.8347	57.1500	0.8319	0.5372	0.1392	0.0000	0.0000	0.0000	0.0000	0.0000	0.0000	0.0000	
116.1012	55.5019	222.8144	128.6855	64.4500	0.8934	0.4271	0.1392	0.0000	0.0000	0.0000	0.0000	0.0000	0.0000	0.0000	
122.0707	40.2529	223.8763	128.5362	71.7500	0.9405	0.3101	0.1392	0.0000	0.0000	0.0000	0.0000	0.0000	0.0000	0.0000	
126.0495	24.3874	224.9381	128.3870	79.0500	0.9722	0.1881	0.1392	0.0000	0.0000	0.0000	0.0000	0.0000	0.0000	0.0000	
127.9776	8.1638	226.0000	128.2377	86.3500	0.9883	0.0630	0.1392	0.0000	0.0000	0.0000	0.0000	0.0000	0.0000	0.0000	
127.9776	-8.1638	226.0000	128.2377	93.6500	0.9883	-0.0630	0.1392	0.0000	0.0000	0.0000	0.0000	0.0000	0.0000	0.0000	
126.0805	-24.3934	224.7131	128.4186	100.9500	0.9722	-0.1881	0.1392	0.6987	-0.0245	0.0047	0.1778	0.6793	-0.1314	0.0972	
122.1308	-40.2727	223.4263	128.5995	108.2500	0.9405	-0.3101	0.1392	1.0322	-0.0351	0.0116	0.2627	0.9707	-0.3201	0.1437	
116.1868	-55.5428	222.1394	128.7803	115.5500	0.8934	-0.4271	0.1392	0.6987	-0.0225	0.0108	0.1778	0.6242	-0.2984	0.0972	
108.2775	-69.9139	221.3776	128.8874	122.8500	0.8319	-0.5372	0.1392	0.6987	-0.0210	0.0136	0.1778	0.5813	-0.3753	0.0972	
98.5981	-83.1745	220.6157	128.9945	130.1500	0.7569	-0.6385	0.1392	1.0322	-0.0282	0.0238	0.2627	0.7813	-0.6591	0.1437	
87.3028	-95.1075	219.8539	129.1015	137.4500	0.6697	-0.7295	0.1392	1.3353	-0.0323	0.0352	0.3398	0.8942	-0.9742	0.1858	
74.5721	-105.5171	219.0920	129.2086	144.7500	0.5715	-0.8087	0.1392	0.0000	0.0000	0.0000	0.0000	0.0000	0.0000	0.0000	
									-0.1637	0.0996	1.3987	4.5311	-2.7585	0.7649	

4.0000															
Coordinates					**Normal**			**Tekscan**	**Friction**			**Normal Forces**			
X	Y	Z	radius	Angle	L	M	N	F	I	j	k	I	j	k	
76.9344	105.8911	207.1380	130.8886	36.0000	0.5821	0.8011	0.1392	0.0000	0.0000	0.0000	0.0000	0.0000	0.0000	0.0000	
89.5115	95.3201	208.0516	130.7602	43.2000	0.6779	0.7219	0.1392	0.0000	0.0000	0.0000	0.0000	0.0000	0.0000	0.0000	
100.6536	83.2679	208.9652	130.6318	50.4000	0.7630	0.6312	0.1392	0.0000	0.0000	0.0000	0.0000	0.0000	0.0000	0.0000	
110.1877	69.9272	209.8789	130.5034	57.6000	0.8361	0.5306	0.1392	0.0000	0.0000	0.0000	0.0000	0.0000	0.0000	0.0000	
117.9520	55.5040	210.9091	130.3586	64.8000	0.8960	0.4216	0.1392	0.0000	0.0000	0.0000	0.0000	0.0000	0.0000	0.0000	
123.8407	40.2383	211.9394	130.2138	72.0000	0.9418	0.3060	0.1392	0.0000	0.0000	0.0000	0.0000	0.0000	0.0000	0.0000	
127.7652	24.3725	212.9697	130.0690	79.2000	0.9727	0.1856	0.1392	0.0000	0.0000	0.0000	0.0000	0.0000	0.0000	0.0000	
129.6679	8.1580	214.0000	129.9242	86.4000	0.9883	0.0622	0.1392	0.0000	0.0000	0.0000	0.0000	0.0000	0.0000	0.0000	
129.6679	-8.1580	214.0000	129.9242	93.6000	0.9883	-0.0622	0.1392	0.0000	0.0000	0.0000	0.0000	0.0000	0.0000	0.0000	
127.7859	-24.3765	212.8197	130.0901	100.8000	0.9727	-0.1856	0.1392	0.0000	0.0000	0.0000	0.0000	0.0000	0.0000	0.0000	
123.8808	-40.2513	211.6394	130.2560	108.0000	0.9418	-0.3060	0.1392	0.0000	0.0000	0.0000	0.0000	0.0000	0.0000	0.0000	
118.0092	-55.5309	210.4591	130.4219	115.2000	0.8960	-0.4216	0.1392	0.0000	0.0000	0.0000	0.0000	0.0000	0.0000	0.0000	
110.2174	-69.9461	209.6289	130.5386	122.4000	0.8361	-0.5306	0.1392	0.0000	0.0000	0.0000	0.0000	0.0000	0.0000	0.0000	
100.6716	-83.2828	208.7986	130.6553	129.6000	0.7630	-0.6312	0.1392	0.0000	0.0000	0.0000	0.0000	0.0000	0.0000	0.0000	
89.5196	-95.3286	207.9683	130.7719	136.8000	0.6779	-0.7219	0.1392	2.3928	-0.0586	0.0624	0.6090	1.6220	-1.7273	0.3330	
76.9344	-105.8911	207.1380	130.8886	144.0000	0.5821	-0.8011	0.1392	1.1989	-0.0252	0.0347	0.3051	0.6979	-0.9605	0.1669	
									-0.0838	0.0971	0.9141	2.3199	-2.6878	0.4999	

5.0000															
Coordinates					**Normal**			**Tekscan**	**Friction**			**Normal Forces**			
X	Y	Z	radius	Angle	L	M	N	F	I	j	k	I	j	k	
79.3191	106.2211	195.1840	132.5687	36.7500	0.5925	0.7935	0.1392	0.0000	0.0000	0.0000	0.0000	0.0000	0.0000	0.0000	
91.7484	95.5074	196.1244	132.4365	43.8500	0.6860	0.7141	0.1392	0.0000	0.0000	0.0000	0.0000	0.0000	0.0000	0.0000	
102.7471	83.3515	197.0648	132.3043	50.9500	0.7690	0.6239	0.1392	0.0000	0.0000	0.0000	0.0000	0.0000	0.0000	0.0000	
112.1494	69.9427	198.0051	132.1722	58.0500	0.8403	0.5240	0.1392	0.0000	0.0000	0.0000	0.0000	0.0000	0.0000	0.0000	
119.8071	55.4856	199.0039	132.0318	65.1500	0.8986	0.4162	0.1392	0.0000	0.0000	0.0000	0.0000	0.0000	0.0000	0.0000	
125.6129	40.2090	200.0026	131.8914	72.2500	0.9431	0.3019	0.1392	0.0000	0.0000	0.0000	0.0000	0.0000	0.0000	0.0000	
129.4816	24.3488	201.0013	131.7511	79.3500	0.9732	0.1830	0.1392	0.0000	0.0000	0.0000	0.0000	0.0000	0.0000	0.0000	
131.3582	8.1493	202.0000	131.6107	86.4500	0.9884	0.0613	0.1392	0.0000	0.0000	0.0000	0.0000	0.0000	0.0000	0.0000	
131.3582	-8.1493	202.0000	131.6107	93.5500	0.9884	-0.0613	0.1392	0.0000	0.0000	0.0000	0.0000	0.0000	0.0000	0.0000	
129.4920	-24.3507	200.9263	131.7616	100.6500	0.9732	-0.1830	0.1392	0.0000	0.0000	0.0000	0.0000	0.0000	0.0000	0.0000	
125.6329	-40.2154	199.8526	131.9125	107.7500	0.9431	-0.3019	0.1392	0.0000	0.0000	0.0000	0.0000	0.0000	0.0000	0.0000	
119.8358	-55.4989	198.7789	132.0634	114.8500	0.8986	-0.4162	0.1392	0.0000	0.0000	0.0000	0.0000	0.0000	0.0000	0.0000	
112.1643	-69.9520	197.8801	132.1897	121.9500	0.8403	-0.5240	0.1392	0.0000	0.0000	0.0000	0.0000	0.0000	0.0000	0.0000	
102.7562	-83.3589	196.9814	132.3160	129.0500	0.7690	-0.6239	0.1392	0.0000	0.0000	0.0000	0.0000	0.0000	0.0000	0.0000	
91.7525	-95.5116	196.0827	132.4423	136.1500	0.6860	-0.7141	0.1392	0.0000	0.0000	0.0000	0.0000	0.0000	0.0000	0.0000	
79.3191	-106.2211	195.1840	132.5687	143.2500	0.5925	-0.7935	0.1392	0.0000	0.0000	0.0000	0.0000	0.0000	0.0000	0.0000	
									0.0000	0.0000	0.0000	0.0000	0.0000	0.0000	

6.0000

Coordinates					Normal			Tekscan	Friction			Normal Forces		
X	Y	Z	radius	Angle	L	M	N	F	I	j	k	I	j	k
81.7254	106.5066	183.2300	134.2487	37.5000	0.6028	0.7856	0.1392	0.0000	0.0000	0.0000	0.0000	0.0000	0.0000	0.0000
94.0009	95.6560	184.1971	134.1128	44.5000	0.6941	0.7063	0.1392	0.0000	0.0000	0.0000	0.0000	0.0000	0.0000	0.0000
104.8514	83.4025	185.1643	133.9768	51.5000	0.7750	0.6165	0.1392	0.0000	0.0000	0.0000	0.0000	0.0000	0.0000	0.0000
114.1181	69.9317	186.1314	133.8409	58.5000	0.8443	0.5174	0.1392	0.0000	0.0000	0.0000	0.0000	0.0000	0.0000	0.0000
121.6664	55.4466	187.0986	133.7050	65.5000	0.9011	0.4107	0.1392	0.0000	0.0000	0.0000	0.0000	0.0000	0.0000	0.0000
127.3871	40.1650	188.0657	133.5691	72.5000	0.9444	0.2978	0.1392	0.0000	0.0000	0.0000	0.0000	0.0000	0.0000	0.0000
131.1988	24.3163	189.0329	133.4331	79.5000	0.9737	0.1805	0.1392	0.4764	-0.0168	-0.0031	0.1212	0.4639	0.0860	0.0663
133.0486	8.1376	190.0000	133.2972	86.5000	0.9884	0.0605	0.1392	0.0000	0.0000	0.0000	0.0000	0.0000	0.0000	0.0000
133.0486	-8.1376	190.0000	133.2972	93.5000	0.9884	-0.0605	0.1392	0.0000	0.0000	0.0000	0.0000	0.0000	0.0000	0.0000
131.1988	-24.3163	189.0329	133.4331	100.5000	0.9737	-0.1805	0.1392	0.0000	0.0000	0.0000	0.0000	0.0000	0.0000	0.0000
127.3871	-40.1650	188.0657	133.5691	107.5000	0.9444	-0.2978	0.1392	0.0000	0.0000	0.0000	0.0000	0.0000	0.0000	0.0000
121.6664	-55.4466	187.0986	133.7050	114.5000	0.9011	-0.4107	0.1392	0.0000	0.0000	0.0000	0.0000	0.0000	0.0000	0.0000
114.1181	-69.9317	186.1314	133.8409	121.5000	0.8443	-0.5174	0.1392	0.0000	0.0000	0.0000	0.0000	0.0000	0.0000	0.0000
104.8514	-83.4025	185.1643	133.9768	128.5000	0.7750	-0.6165	0.1392	0.0000	0.0000	0.0000	0.0000	0.0000	0.0000	0.0000
94.0009	-95.6560	184.1971	134.1128	135.5000	0.6941	-0.7063	0.1392	0.0000	0.0000	0.0000	0.0000	0.0000	0.0000	0.0000
81.7254	-106.5066	183.2300	134.2487	142.5000	0.6028	-0.7856	0.1392	0.0000	0.0000	0.0000	0.0000	0.0000	0.0000	0.0000
									-0.0168	-0.0031	0.1212	0.4639	0.0860	0.0663

Normal Planes

Lumbar and Abdomen Area

Normal Plane - Lumbar								
Intercepts								
					For Friction:			
	X	Y	Z		X	Y	Z	
A1	30	122.4053	267.5		0	0	1138.459	
H3	6	134.70263	180		0	-122.4053	267.5000	
M5	-18	143.48643	117.5					
(H3-A1)U	-24	12.297323	-87.5		0	122.4053	870.959	
(M5-A1)V	-48	21.081125	-150					
					0	**0.1391731**	**0.9902681**	
U X V	1.819E-12	600	84.324501					
Normal Unit	**3.002E-15**	**0.9902681**	**0.1391731**					

Normal Plane - Abdomen				
Intercepts				
	X	Y	Z	
A1	-30.0000	-122.4053	267.5000	
H3	-6	-134.70263	180	
M5	18	-143.48643	117.5	
(H3-A1)U	24	-12.297323	-87.5	
(M5-A1)V	48	-21.081125	-150	
U X V	-1.819E-12	-600	84.324501	
Normal Unit	**-3.002E-15**	**-0.9902681**	**0.1391731**	

Sample data set – Normal plane calculation

Sample Data Set:

For:

$$\theta = 12^o$$
$$r = 161mm$$

Coordinates of the point:

$$x = r\cos\theta$$
$$x = (161)\cos(12)$$
$$x = 157.5mm$$

$$y = r\sin\theta$$
$$y = (161)\sin(12)$$
$$y = 33.47mm$$

The coordinates of point 'P' are (157.5, 33.47)

Tangent line at point P:

$$x^2 + y^2 = r^2$$
$$x^2 + y^2 = (161)$$

Using implicit differentiation:

$$2x + 2yy' = 0$$
$$yy' = -x$$
$$y' = -\frac{x}{y} = m$$
$$m = -(\frac{157.5}{33.47})$$
$$m = -4.7$$

Using the point-slope form:

$$(y - y_0) = (m)(x - x_0)$$
$$(y - 33.5) = (-4.7)(x - 157.5)$$

For the x-intercept, set y=0

$$(y-33.5)=(-4.7)(x-157.5)$$
$$(0-33.5)=(-4.7)(x-157.5)$$
$$x=164.6$$

For the y-intercept, set x=0

$$(y-33.5)=(-4.7)(x-157.5)$$
$$(y-33.5)=(-4.7)(0-157.5)$$
$$y=773.8$$

Therefore the three intercepts of the resulting plane where $\theta=12^{o}$ are:

$$A=(164.6,0,0)$$
$$B=(0,773.8,0)$$
$$C=(0,0,1145.6)$$

$$\vec{u}=B-A$$
$$\vec{u}=((0-164.6),(773.8-0),(0-0)$$
$$\vec{u}=(-164.6,773.8,0)$$

$$\vec{v}=C-A$$
$$\vec{v}=((0-164.6),(0-0),(1145.6-0))$$
$$\vec{v}=(-164.6,0,1145.6)$$

$$\vec{n}=\vec{u}\times\vec{v}$$
$$\vec{n}=((773.8*1145.6-0*0),(0*0-(-164.6*1145.6)),(-164.6*0-(773.8*(-164.6))))$$
$$\vec{n}=(886465.3,188565.8,127367.5)$$

Unitvector :

$$\vec{n}=(0.97,0.21,0.14)$$

For z=0																										
		A													U			V								
r=		160	mm		Tangent intercepts										Vector						cross product			unit vector		
		Coordinates			X			Y			Z			XY			XZ									
Angle (from y)	radians	X	Y	Z	X	Y	Z	X	Y	Z	X	Y	Z											x	y	z
0	0	0	160	0	#DIV/0!	0	0	0	160	0	0	0	1138.5	#DIV/0!	160	0	#DIV/0!	0	1138.46	182153	#DIV/0!	####	#DIV/0!	#DIV/0!	#DIV/0!
1	0.017453	2.7924	159.98	0	9167.8	0	0	0	160	0	0	0	1138.5	-9167.8	160.02	0	-9167.79	0	1138.46	182181	-1E+07	1E+06	0.0173	-0.99	0.1392
2	0.034907	5.5839	159.9	0	4584.6	0	0	0	160.1	0	0	0	1138.5	-4584.6	160.1	0	-4584.59	0	1138.46	182264	-5E+06	7E+05	0.0346	-0.99	0.1392
3	0.05236	8.3738	159.78	0	3057.2	0	0	0	160.2	0	0	0	1138.5	-3057.2	160.22	0	-3057.17	0	1138.46	182403	-3E+06	5E+05	0.0518	-0.989	0.1392
4	0.069813	11.161	159.61	0	2293.7	0	0	0	160.4	0	0	0	1138.5	-2293.7	160.39	0	-2293.69	0	1138.46	182598	-3E+06	4E+05	0.0691	-0.988	0.1392
39.75	0.693768	102.31	123.01	0	250.22	0	0	0	208.1	0	0	0	1138.5	-250.22	208.11	0	-250.219	0	1138.46	236919	-284864	52072	0.6332	-0.761	0.1392
46.45	0.810705	115.96	110.24	0	220.76	0	0	0	232.2	0	0	0	1138.5	-220.76	232.22	0	-220.759	0	1138.46	264379	-251325	51266	0.7177	-0.682	0.1392
53.15	0.927642	128.03	95.956	0	199.95	0	0	0	266.8	0	0	0	1138.5	-199.95	266.79	0	-199.948	0	1138.46	303730	-227633	53344	0.7924	-0.594	0.1392
59.85	1.04458	138.35	80.362	0	185.03	0	0	0	318.6	0	0	0	1138.5	-185.03	318.56	0	-185.032	0	1138.46	362664	-210652	58943	0.8563	-0.497	0.1392
66.55	1.161517	146.79	63.672	0	174.4	0	0	0	402.1	0	0	0	1138.5	-174.4	402.06	0	-174.404	0	1138.46	457731	-198552	70121	0.9085	-0.394	0.1392
73.25	1.278454	153.21	46.111	0	167.09	0	0	0	555.2	0	0	0	1138.5	-167.09	555.18	0	-167.089	0	1138.46	632047	-190224	92764	0.9483	-0.285	0.1392
79.95	1.395391	157.54	27.921	0	162.49	0	0	0	916.9	0	0	0	1138.5	-162.49	916.87	0	-162.493	0	1138.46	1043814	-184992	1E+05	0.9751	-0.173	0.1392
86.65	1.512328	159.73	9.3496	0	160.27	0	0	0	2738	0	0	0	1138.5	-160.27	2738.1	0	-160.274	0	1138.46	3117186	-182465	4E+05	0.9886	-0.058	0.1392
93.35	1.629265	159.73	-9.35	0	160.27	0	0	0	-2738	0	0	0	1138.5	-160.27	-2738	0	-160.274	0	1138.46	-3E+06	-182465	-4E+05	-0.989	-0.058	-0.1392
100.05	1.746202	157.54	-27.92	0	162.49	0	0	0	-917	0	0	0	1138.5	-162.49	-916.9	0	-162.493	0	1138.46	-1E+06	-184992	-1E+05	-0.975	-0.173	-0.1392
106.75	1.863139	153.21	-46.11	0	167.09	0	0	0	-555	0	0	0	1138.5	-167.09	-555.2	0	-167.089	0	1138.46	-632047	-190224	-92764	-0.948	-0.285	-0.1392
113.45	1.980076	146.79	-63.67	0	174.4	0	0	0	-402	0	0	0	1138.5	-174.4	-402.1	0	-174.404	0	1138.46	-457731	-198552	-70121	-0.908	-0.394	-0.1392
120.15	2.097013	138.35	-80.36	0	185.03	0	0	0	-319	0	0	0	1138.5	-185.03	-318.6	0	-185.032	0	1138.46	-362664	-210652	-58943	-0.856	-0.497	-0.1392
126.85	2.21395	128.03	-95.96	0	199.95	0	0	0	-267	0	0	0	1138.5	-199.95	-266.8	0	-199.948	0	1138.46	-303730	-227633	-53344	-0.792	-0.594	-0.1392
133.55	2.330887	115.96	-110.2	0	220.76	0	0	0	-232	0	0	0	1138.5	-220.76	-232.2	0	-220.759	0	1138.46	-264379	-251325	-51266	-0.718	-0.682	-0.1392
140.25	2.447824	102.31	-123	0	250.22	0	0	0	-208	0	0	0	1138.5	-250.22	-208.1	0	-250.219	0	1138.46	-236919	-284864	-52072	-0.633	-0.761	-0.1392
146.95	2.564761	87.259	-134.1	0	293.38	0	0	0	-191	0	0	0	1138.5	-293.38	-190.9	0	-293.378	0	1138.46	-217316	-333999	-56002	-0.54	-0.83	-0.1392
153.65	2.681698	71.017	-143.4	0	360.48	0	0	0	-179	0	0	0	1138.5	-360.48	-178.6	0	-360.479	0	1138.46	-203274	-410391	-64364	-0.44	-0.887	-0.1392
160.35	2.798635	53.804	-150.7	0	475.8	0	0	0	-170	0	0	0	1138.5	-475.8	-169.9	0	-475.803	0	1138.46	-193417	-541682	-80836	-0.333	-0.933	-0.1392
167.05	2.915573	35.856	-155.9	0	713.96	0	0	0	-164	0	0	0	1138.5	-713.96	-164.2	0	-713.965	0	1138.46	-186907	-812820	-1E+05	-0.222	-0.965	-0.1392
173.75	3.03251	17.419	-159	0	1469.7	0	0	0	-161	0	0	0	1138.5	-1469.7	-161	0	-1469.68	0	1138.46	-183243	-2E+06	-2E+05	-0.108	-0.984	-0.1392
180.45	3.149447	-1.2566	-160	0	-20372	0	0	0	-160	0	0	0	1138.5	20372	-160	0	20372.04	0	1138.46	-182159	2.3E+07	3E+06	-0.008	0.9902	0.1392
187.15	3.266384	-19.915	-158.8	0	-1285.5	0	0	0	-161	0	0	0	1138.5	1285.48	-161.3	0	1285.477	0	1138.46	-183581	1463463	2E+05	-0.123	0.9826	0.1392

193.85	3.383321	-38.301	-155.3	0	-668.39	0	0	0	-165	0	0	0	1138.5	668.391	-164.8	0	668.391	0	1138.46	-187608	760936	1E+05	-0.237	0.9615	0.1392
200.55	3.500258	-56.164	-149.8	0	-455.81	0	0	0	-171	0	0	0	1138.5	455.808	-170.9	0	455.8084	0	1138.46	-194532	518919	77886	-0.348	0.9273	0.1392
207.25	3.617195	-73.26	-142.2	0	-349.44	0	0	0	-180	0	0	0	1138.5	349.441	-180	0	349.4412	0	1138.46	-204893	397825	62890	-0.453	0.8804	0.1392
213.95	3.734132	-89.355	-132.7	0	-286.5	0	0	0	-193	0	0	0	1138.5	286.497	-192.9	0	286.4974	0	1138.46	-219588	326166	55260	-0.553	0.8215	0.1392
220.65	3.851069	-104.23	-121.4	0	-245.61	0	0	0	-211	0	0	0	1138.5	245.611	-210.9	0	245.611	0	1138.46	-240085	279618	51796	-0.645	0.7513	0.1392
227.35	3.968006	-117.68	-108.4	0	-217.54	0	0	0	-236	0	0	0	1138.5	217.537	-236.2	0	217.5373	0	1138.46	-268854	247657	51373	-0.728	0.6709	0.1392
234.05	4.084943	-129.52	-93.93	0	-197.65	0	0	0	-273	0	0	0	1138.5	197.646	-272.5	0	197.6456	0	1138.46	-310271	225011	53865	-0.802	0.5814	0.1392
240.75	4.201188	-139.6	-78.18	0	-183.38	0	0	0	-327	0	0	0	1138.5	183.382	-327.5	0	183.3819	0	1138.46	-372791	208773	60049	-0.864	0.4839	0.1392
247.45	4.318817	-147.77	-61.36	0	-173.25	0	0	0	-417	0	0	0	1138.5	173.245	-417.2	0	173.2454	0	1138.46	-474989	197233	72282	-0.915	0.3798	0.1392
254.15	4.435754	-153.92	-43.7	0	-166.32	0	0	0	-586	0	0	0	1138.5	166.324	-585.8	0	166.3236	0	1138.46	-666936	189353	97436	-0.953	0.2705	0.1392
260.85	4.552691	-157.96	-25.44	0	-162.06	0	0	0	-1006	0	0	0	1138.5	162.062	-1006	0	162.0622	0	1138.46	-1E+06	184501	2E+05	-0.978	0.1575	0.1392
267.55	4.669628	-159.85	-6.84	0	-160.15	0	0	0	-3743	0	0	0	1138.5	160.146	-3743	0	160.1464	0	1138.46	-4E+06	182320	6E+05	-0.989	0.0423	0.1392
274.25	4.786565	-159.56	11.857	0	-160.44	0	0	0	2159	0	0	0	1138.5	160.441	2159	0	160.4412	0	1138.46	2457930	182656	-3E+05	0.9875	0.0734	-0.1392
280.95	4.903503	-157.09	30.392	0	-162.97	0	0	0	842.3	0	0	0	1138.5	162.967	842.32	0	162.9671	0	1138.46	958943	185531	-1E+05	0.9722	0.1881	-0.1392
287.65	5.02044	-152.47	48.512	0	-167.9	0	0	0	527.7	0	0	0	1138.5	167.904	527.7	0	167.9038	0	1138.46	600767	191152	-88603	0.9437	0.3003	-0.1392
294.35	5.137377	-145.77	65.97	0	-175.62	0	0	0	388.1	0	0	0	1138.5	175.623	388.06	0	175.6227	0	1138.46	441788	199939	-68152	0.9022	0.4083	-0.1392
301.05	5.254314	-137.07	82.526	0	-186.76	0	0	0	310.2	0	0	0	1138.5	186.759	310.21	0	186.7593	0	1138.46	353157	212618	-57934	0.8484	0.5108	-0.1392
307.75	5.371251	-126.51	97.955	0	-202.36	0	0	0	261.3	0	0	0	1138.5	202.355	261.35	0	202.355	0	1138.46	297531	230373	-52884	0.783	0.6063	-0.1392
314.45	5.488188	-114.22	112.05	0	-224.13	0	0	0	228.5	0	0	0	1138.5	224.133	228.48	0	224.133	0	1138.46	260113	255166	-51209	0.7069	0.6935	-0.1392
321.15	5.605125	-100.37	124.61	0	-255.07	0	0	0	205.4	0	0	0	1138.5	255.068	205.45	0	255.068	0	1138.46	233893	290385	-52403	0.6212	0.7712	-0.1392
327.85	5.722062	-85.142	135.47	0	-300.67	0	0	0	189	0	0	0	1138.5	300.674	188.98	0	300.6741	0	1138.46	215144	342305	-56821	0.527	0.8384	-0.1392
334.55	5.838999	-68.756	144.47	0	-372.33	0	0	0	177.2	0	0	0	1138.5	372.333	177.19	0	372.3326	0	1138.46	201729	423885	-65975	0.4255	0.8942	-0.1392
341.25	5.955936	-51.43	151.51	0	-497.76	0	0	0	169	0	0	0	1138.5	497.761	168.97	0	497.7609	0	1138.46	192362	566680	-84105	0.3183	0.9377	-0.1392
347.95	6.072873	-33.402	156.47	0	-766.41	0	0	0	163.6	0	0	0	1138.5	766.411	163.6	0	766.4112	0	1138.46	186258	872528	-1E+05	0.2067	0.9684	-0.1392
354.65	6.18981	-14.918	159.3	0	-1716	0	0	0	160.7	0	0	0	1138.5	1716.01	160.7	0	1716.011	0	1138.46	182950	195360	-3E+05	0.0923	0.986	-0.1392
361.35	6.306747	3.7696	159.96	0	6791.2	0	0	0	160	0	0	0	1138.5	-6791.2	160.04	0	-6791.24	0	1138.46	182204	-8E+06	1E+06	0.0233	-0.99	0.1392

Appendix C - Data Acquisition Procedures

A) Force Plate

The raw voltage data were obtained from the acquisition software. The output was in six columns, representing Fx, Fy, Fz, Mx, My, and Mz. The average value for 400 points, measured at 50Hz, was calculated for each of the six measurements. These values were imported into an Excel spreadsheet.

The baseline data were obtained with the acquisition of a data file measuring the forces applied by the SLT and the frame on the load cell, with all instrumentation affixed, but with no external forces applied.
The calibration or baseline file was subtracted from the averages to reduce the effects of noise and baseline inequalities. The calibrated voltages were then converted to forces with the application of conversion formulas and corresponding sensitivity values, designated by the manufacturer, for each measured voltage.

For conversion to Newtons from the given voltage, the following equation was used:

$$\mathbf{V_o = 0.000001 \times S \times V_{exc} \times G \times Input}$$

Where:

V_o= the output voltage from the amplifier used
0.000001= volts/micro-volt, units for sensitivity
S= the sensitivity
V_{exc}= the bridge excitation voltage
G= the amplifier gain
Input= the input force or moment

Rearranging the equation to solve for the input force or moment:

$$Input = \frac{V_0}{0.000001 \times S \times V_{exc} \times G}$$

Where:

Excitation voltage = 10V
Gain = 4000
Sensitivities:

$$F_x = 1.526 \frac{Microvolts/Volt}{Pound}$$

$$F_y = 1.526 \frac{Microvolts/Volt}{Pound}$$

$$F_z = 0.389 \frac{Microvolts/Volt}{Pound}$$

$$M_x = 0.496 \frac{Microvolts/Volt}{Pound}$$

$$M_y = 0.696 \frac{Microvolts/Volt}{Pound}$$
$$M_z = 1.134 \frac{Microvolts/Volt}{Pound}$$

The measured forces Fx, Fy, and Fz were resolved to a single resultant force. The moments were used to calculate the coordinates of the applied force.

$$M_x = F_y \times y$$
$$M_y = F_z \times z$$
$$M_z = F_x \times x$$

Where x,y,z are the coordinates of the applied resultant force. These coordinates were compared to the estimated point of application measured on the SLT.

A2) Centre of Pressure Calculations

The calculated COP coordinates (x,y) for a force platform are as follows:

$$COP(x) = \left[\frac{M_y + (Z_{off} \times F_x)}{F_z} \right] \times (-1)$$
$$COP(y) = \left[\frac{M_x + (Z_{off} \times F_y)}{F_z} \right] \times (-1)$$

where:
COP(x) = The x coordinate of the center of pressure
COP(y) = The y coordinate of the center of pressure
Zoff = The vertical offset from the top plate to the origin of the force platform (a negative #)
Fx = The force along the x axis
Fy = The force along the y axis
Fz = The force along the z axis
Mx = The moment about the x axis
My = The moment about the y axis
Mz = The moment about the z axis

Centre of Pressure Results

Table C.1 Centre of Pressure – Expected vs. Calculated Results

Expected		Calculated	
X	Y	X	Y
0	0	-0.3017	0.07745
0	0	-0.6734	0.1237
0	0	-0.4527	0.09911
0	-12	-1.0035	-11.461
0	-12	-1.7965	-11.803
0	-12	-1.5253	-12.127
0	12	-0.8911	11.3121
0	12	-1.2318	13.0101
0	12	-1.2497	12.4381
-6	-5	-5.013	-5.4783
-6	-5	-5.5938	-5.4778
-6	-5	-5.5634	-5.4583
5	-6	4.36473	-5.7219
5	-6	4.17275	-5.6334
5	-6	4.21495	-5.5484
-5	6	-5.8456	6.34528
-5	6	-5.6531	6.41828
-5	6	-5.7082	6.30707

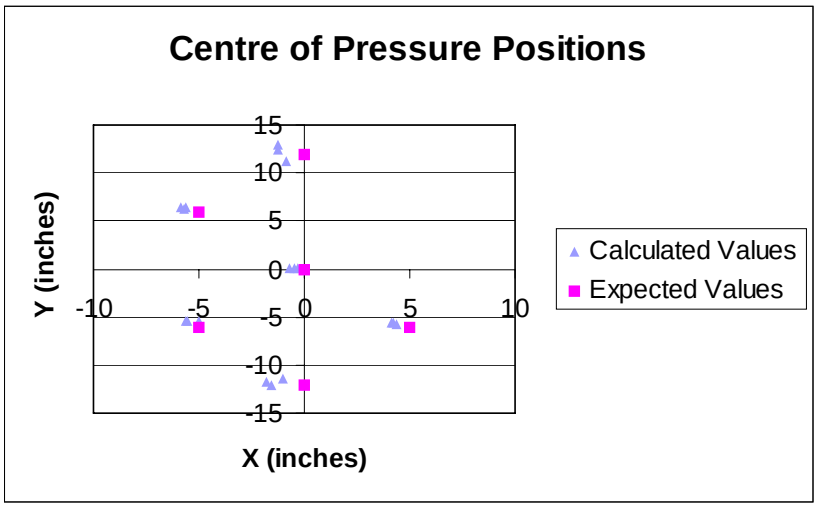

Figure C.1 Plot of Expected vs. Calculated Results

Table C.2 Standard Deviation and Standard Error for Centre of Pressure

		Standard Deviation		Standard Error	
X	Y	X	Y	X	Y
0	0	0.10794	0.01336	0.18696316	0.02314
0	-12	0.23269	0.19233	0.40303821	0.33312
0	12	0.40304	0.33312	0.23269422	0.19233
-5	-6	0.11669	0.11142	0.20210536	0.11211
5	-6	0.10089	0.08672	0.05824992	0.05007
-5	6	0.05725	0.03262	0.09916766	0.05651
5	6	0.32688	0.0114	0.18872288	0.00658

A3) Force Plate Calibration

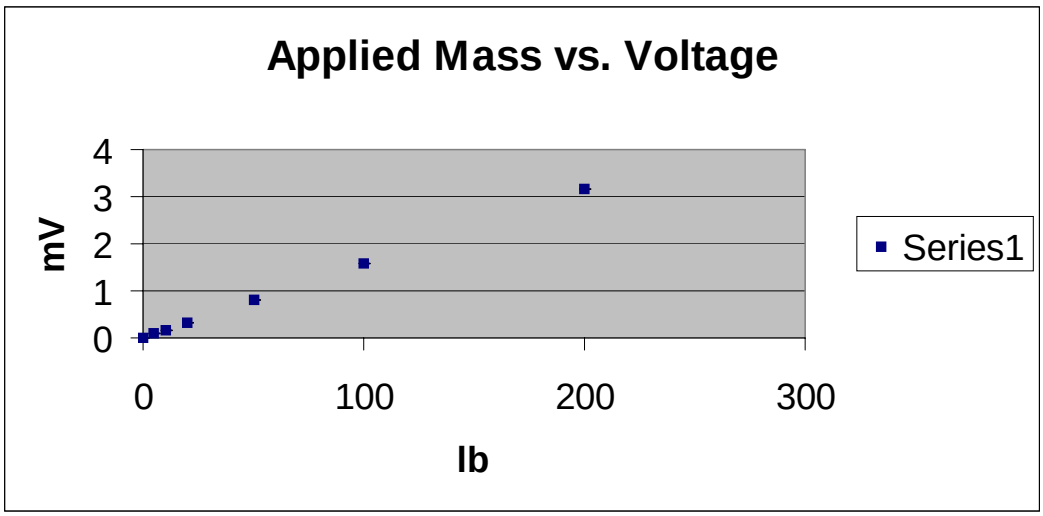

Figure C.2 Applied Mass vs. Voltage

Table C.3 Regression Analysis for Logarithmic Loading

Regression Statistics	
Multiple R	0.999991447
R Square	0.999982895
Adjusted R Square	0.999979474
Standard Error	0.005180357
Observations	7

ANOVA

	df	*SS*	*MS*	*F*	*Significance F*
Regression	1	7.844305377	7.844305377	292304.2435	4.10866E-13
Residual	5	0.00013418	2.68361E-05		
Total	6	7.844439557			

	Coefficients	*Standard Error*	*t Stat*	*P-value*
Intercept	0.014328576	0.002526366	5.671615104	0.002371385
X Variable 1	0.015693598	2.90272E-05	540.6516841	4.10866E-13

	Lower 95%	*Upper 95%*	*Lower 95.0%*	*Upper 95.0%*
Intercept	0.007834356	0.020822796	0.007834356	0.020822796
X Variable 1	0.015618982	0.015768215	0.015618982	0.015768215

B) Force Gauge

The coordinates of the applied force were calculated from the centre point of the application. The force was resolved with the angle of application into Fx, Fy, and Fz. Moments created by the applied force were calculated using the coordinates of the point of application with respect to the origin of the force plate axes. The distances in each direction in relation to the coordinate system of the force plate were calculated from the position of the origin of the coordinate system for the SLT measurements. The relation of the point on the SLT with reference to the coordinate system of the force plate was calculated by adding the coordinates of the origin of the SLT system to the coordinates of the point in the FP system. This procedure was repeated five times.

These values were compared to those of the measured forces from the force plate.

Table C.4 Push-Pull Gauge Calibration Results

		Applied Force (lb)					
Trial		2	10	10.1	11	20.5	50.5
	1	2	10	10.1	11	20.5	50.3
	2	1.95	9.95	10.15	11	20.45	50.4
Measured	3	2	9.95	10.1	11	20.5	50.6
	4	2.05	10	10.1	10.95	20.5	50.5
	5	2	10	10.05	11	20.45	50.5
Average		2	9.98	10.1	10.99	20.48	50.46

C) Tekscan™ Data Acquisition

Two hundred data points for each sensel were recorded with the Tekscan™ acquisition software. In order to minimize effects of start-up and drift, the middle 50 points were chosen and averaged.
The recorded pressures were converted to forces by division of the area of each sensel. The sensel area was considered equal for each sensel and was defined by the manufacturer as 161mm^2.

D) Strap Force Transducers

The force transducers were sewn into the webbing strap on one side of the buckle and measure the tension in the strap. The voltage across the transducer was collected with a voltage meter. It was assumed that the tension was constant throughout the length of the strap. It was seated firmly in the belt and then the voltage meter was zeroed.
Masses were hung from the belt in a random order. The measured voltages were plotted against the applied forces. A trend line was created with an equation for the calibration curve as seen in Figure C.3.

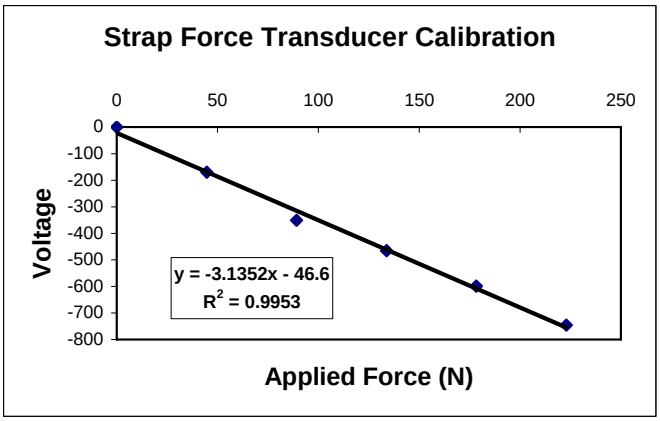

Figure C.3 Strap Force Transducer Calibration

The equation of the trend line was used for conversion of the output voltages to forces in Newtons.

Appendix D - System Calibration

System Calibration

The set-up can be seen below:

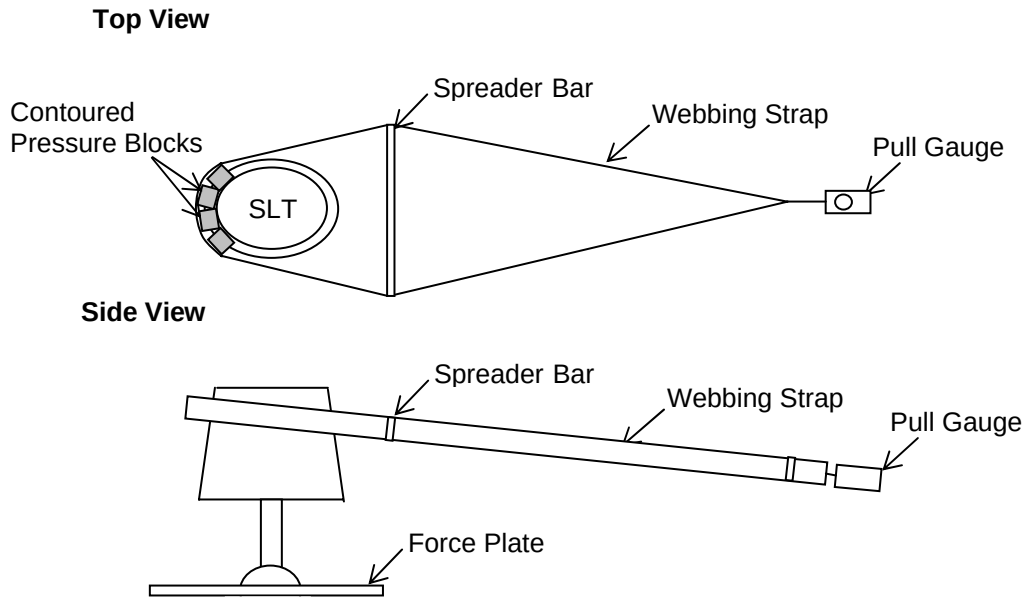

Figure D.1 Calibration Set-up

The free-body diagram is seen below:

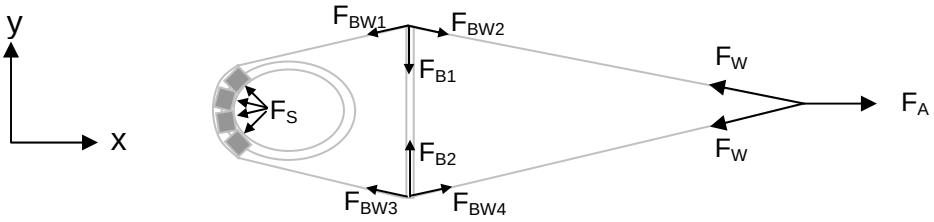

Figure D.2 Free body diagram of calibration set-up

The equilibrium equations are shown below.

The system is static, therefore:

$\Sigma F_x=0$
$\Sigma F_y=0$

From the orientation of the webbing it was shown that:

$F_A = 2F_W$

The resultant forces from this applied force are acted on the SLT.

$F_A - \Sigma F_{Sx} = 0$

The symmetry of the SLT about the x-axis caused the forces acting on it in the y-direction to cancel out.

$\Sigma F_{Sy} = 0$

The spreader bar was an internal component of the system and the forces that acted on it canceled in both directions.

$\Sigma F_B = 0$
$F_{B1} + F_{BW1} + F_{BW2} = F_{B2} + F_{BW3} + F_{BW4}$

Calibration of Flat Lumbar and Abdominal Sensors

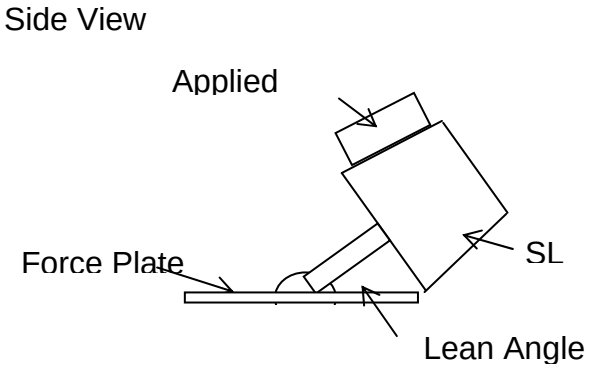

Figure D.3 Calibration set-up for lumbar and abdominal areas

Results of Initial Calibration

Table D.1 Force Gauge (Expected) vs. Tekscan (Measured)

Trial	Force	Expected (N)			Measured (N)			Standard Deviation		
	(N)	X	Y	Z	X	Y	Z	X	Y	Z
1	91.4	90.5	0.0	12.7	40.4	-3.5	6.9	35.4	2.5	4.1
2	87.4	86.5	0.0	12.2	35.2	-4.7	6.2	36.3	3.4	4.2
3	119.5	118.3	0.0	16.6	61.7	-7.1	10.5	40.0	5.0	4.4
4	68.7	68.0	0.0	9.6	28.2	1.1	5.0	28.2	0.8	3.2
5	72.2	71.5	0.0	10.1	29.0	-3.8	5.2	30.1	2.7	3.5
6	85.6	84.8	0.0	11.9	35.7	-3.2	6.2	34.7	2.3	4.1
7	104.3	103.3	0.0	14.5	48.6	-4.7	8.3	38.7	3.4	4.4
8	103.7	102.7	0.0	14.4	44.6	-5.3	7.8	41.1	3.8	4.7
9	67.8	67.1	0.0	9.4	37.0	-1.5	6.2	21.3	1.0	2.3
10	93.2	92.3	0.0	13.0	58.1	-2.6	9.6	24.2	1.8	2.4
11	90.1	89.2	0.0	12.5	47.7	-2.8	8.1	29.3	2.0	3.1

Table D.2 Force Gauge vs. Force Plate

Force Gauge -resolved			Force plate			Standard Deviation		
X	Y	Z	X	Y	Z	X	Y	Z
136.0	0.0	18.9	136.4	-0.3	16.0	0.3	0.2	2.1
107.0	0.0	14.9	109.4	-0.6	13.1	1.7	0.4	1.3
122.2	0.0	17.0	123.6	-0.5	13.9	1.0	0.4	2.2
100.3	0.0	14.0	102.8	-0.8	12.2	1.8	0.6	1.2
91.9	0.0	12.8	94.8	-0.9	11.7	2.1	0.6	0.8
77.6	0.0	10.8	80.4	-1.1	10.5	2.0	0.8	0.2
78.5	0.0	10.9	81.8	-0.9	8.3	2.4	0.7	1.8
83.8	0.0	11.7	86.3	-0.9	8.4	1.8	0.6	2.3
99.9	0.0	13.9	103.3	-0.6	10.3	2.5	0.4	2.5
78.0	0.0	10.9	81.3	-0.8	8.7	2.3	0.6	1.6
78.5	0.0	10.9	80.9	-0.9	8.5	1.7	0.7	1.7
84.7	0.0	11.8	87.4	-1.2	8.6	2.9	0.4	2.9

	Load Cell Expected						Force Plate Actual					
Trial	Fx	Fy	Fz	Mx	My	Mz	X	Y	Z	Mx	My	Mz
1	136	0	18.9	0	38.4	0	136.4	-0.3	16	4.8	43.2	1.3
2	107	0	14.9	0	30.2	0	109.4	-0.6	13.1	2.1	22.1	2.5
3	122.2	0	17	0	34.5	0	123.6	-0.5	13.9	2.5	29.9	3.3
4	100.3	0	14	0	28.4	0	102.8	-0.8	12.2	6.2	32.7	8.2
5	91.9	0	12.8	0	26.0	0	94.8	-0.9	11.7	5.6	23.9	1.6
6	77.6	0	10.8	0	21.9	0	80.4	-1.1	10.5	6.1	25	1.8
7	78.5	0	10.9	0	22.2	0	81.8	-0.9	8.3	4.7	11.3	2.9
8	83.8	0	11.7	0	23.7	0	86.3	-0.9	8.4	3.5	21.6	3.1
9	99.9	0	13.9	0	28.2	0	103.3	-0.6	10.3	3.6	34.8	1.2
10	78	0	10.9	0	22.1	0	81.3	-0.8	8.7	4.7	31.6	1.8
11	78.5	0	10.9	0	22.2	0	80.9	-0.9	8.5	4.9	31.2	1.8
12	84.7	0	11.8	0	23.9	0	87.4	-1.2	8.6	11	26.4	0.9

Table D.3 Results of the Initial Sum of Squared Error Calculations

Sensor	Friction	Area	SSE	RMS
01	-----	-----	-----	-----
03	0.26	4.87	289.39	7.61
05	-----	-----	-----	-----
06	0.26	4.82	122.33	6.39
07	0.26	5.96	227.29	7.54
09	0.25	4.51	66.47	4.71
10	0.26	4.82	122.33	6.39
12	0.24	4.26	103.49	5.87
13	0.26	4.87	289.39	7.61
15	0.25	5.84	245.71	6.40

Table D.4 Results of Sum of Squared Error using Constant coefficient of Friction

Sensor	Friction	Area	SSE	RMS
01	0.257	-----	-----	-----
03	0.257	4.87	290.02	7.62
05	0.257	-----	-----	-----
06	0.257	4.82	127.37	6.52
07	0.257	5.96	229.44	7.57
09	0.257	4.51	66.52	4.71
10	0.257	4.82	127.37	6.52
12	0.257	4.26	108.30	6.01
13	0.257	4.87	290.02	7.62
15	0.257	5.84	245.93	6.40

Appendix E - Determination of Static Coefficient of Friction

$$F_r = \mu \times F_n$$

The force of friction on a flat surface is:

$$F_r = force\_of\_friction$$
$$\mu = Coefficient\_of\_friction$$
$$F_n = Normal\_Force$$

Where:

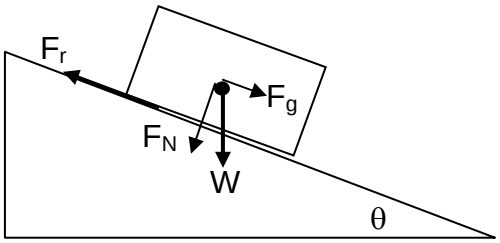

Figure E.1 Friction on an inclined plane

On an inclined surface:

$$F_r = \mu \times \cos\theta \times W$$

Gravity also has an effect on the inclined surface:

$$F_g = \sin\theta \times W$$
$$F_g \geq F_r$$

The object will slide when

Therefore, solving for coefficient of friction

$$F_g = F_r$$
$$\mu \times \cos\theta \times W = \sin\theta \times W$$
$$\mu = \frac{\sin\theta}{\cos\theta}$$
$$\mu = \tan\theta$$

This value was the maximum friction, or static friction coefficient. The actual coefficient when movement was occurring was not measurable. Therefore, the static friction value was used as an upper limit and an estimated sliding coefficient was calculated by optimizing the results over a series of trials. The sliding coefficient of friction is generally 25% lower than that of the static coefficient of friction (Hibbeler, 1993). Three different surface configurations were used:

A) Sensor on wood, smooth steel block
B) Sensor on wood, steel block on foam and webbing
C) Sensor on wood and BockliteTM, steel block on foam and webbing

The measurements are seen below in Table E.1.

Trial C averaged a static coefficient of 0.31 which resulted in a sliding coefficient of 0.23.

Table E.1 Inclined Plane Calculations

Inclined Plane Calculations							
Trial A				Trial B			
Mass:	2.75	Lb		Mass:	2.78	lb	
Mass Mat'l:	Steel block			Mass Mat'l:	Steel block on foam and webbing		
Surface:	Sensor on wood			Surface:	Sensor on wood		
Trial	Angle (degrees)	Coefficient		Trial	Angle (degrees)	Coefficient	
1	23	0.4244748		1	22	0.4040262	
2	19	0.3443276		2	22	0.4040262	
3	21	0.383864		3	19	0.3443276	
4	23	0.4244748		4	19	0.3443276	
5	21	0.383864		5	20	0.3639702	
6	21	0.383864		6	19	0.3443276	
7	19	0.3443276		7	18	0.3249197	
8	21	0.383864		8	21	0.383864	
9	22	0.4040262		9	20	0.3639702	
10	22	0.4040262		10	19	0.3443276	
	Average:	0.3881113			Average:	0.3622087	
Trial C							
Mass:	5.8	Lb					
Mass Mat'l:	Steel block on foam and webbing						
Surface:	Sensor on wood and Bocklite						
Trial	Angle (degrees)	Coefficient					
1	20	0.3639702					
2	17	0.3057307					
3	18	0.3249197					
4	16	0.2867454					
5	18	0.3249197					
6	16	0.2867454					
7	18	0.3249197					
8	16	0.2867454					
9	17	0.3057307					
10	16	0.2867454					
	Average:	0.3097172					

Appendix F - Strap Force Transducer and Tekscan Sensor Testing

The Tekscan data was summed as in Figure 5.6, seen below in Table F.1.

Table F.1 Tekscan Data for Strap Tension Comparison

Trial	Strap Force (N)	X-LHS	X-RHS	Y-Lumbar	Y-Abdomen
1	41.9800825	90.760884	-63.83545	141.8743913	-56.8092693
2	42.97256854	98.439224	-106.7235	158.2459341	-66.0045776
3	47.43875573	107.73225	-97.65042	179.4105244	-71.6257236
4	44.4612976	91.45464	-44.78245	139.525006	-57.5580078
5	59.34858822	116.88149	-79.11695	150.2285888	-64.6015177
6	54.38615801	122.88968	-104.1704	168.0928385	-65.7241582

The values of measured force in Table F.1 were divided by the strap force tension in order to normalize the values. As the strap tensions varied slightly throughout trials, they are not directly comparable in Figure F.1.

Table F.2 Averaged (Absolute) Values with Factor for Strap Tension – X Values

	LHS Factor	RHS Factor	Average Factor
X Values	2.16199872	-1.52061289	1.841305802
	2.29074564	-2.4835259	2.387135772
	2.27097554	-2.05845248	2.164714007
	2.05694941	-1.00722323	1.53208632
	1.96940649	-1.33308898	1.651247733
	2.2595764	-1.91538426	2.08748033
Average	2.16827537	-1.71971462	1.943994994

Table F.3 Averaged (Absolute) Values with Factor for Strap Tension – Y Values

	Strap Force (N)	Lumbar factor	Abdomen factor	Average Factor
Y Values	41.9800825	3.379564376	-1.353243393	2.366403884
	42.97256854	3.68248721	-1.535970034	2.609228622
	47.43875573	3.781939928	-1.509856708	2.645898318
	44.4612976	3.138122671	-1.294564281	2.216343476
	59.34858822	2.531291701	-1.088509764	1.809900732
	54.38615801	3.090728314	-1.208472166	2.14960024
Average	48.43124177	3.2673557	-1.331769391	2.299562545

Appendix G - Pack-On Testing Procedure

Where:

F_p = Force of gravity acting on the pack
F_a = Applied force by pull gauge to steady pack on system

Both of these forces are constants throughout each trial.

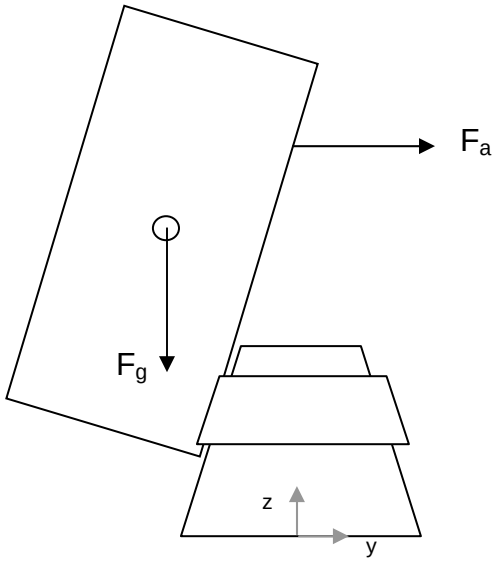

Isolation of the forces acting on the lumbar area:

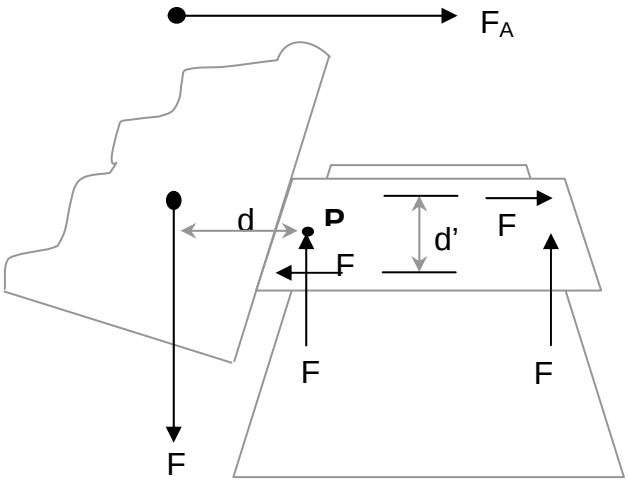

DOCUMENT CONTROL DATA
(Security classification of the title, body of abstract and indexing annotation must be entered when the overall document is classified)

1. ORIGINATOR (The name and address of the organization preparing the document, Organizations for whom the document was prepared, e.g. Centre sponsoring a contractor's document, or tasking agency, are entered in section 8.)

Publishing: DRDC Toronto

Performing: Ergonomics Research Group, Queen's University, Kingston, Ontario K7L 3N6

Monitoring:

Contracting: DRDC Toronto

2. SECURITY CLASSIFICATION (Overall security classification of the document including special warning terms if applicable.)

UNCLASSIFIED

3. TITLE (The complete document title as indicated on the title page. Its classification is indicated by the appropriate abbreviation (S, C, R, or U) in parenthesis at the end of the title)

Development of a Dynamic Biomechanical Model for Load Carriage: Phase III Part C1: Pressure and Force Distribution Measurement for the Design of Waist Belts in Personal Load Carriage Systems (U)

4. AUTHORS (First name, middle initial and last name. If military, show rank, e.g. Maj. John E. Doe.)

L.J. Hadcock

5. DATE OF PUBLICATION (Month and year of publication of document.)

August 2005

6a NO. OF PAGES (Total containing information, including Annexes, Appendices, etc.)

117

6b. NO. OF REFS (Total cited in document.)

38

7. DESCRIPTIVE NOTES (The category of the document, e.g. technical report, technical note or memorandum. If appropriate, enter the type of document, e.g. interim, progress, summary, annual or final. Give the inclusive dates when a specific reporting period is covered.)

Contract Report

8. SPONSORING ACTIVITY (The names of the department project office or laboratory sponsoring the research and development − include address.)

Sponsoring:

Tasking:

9a. PROJECT OR GRANT NO. (If appropriate, the applicable research and development project or grant under which the document was written. Please specify whether project or grant.)

12CM03

9b. CONTRACT NO. (If appropriate, the applicable number under which the document was written.)

W7711−0−7632−06

10a. ORIGINATOR'S DOCUMENT NUMBER (The official document number by which the document is identified by the originating activity. This number must be unique to this document)

DRDC Toronto CR 2005−121

10b. OTHER DOCUMENT NO(s). (Any other numbers under which may be assigned this document either by the originator or by the sponsor.)

11. DOCUMENT AVAILABILITY (Any limitations on the dissemination of the document, other than those imposed by security classification.)

Unlimited distribution

12. DOCUMENT ANNOUNCEMENT (Any limitation to the bibliographic announcement of this document. This will normally correspond to the Document Availability (11), However, when further distribution (beyond the audience specified in (11) is possible, a wider announcement audience may be selected.))

Unlimited announcement

DOCUMENT CONTROL DATA
(Security classification of the title, body of abstract and indexing annotation must be entered when the overall document is classified)

13. ABSTRACT (A brief and factual summary of the document. It may also appear elsewhere in the body of the document itself. It is highly desirable that the abstract of classified documents be unclassified. Each paragraph of the abstract shall begin with an indication of the security classification of the information in the paragraph (unless the document itself is unclassified) represented as (S), (C), (R), or (U). It is not necessary to include here abstracts in both official languages unless the text is bilingual.)

(U) In previous studies, two biomechanical models were developed that used pack and person geometry as well as pack mass to determine the reaction forces on the body. One perpetual problem has been determining the pack−person interface forces using TekscanTM pressure sensors on rounded surfaces such as the shoulder and waist. The goal of this study was to determine design factors that affect force distribution of the backpack waist belt. A human−sized symmetrical lower torso (SLT) was created of wood and covered with BockliteTM. A method of calculating the directional coordinates of applied forces was developed in order to understand the reactions between pack and person. TekscanTM Sensors were used on the surface to measure the surface pressures between the torso and the waist belt. These were converted to normal force measures based on the mathematical coordinates of each sensel. A strategy was developed for calibration of TekscanTM on a curved surface. Calibration factors, a factor of effective sensel area and a frictional coefficient for the in situ orientation of each sensor were calculated and used for the calculation of the directional forces. Then, using selected sites on the waist belt, known forces were applied and the resulting directional forces correlated moderately well with the known applied forces (19%). The pressure distributions of three waist belts were compared and the design features were examined to account for differences in distribution. The distributions were compared to results of the previous biomechanical models and determined to be too complex to be resolved with the simplified hoop stress theory. The study determined the importance of waist belt design, frictional force from belt tightening, and influence of load in understanding the force distribution of a waist belt. A limiting factor was the lack of precision of TekscanTM and its inability to measure shearing frictional forces, a key variable in understanding how a backpack works. It is recommended that each pack and load condition be tested using this approach if one wishes to use the waist strap force gauge to determine compressive forces on the lumbar spine and on the hips.

14. KEYWORDS, DESCRIPTORS or IDENTIFIERS (Technically meaningful terms or short phrases that characterize a document and could be helpful in cataloguing the document. They should be selected so that no security classification is required. Identifiers, such as equipment model designation, trade name, military project code name, geographic location may also be included. If possible keywords should be selected from a published thesaurus, e.g. Thesaurus of Engineering and Scientific Terms (TEST) and that thesaurus identified. If it is not possible to select indexing terms which are Unclassified, the classification of each should be indicated as with the title.)

(U) Load carriage; Dynamic Biomechanical Model; Lower Torso Model; Waist Belt Model; Pressure and Force Distribution; Contact pressure Sensors; Strap Force Tension; Tekscan